NATIONAL TECHNICAL UNIVERSITY OF ATHENS
School of Civil Engineering
Laboratory for Earthquake Engineering
Interdepartmental Postgraduate Program ***"Analysis and Design of Structures"***

"Structural Health Monitoring using the Continuous Wavelet Transform Method"

P O S T G R A D U A T E T H E S I S

Nikolaos S. Smyrniotis

Supervisor:
Dr. Michalis Fragiadakis, Associate Professor NTUA

Athens, March 2024

Copyright © Νικόλαος Σ. Σμυρνιώτης, 2024
Με επιφύλαξη παντός δικαιώματος
Απαγορεύεται η αντιγραφή, αποθήκευση σε αρχείο πληροφοριών, διανομή, αναπαραγωγή, μετάφραση ή μετάδοση της παρούσας εργασίας, εξ ολοκλήρου ή τμήματος αυτής, για εμπορικό σκοπό, υπό οποιαδήποτε μορφή και με οποιοδήποτε μέσο επικοινωνίας, ηλεκτρονικό ή μηχανικό, χωρίς την προηγούμενη έγγραφη άδεια του συγγραφέα. Επιτρέπεται η αναπαραγωγή, αποθήκευση και διανομή για σκοπό μη κερδοσκοπικό, εκπαιδευτικής ή ερευνητικής φύσης, υπό την προϋπόθεση να αναφέρεται η πηγή προέλευσης και να διατηρείται το παρόν μήνυμα. Ερωτήματα που αφορούν στη χρήση της εργασίας για κερδοσκοπικό σκοπό πρέπει να απευθύνονται προς τον συγγραφέα. Η έγκριση της διπλωματικής εργασίας από τη Σχολή Πολιτικών Μηχανικών του Εθνικού Μετσόβιου Πολυτεχνείου δεν υποδηλώνει αποδοχή των απόψεων του συγγραφέα (Ν. 5343/1932, Άρθρο 202).

Copyright © Nikolaos S. Smyrniotis, 2024
All Rights Reserved
Neither the whole nor any part of this diploma thesis may be copied, stored in a retrieval system, distributed, reproduced, translated, or transmitted for commercial purposes, in any form or by any means now or hereafter known, electronic or mechanical, without the written permission from the author. Reproducing, storing and distributing this thesis for non–profitable, educational or research purposes is allowed, without prejudice to reference to its source and to inclusion of the present text. Any queries in relation to the use of the present thesis for commercial purposes must be addressed to its author. Approval of this diploma thesis by the School of Civil Engineering of the National Technical University of Athens (NTUA) does not constitute in any way an acceptance of the views of the author contained herein by the said academic organization (L. 5343/1932, art. 202).

Νικόλαος Σ. Σμυρνιώτης (2024)
Διπλωματική Εργασία
Παρακολούθηση της Δομικής Υγείας
με χρήση της Μεθόδου του Συνεχή Μετασχηματισμού Κυματιδίων
Εργαστήριο Αντισεισμικών Ερευνών, Εθνικό Μετσόβιο Πολυτεχνείο, Αθήνα

Nikolaos S. Smyrniotis (2024)
Diploma Thesis
Structural Health Monitoring using the Continuous Wavelet Transform Method
Laboratory for Earthquake Engineering, National Technical University of Athens, Greece

Contents

Acknowledgements

The completion of this postgraduate thesis marks the end of my journey in the program “Analysis and Design of Structures”, provided by the School of Civil Engineering at NTUA. A journey full of new knowledge, acquaintances and goals, opening my horizons in the subject of engineering, and now it constitutes an achievement of personal fulfillment.

First of all, I would like to express my gratitude to my supervisor, Associate Professor Michalis Fragiadakis, for his cooperation, continuous help, understanding and the opportunity he gave me to deal with such an interesting field. I am also grateful to all the professors of the program for the knowledge and the scientific background they provided us and, of course, to all the members of the academic community for their help and support.

Finally, I would like to express my profound thankfulness to my parents, Stefanos and Ioanna, family members and all my friends, who extremely supported me all these years through my pre– and post–graduate studies.

Abstract

Structural Health Monitoring (SHM) is a process of implementing a damage detection strategy in structures to evaluate the condition of existing structures to ensure the safety of users in the future. The changes in the material, geometric and/or structural properties affect structural responses, which can be captured and analyzed for condition assessment. Various vibration–based damage detection algorithms have been developed in the past decades. Among them, the method of the Continuous Wavelet Transform (CWT) gained popularity as an efficient method of signal processing to create a framework to identify model properties and detect damage in structures. In this study, the application of wavelet transform for identification of modal parameters and damage detection is presented and numerically verified through verification examples. The method is developed in MATLAB and then, it is used in various cases, such as in the Z24 road bridge in Switzerland. The results are compared with those obtained from other calculation methods as the Fast Fourier Transform (FFT), and moreover with the use of the Modal Analysis Software "ARTeMIS Modal". It is shown that the CWT used for output–only identification and damage detection yields good agreement with the results from ARTeMIS Modal. The incorporation of noise in the signals and the methods' sensitivity in modal parameter identification are also investigated. Furthermore, an attempt is made to reconstruct the signals in non–significant noise situations, through the Hilbert transform and the analytical signal.

Περίληψη

Η Παρακολούθηση της Δομικής Υγείας – Structural Health Monitoring (SHM) – είναι μία διαδικασία εφαρμογής στρατηγικής ανίχνευσης αστοχιών για την αξιολόγηση της κατάστασης υφιστάμενων κατασκευών, ώστε να διασφαλισθεί η ασφάλεια των χρηστών στο μέλλον. Οι αλλαγές στο υλικό, στις γεωμετρικές ή/και δομικές ιδιότητες επηρεάζουν τις δομικές αποκρίσεις, οι οποίες μπορούν να αποτυπωθούν και να αναλυθούν για την εκτίμηση της κατάστασης της κατασκευής. Διάφοροι αλγόριθμοι ανίχνευσης αστοχιών που βασίζονται σε κραδασμούς έχουν αναπτυχθεί τις τελευταίες δεκαετίες. Μεταξύ αυτών, η μέθοδος του Συνεχή Μετασχηματισμού Κυματιδίων – Continuous Wavelet Transform Method (CWT) – κέρδισε δημοτικότητα ως μία αποτελεσματική μέθοδος στην επεξεργασία σημάτων για την δημιουργία ενός πλαισίου για τον εντοπισμό των ιδιοχαρακτηριστικών της κατασκευής και την ανίχνευση αστοχιών. Σε αυτήν την μελέτη παρουσιάζεται η εφαρμογή της μεθόδου του Συνεχή Μετασχηματισμού Κυματιδίων για την αναγνώριση των ιδιοτιμών αυτών και την ανίχνευση αστοχιών και επαληθεύεται αριθμητικά μέσω παραδειγμάτων. Η μέθοδος έχει αναπτυχθεί στο MATLAB και εφαρμόστηκε σε διάφορες περιπτώσεις, όπως στην περίπτωση της οδικής γέφυρας Z24 στην Ελβετία. Τα αποτελέσματα συγκρίνονται με αυτά που προέκυψαν από άλλες μεθόδους υπολογισμού όπως ο Fast Fourier Transform (FFT) και με την χρήση του λογισμικού ιδιομορφικής ανάλυσης “ARTeMIS Modal”. Αποδεικνύεται ότι ο CWT ως μέθοδος output–only και ανίχνευσης αστοχιών, αποδίδει καλή συμφωνία με τα αποτελέσματα του ARTeMIS Modal. Διερευνάται, επίσης, η ενσωμάτωση του θορύβου στα σήματα και η ευαισθησία των μεθόδων στην ταυτοποίηση των παραμέτρων των συστημάτων λόγω του θορύβου αυτού. Επιπλέον, γίνεται προσπάθεια ανακατασκευής των σημάτων σε καταστάσεις μη σημαντικού θορύβου, μέσω του μετασχηματισμού Hilbert και του αναλυτικού σήματος.

Acronyms, Abbreviations and Symbols

SHM	Structural Health Monitoring
CWT	Continuous Wavelet Transform
ACWT	Averaged Continuous Wavelet Transform
WT	Wavelet Transform
RDT	Random Decrement Technique
SNR	Signal–to–Noise Ratio
DOF	Degree of Freedom
FFT	Fast Fourier Transform
FT	Fourier Transform
FRF	Frequency Response Function
TF	Time Frequency
EMA	Experimental Modal Analysis
OMA	Operational Modal Analysis
MDOF	Multi Degree of Freedom system
SDOF	Single Degree of Freedom system
STFT	Short Time Fourier Transform
$sgn(\omega)$	Sign function of a real number, equal to: $$sgn(\omega)=\begin{cases}-1, & \text{if } \omega < 0.\\ 0, & \text{if } \omega = 0.\\ 1, & \text{if } \omega > 0.\end{cases}$$
$\Theta(\omega)$	Heaviside step function, equal to: $$\Theta(\omega)=\begin{cases}1, & \text{if } \omega \geq 0.\\ 0, & \text{if } \omega < 0.\end{cases}$$
ω	Angular frequency or Undamped angular frequency [rad/sec]
f	Frequency [Hz]
F_s	Sampling frequency [Hz]
T	Period [*sec*]
dt	Sampling period [*sec*]
$\widetilde{\omega}$	Damped angular natural frequency of the system [rad/sec]
m	Mass
c	Damping constant
c_{cr}	Critical damping coefficient

$\boldsymbol{u}(t)$	Displacement vector vector
$\dot{u}(t)$	Velocity vector
$\ddot{u}(t)$	Acceleration vector
$\mathbf{M}$	Mass matrix
$\mathbf{C}$	Damping matrix
$\mathbf{K}$	Stiffness matrix
$\mathbf{\Phi}$	Mode shape matrix
$u(t)$	Real valued signal
$Z_u(t)$	Analytic signal
$T_\psi[u](b, a)$	Continuous wavelet transform of a signal $u(t)$
t_ψ	Mother wavelet center time
ω_ψ	Mother wavelet center frequency
Δt_ψ	Duration of the mother wavelet
$\Delta\omega_\psi$	Bandwidth of the mother wavelet
a	Scale parameter of the CWT
b	Time translation parameter of the CWT
$a_r(b)$	Ridge of the CWT
$A(t)$	Instantaneous amplitude
$\varphi(t)$	Instantaneous phase
$\omega(t)$	Instantaneous angular frequency
$\psi(t)$	Mother wavelet defined in the time domain
$\hat{\psi}(\omega)$	Mother wavelet defined in the frequency domain
$\bar{z}$	Complex conjugate of a complex number z
$x * y$	Convolution of x and y
$\hat{g}$	Fourier transform of a function g
$\langle x, y \rangle$	Inner product of x and y
$\|\| \cdot \|\|$	Norm of a function, vector or matrix
$\angle$	Phase of the function/signal
$\mathrm{Re}()$	Real part of a complex number
$\mathrm{Im}()$	Imaginary part of a complex number
$\mathbb{C}$	The set of all complex numbers
$\mathbb{R}$	The set of all real numbers
$\mathbb{R}_+^*$	The set of all real positive numbers excluding zero
$\mathbb{Z}$	The set of integers (positive, negative, zero)

1. Introduction

1.1 Introduction in Structural Health Monitoring

Structural Health Monitoring (SHM) is defined as the process of using an on–structure sensing system to monitor its performance and evaluate the health state. The changes of material and geometric properties of structures including boundary condition, changes in loading conditions, deterioration with age, etc. affect the structure performance and can cause damage. While some damage is visible, others may be difficult to spot. Structural damage caused results in observable changes in the vibratory responses of the structure, hence the analysis of these outputs can allow the estimation of the decreased stiffness matrix. The vibration based SHM process involves the observation of a system over time using periodically sampled dynamic response measurements from an array of sensors. In addition, SHM uses the extraction of damage–sensitive features, such as vibration characteristics and the statistical analysis to determine the current state of system health. Furthermore, measured vibration data can be employed for validating and updating finite–element–models used in the analysis, even in the design phase for some cases of complex and large–scale structures where experiments and tests are also performed. [41]

Sensors are placed on the structure to allow communication between sensors as well as the location of the damage. As the density of sensors increases on a structure, the quality and resolution of damage information also increases. However, sensor installation costs, sensor power consumption, and data processing capacity act as limiting factors for sensor density. Sensors measure structure quantities such as strain, displacement, and acceleration as well as environmental conditions like temperature, wind, and moisture. The output of this process periodically updates information regarding the ability of the structure to perform its intended function and degradation results from operational environments for long term serviceability. [41]

This concept is widely used in various types of engineering structures to reduce monetary losses and guarantee and ensure the safety of users.

SHM is used to provide rapid, real and reliable information regarding the functions of the structure. A complete SHM approach consists of five basic steps which involve:

(1) Detection – Identification of damage occurrence in the structure, if any
(2) Localization – Identification of single or multiple damage locations
(3) Assessment – Quantification of the level of damage
(4) Prognosis – Evaluation of structural performance and its useful remaining life
(5) Remediation – Determination, implementation, and evaluation of effective remediation and repair efforts

1.2 Modal Parameter Identification

Dynamic and vibration characteristics may be identified through the process of Modal Analysis. Modal parameter identification is a fundamental part of structural

engineering, used in the monitoring or the assessment of existing structures under dynamic loading conditions as well as the design phase of new structures. In existing structures, modal parameter identification consists in general of three main steps: excitation and data acquisition, signal processing, and modal parameters estimation.

Focusing on the first step, vibration measurements can be obtained by performing Experimental Modal Analysis (EMA), where the structure is subjected to a controlled input (excitation) and its output (response) is being recorded, or Operational Modal Analysis (OMA), where the modal properties are identified based on vibration data (wind, traffic, machine vibration etc.) collected during operating conditions of the under–study structure. In many cases, OMA is used instead of classical modal analysis, as it provides the advantages of not requiring special equipment and evacuation of the structure during the measurements and it can be applied in situations where it is difficult or impossible to artificially excite the structure.

The signal processing techniques are used for the estimation of modal parameters. The most common classification of these methods is done according to the domain where the data are processed: time domain, frequency domain and time–frequency domain. In general, time domain models tend to provide the best results when a wide frequency range or large number of modes exist in the data, whereas frequency domain models tend to provide the best results when the frequency range of interest is limited and the number of modes is relatively small. However, frequency domain methods do not provide any information about the time where the components of the frequency content of the under signal are present. For a long time, frequency domain identification and time domain identification were considered as competing methods to solve the same problem. A main conclusion of Ljung and Glover [13] back in 1979, was that these two approaches are complementary rather than rivalling. Thus, taking it one step further, the need to overcome the inability of the frequency domain approach to capture time–varying features of a structure but retain the advantage of the frequency content information, led to the development of the time–frequency domain methods. These methods study a signal in both the time and frequency domains simultaneously. Subsequently, they were widely applied and used in system identification and damage detection.

1.3 The wavelet transform (WT)

The wavelet transform (WT) originated in the early 1980s in the works of Morlet [15] who used it in seismology and then Grossman and Morlet [16] who developed the geometrical formalism of the continuous wavelet transform. The Continuous wavelet transform (CWT) is a time–frequency domain output–only modal identification method and was first proposed by Staszewski and Cooper [23] in 1995 to estimate structural parameters. Since then, the potential of modal parameter identification using the CWT has been receiving considerable attention in the literature. Early works were focused on exploring and developing methods and techniques for the estimation of a system's natural frequencies, damping ratios and gradually mode shapes. [25]

The CWT is a linear transform by definition and thus, appropriate for multi–component signals. Compared with other identification techniques, CWT has two fundamental advantages in structural parameter identification [24]. The first is the multi–resolution ability inherent to wavelet analysis. This property enables the separation of the close frequency components of a coupled frequency signal, allowing MDOF systems to be handled directly. Additionally this ability ensures that CWT can work as a band–pass filter

and automatically filter out noise from the signal. Hence, this method can handle very noisy measurements. The second advantage is that CWT can resolve multiple structural parameters from a single signal without knowledge of the applied force acting on the structure. This advantage makes it a promising output–only identification method that is widely utilized in both EMA and OMA. Another important advantage of the CWT is that it can be used to analyze time series that contain non–stationary power at many different frequencies [4], and therefore it can process non–stationary vibration measurements. Lastly, the use of the CWT allows to determine the time variation of instantaneous amplitude and phase of each component within the signal [10] a property that facilitates the identification procedure of modal parameters through the identification of ridges and the reconstruction of the signal.

1.4 Objective

The objective of this thesis is the application of the Continuous Wavelet Transform (CWT) on ambient vibration responses, with the aim of the identification of their modal parameters and subsequently of the damage detection for SHM.

The implementation of the algorithms, the calculations and the visualizations are done with MATLAB ver.R2023a, using the standard features and additionally the Signal Processing Toolbox and the Wavelet Toolbox. MATLAB simulations are used to develop algorithms and subjected to acquire acceleration data analysis. The advantages of the CWT method are identified and compared to the widely used Fourier analysis. The comparison of the results is done with the Modal Analysis Software ARTeMIS Modal ver. 7.2. Moreover, the methods' sensitivity in embedding of additional noise is tested, aiming to prove the dominance of CWT.

1.5 Thesis outline

The thesis contains 8 main chapters.

Chapter 1 is the Introduction.

In **Chapters 2** the definition, the importance and basic steps of structural health monitoring are presented.

Chapters 3 and 4 present the essential engineering, physical and mathematical theoretical background that is required to comprehend the contents and the methods applied.

Chapter 5 provides an essential background on structural dynamics.

Chapter 6 describes the methods that will be applied for ridge extraction, reconstruction of the signals, modal parameters identification and the system dynamic characterization.

Chapter 7 presents three numerical applications, a 4–storey building, an 8–storey building, and a real project conducted in Aristotle University of Thessaloniki called EuroProteas.

Chapter 8 presents the modal parameter identification and damage detection of the Z24 Bridge in Switzerland. The time–frequency representation is generated for different damage scenarios took place throughout a period of one month. The eigen–frequencies, damping ratios and mode shapes are obtained and compared for each scenario in order to assess the integrity of the bridge. The results obtained from ARTeMIS Modal are also compared.

2. Structural Health Monitoring (SHM)

2.1 Structural Health Monitoring Methods

2.1.1 Visual Inspection

The first and foremost basic structural health monitoring system is visual inspection. That is, visually inspect the cracks, delaminated areas, deformations of structural members in order to clarify the structural healthiness of the structure. Even though this is helpful as an initial inspection method, this has several drawbacks and inconsistency of results depending on the experience of the inspectors. Hence, there is a special need of using consistent reliable methods in order to overcome these drawbacks. [41]

2.1.2 Non–contact Monitoring

Contacting sensors have to be mounted directly onto the measuring points of structures and be connected to a neighboring stationary reference point. For practical infrastructures, it is difficult to find an ideal stationary reference point near the measuring point, and it is also inconvenient for the connection between sensors and stationary reference points. Therefore contacting sensors troublesome in installation and expensive in maintenance too (Malesa et al. 2010). Non–contacting sensors can be located outside the infrastructures without being connected to a stationary reference point directly which is quite convenient for SHM compared to contact technologies for health monitoring. [41]

The development of innovative non–contact systems for vibration measurement is convenient to use compared to contact technologies and has recently drawn the attention of several researchers for non–contact technologies. Non–contact sensors include Laser Doppler Vibrometer (Cunha and Caetano 1999), Global Positioning Systems (Nickitopoulou et al. 2006,) and vision–based systems using digital image processing techniques etc. In addition, the microwave interferometry has recently emerged as an innovative technology, suitable to the non–contact vibration monitoring of large structures. [41]

2.1.3 Vibration Based Structural Health Monitoring

Vibration Based Structural Health Monitoring (VBSHM) has drawn significant attention in health monitoring techniques. The basic characteristic of this method is that the characteristic changes in structures such as mass, stiffness and damping will affect to the global vibration response of the monitored structure. Thus, unknown properties of the structure can be identified by studying the changes of the measured vibration behavior. When the changes in structural properties inversely affect to the performance of structure, it will be defined as damage (Guan and Karbhari 2008). The process of identifying those structural changes is referred as vibration based damage identification or vibration based damage detection. Compared to other monitoring system, this method has the advantage of monitoring the global nature of the vibration characteristics. The capability of identifying

the modal parameters such as natural frequencies and mode shapes, pave the path to monitor not only a single individual structural component but the entire structure. Hence, large civil engineering structures such as bridges can be effectively monitored with limited number of sensors and equipment. [41]

Structural dynamic response measurements are achieved with an instrumentation system which includes sensors, transmission and storage of dynamic response data. Sensor type, sampling frequencies need to be customized according to the application. Acceleration, velocity and displacement are the most common dynamic response measurements. The instrumentation system must be designed to manage a data collection if continuous monitoring of a structure is needed with large amount of data. [41]

Dynamic response of the structure is utilized in order to find the corresponding modal parameters which contain important characteristics of the structural dynamic response. Those are easy to use in further analysis and storage compared to actual raw data. [41]

2.2 Data Acquisition Methods

2.2.1 Wired Sensor Networks

Wired sensor networks are consists of cables to carry different electrical signals from one end to the other. The speed of operation is high compared to wireless networks but installation is cumbersome and requires more time. In wired sensor network, the mobility is limited as it operates in an area covered by a connected system. Channel interference is less as one wired network will not affect the other. [41]

2.2.2 Wireless Sensor Networks

A wireless sensor network consists of bunch of multi–functional sensor nodes having sensing, computational and communication capabilities for responses in structures. It consists of four basic components which are sensor unit, Analog Digital Converter (ADC), Central Processing Unit (CPU), and a power unit. Sensor nodes sense or capture the physical data at the area of interest. The sensed data by sensors is digitized by ADC and sent to controllers for further processing. Wireless sensor nodes are usually a small electronic device which can only be equipped with limited power. This network can set up without any fixed infrastructure and ideal for non–reachable places such as mountains, deep forests, sea, and rural area. Implementation is comparatively cheaper than wired sensors. [41]

2.3 Wavelet Transform for Structural Health Monitoring

Wavelet Transform (WT) has achieved the ability to overcome many of the limitations in Fourier analysis. Hence, WT is widely used not only in civil engineering field but in many fields including mechanical systems and aerospace as a signal processing tool in structural health monitoring showing its generality. WT is based on dilated scales and shifted windows which has the ability to perform a good time frequency resolution of a data signal contributed to widespread applications in engineering. A time domain signal is

converted into WT in terms of the projection of the original signal onto a family of functions that are normalized dilations and translations of wavelet transform. A function $\psi(t)$ is defined as the mother wavelet and it dilates (scaled) and translates (shifted) as daughter wavelets. Scaling in WT means stretching or compressing it in the time domain. Smaller scales represent more compressed wavelets while larger scales produce more stretched wavelets. Major applications in WT were focused on feature extraction and pattern recognition. [41]

Wavelet based in depth analysis of the status and estimation of a system's remaining useful life was performed by Farrar et al. (2004). Patsias and Staszewski (2002) presented the possibility of damage detection using WT from optically observed mode shapes. Kumara et al. (1999) and Sohn et al. (2003) showed delamination detection of composite structures using CWT. Damage detection is performed by analyzing the structural response collected from piezoelectric sensors and observing the dissimilarity in modal parameters of the system.

3. Signal Processing

This chapter presents some fundamental concepts and definitions used in signal processing, so that they can be utilized for the wavelet analysis theory and its application on the estimation of modal parameters (natural frequencies, damping ratios and mode shapes) that will be described in the following chapters.

3.1 Signal definition

A signal can be defined as a physical quantity that varies with time, space, or any other independent variable (or variables) [19]. In signal processing, a signal is a function that conveys information about a phenomenon and can be represented in the time domain, the frequency domain, and the time–frequency domain.

Typical examples of signals are: human speech, whale song, music, photographs and videos, electrocardiograms, encephalograms, etc. Noise is also a signal, but the information conveyed by it, is unwanted in general, hence it is considered as undesirable. In structural dynamics, the most commonly used signals are those that provide information about the acceleration, velocity, and displacement response of structures during an earthquake or any other kind of vibration. One example of such a signal is an accelerogram.

A system may be defined as a physical device that performs an operation such as analysis, modification, filtering, synthesis, etc. on a signal. “Passing” a signal through a system is called Signal Processing.

3.2 Traditional Signal Representation

3.2.1 Time domain representation

A typical representation of a signal u is as a function of time, called temporal or time–domain representation $u(t)$ (*Figure 3.2(a)*). The time domain representation, $u(t)$, provides information about the actual presence of the signal, its start and end time point, it’s duration in time, its strength and temporal evolution, and it indicates how the signal’s energy (*equations 3.21* and *3.22*) is distributed along the t axis. The observation and recording of physical phenomena from instruments is usually performed in relation to time, and therefore the signals obtained are in the time domain, for example an accelerogram or the displacement response of a structure during an earthquake.

3.2.2 Frequency domain representation

Another typical representation of a signal u is as a function of frequency, called the spectral or frequency domain representation $u(\omega)$ (*Figure 3.2(b)*). The frequency domain representation, $u(\omega)$, provides information about which frequencies are present in the signal, their relative magnitudes, minimum frequency, maximum frequency, and the bandwidth formed by their difference. A signal represented in time domain can be also

represented in the frequency domain by applying a pair of mathematical operators called a transform. An example is the Fourier Transform (FT) (*equation 4.9*) which decomposes a function into the sum of a (potentially infinite) number of sine wave frequency components. The inverse Fourier transform (*equation 4.10*) converts the frequency domain function back to a time function.

3.2.3 Time – frequency representation

Most signals from the nature are intrinsically non−stationary, in the sense that their frequencies vary along time. Using a time–frequency representation, the signal is represented on a time–frequency plane, providing both temporal information and spectral information simultaneously. This illustration on the time–frequency plane allows the determination of the variation of the instantaneous amplitude and phase of each component within a signal in time.

Depending on the application, a time–frequency representation is more advantageous: the time–domain representation does not provide information about the frequency content of a signal and the frequency domain representation does not not locate in time the frequency content of the signal, whereas the time–frequency representation illustrates information on both variables (*Figures 3.1* and *3.2*).

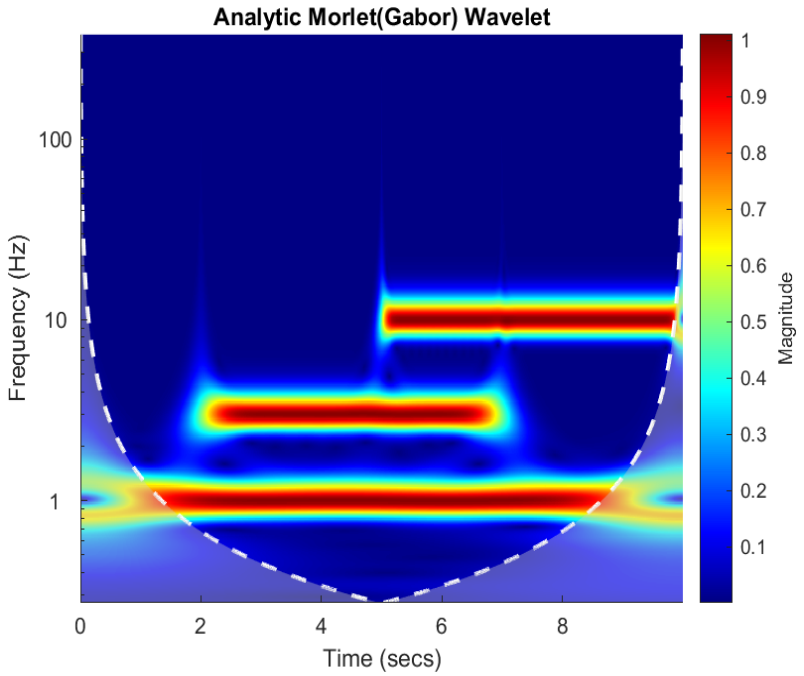

Figure 3.1: Time–frequency domain representation of a non stationary signal. It can be observed that it illustrates information on both. time t and frequency f. [25]

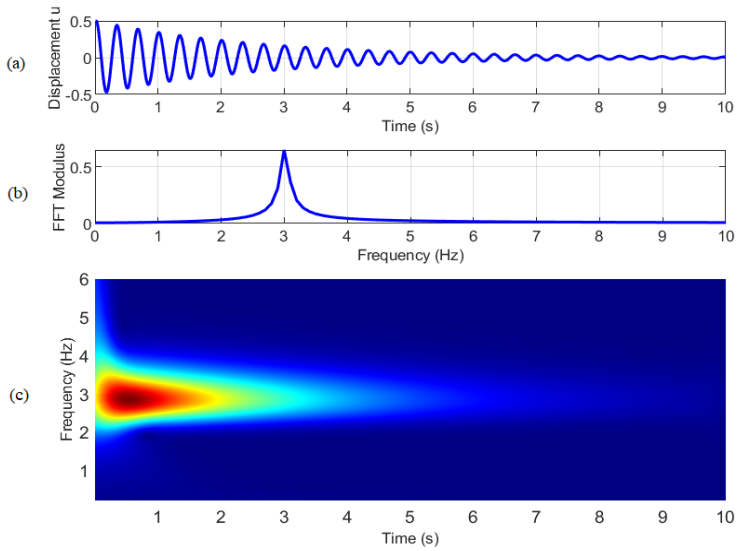

Figure 3.2: Three representations of free decay response u of a SDOF system: (a) time domain, (b) frequency domain, and (c) joint time–frequency domain. [25]

3.3 Complex Numbers

This section provides a brief reference to basic definitions and properties of complex numbers. In mathematics, a complex number is an element of a number system that extends the real numbers with a specific element denoted i, called the imaginary unit and satisfies the equation $i^2 = -1$. Every complex number can be expressed in the form $z = x + yi$, where $\mathrm{Re}(z) = x$ and $\mathrm{Im}(z) = y$ are real numbers [26]. Fundamental concepts of oscillatory motion involve the use of complex numbers. Additionally, the mother wavelets used are complex, which results in the CWT also being complex.

- *Modulus and argument*

i. The modulus of a complex number $z = x + yi$, is defined as:

$$r = \|z\| = \sqrt{x^2 + y^2} \tag{3.1}$$

ii. The argument of a complex number $z = x + yi$, denoted $\varphi = arg(z)$, is defined as:

$$\varphi = \arctan\left(\frac{y}{x}\right), \text{ or } \varphi = \mathrm{atan}[\mathrm{Re}(z), \mathrm{Im}(z)] \tag{3.2}$$

- *Euler's formula*

Euler's formula, establishes the fundamental relationship between the trigonometric functions and the complex exponential function and is expressed as:

$$e^{i\varphi} = \cos\varphi + i\sin\varphi \tag{3.3}$$

Using Euler's formula, trigonometric functions can be expressed as:

$$\cos\varphi = \frac{e^{i\varphi} + e^{-i\varphi}}{2} \tag{3.4}$$

and

$$\sin\varphi = \frac{e^{i\varphi} - e^{-i\varphi}}{2i} \tag{3.5}$$

- *Polar form*

The polar form of a complex number with modulus r and argument φ denoted as: $z = r\angle\varphi$, is defined:

$$z = |z|e^{i\varphi} = |z|(\cos\varphi + i\sin\varphi) \tag{3.6}$$

- *Complex conjugate*

The complex conjugate of a complex number $z = x + yi$ is defined as:

$$\bar{z} = x - yi \text{ , or } \bar{z} = |z|e^{-i\varphi} \tag{3.7}$$

3.4 Simple Harmonic Motion

Simple harmonic motion (a special class of oscillatory motion) can serve as a mathematical model for a variety of phenomena as it provides a basis for the characterization of more complicated periodic motion. Thus, this section provides some basic definitions and concepts which will be used in the following chapters.

3.4.1 Trigonometric Notation for Simple Harmonic Motion

Let the motion of a given point be described by the equation:

$$u(t) = A\sin(\omega t + \varphi) \text{ or } u(t) = A\cos(\omega t + \varphi) \tag{3.8}$$

where
$u(t)$ is the displacement from the equilibrium position in *m*, *cm*, etc.,
A the displacement magnitude of the oscillation in *m*, *cm*, etc.,
ω the angular frequency in *rad*/*s*,
φ the phase angle in *rad*,
and t the time.
The quantity A is the single–peak amplitude; $u(t)$ moves between the limits $\pm A$, so the peak to peak amplitude (also known as double amplitude) is $2A$. The time history of this simple harmonic displacement is shown in *Figure 3.3*.

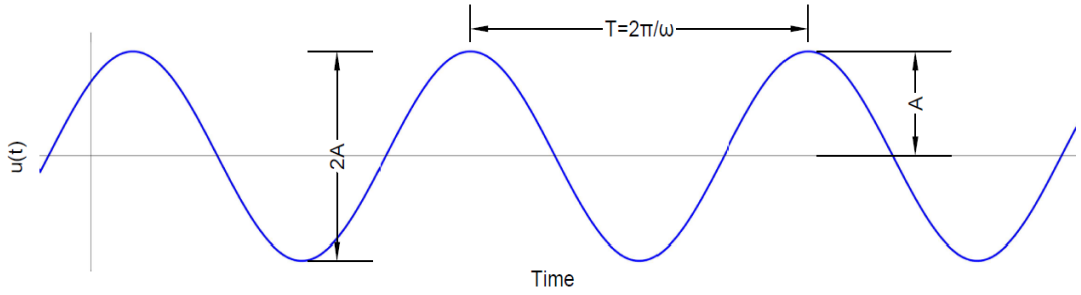

Figure 3.3: Time history of simple harmonic displacement.[25]

The angular frequency ω is is the rate of change of the phase angle φ with time t:

$$\omega = \frac{d\varphi}{dt} \tag{3.9}$$

The angular frequency ω is also related with the frequency $f = 1/T$ (units in hertz) and the period $T = 1/f$ (units in seconds) through the following relations:

$$\omega = 2\pi f \tag{3.10}$$

and

$$\omega = \frac{2\pi}{T} \tag{3.11}$$

Simple harmonic motion can also be described as the sum of a sine function and a cosine function, that is:

$$u(t) = a\cos(\omega t) + b\sin(\omega t) \tag{3.12}$$

As seen in *Figure 3.4* the sum of the sine and cosine functions is also a sinusoidal that oscillates at angular frequency, ω. The motion described by *equation 3.13* can be expressed in the form of *equation 3.9*, with amplitude $A = \sqrt{a^2 + b^2}$ and phase angle $\varphi = \arctan(a/b)$.

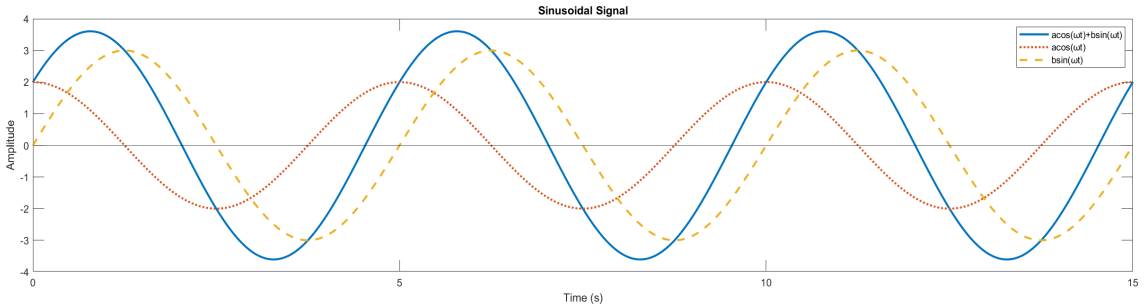

Figure 3.4: Summation of sine and cosine functions of the same frequency produces a sinusoid of the same frequency. Amplitude and phase of the sinusoid depends on the amplitudes of the sine and cosine functions. [25]

3.4.2 Complex Notation for Simple Harmonic Motion

Trigonometric descriptions of simple harmonic motion use familiar functions that are easy to visualize. However, for many dynamic analyses, the use of trigonometric notation complicates considerably many operations, particularly the solution of differential equations. These analyses become much simpler when motions are described using complex notation, which can be derived directly from trigonometric notation using Euler's formula (*equation 3.4*)., by substituting *equations 3.5* and *3.6* in *equation 3.13*:

$$u(t) = \frac{a - ib}{2} e^{i\omega t} + \frac{a + ib}{2} e^{-i\omega t} \tag{3.13}$$

3.4.3 Displacement, Velocity, Acceleration

Differentiating with respect to time the expression for simple harmonic displacement produces expression for velocity and differentiating again produces the expression for acceleration, i.e for $\varphi = 0$:
In trigonometric notation:

$$u(t) = A\sin(\omega t) \tag{3.14}$$

$$\dot{u}(t) = \omega A\cos(\omega t) = \omega A\sin\left(\omega t + \frac{\pi}{2}\right) \tag{3.15}$$

$$\ddot{u}(t) = -\omega^2 A\sin(\omega t) = \omega^2 A\sin(\omega t + \pi) \tag{3.16}$$

In complex notation:

$$u(t) = Ae^{i\omega t} \tag{3.17}$$

$$\dot{u}(t) = i\omega Ae^{i\omega t} \tag{3.18}$$

$$\ddot{u}(t) = -\omega^2 A e^{i\omega t} \tag{3.19}$$

3.5 Classification of signals

The methods employed in processing a signal depend heavily on the characteristics of that particular signal, for example, there are techniques that apply only to specific families of signals. Consequently, any investigation in signal processing requires knowledge of the classification of the signals that are involved in each application.
Signals can be classified according to many criteria into the following categories:

- *Continuous–time and Discrete–time signals.*

This classification's criteria is based on the characteristics of the time (independent) variable and the values they take. Let $u(t)$ be a function (signal) of the independent variable t, defined in the time domain:

If the independent variable t is continuous, $t \in \mathbb{R}$, i.e. between any two points in time there is an infinite number of other points in time, then the corresponding signal is a *continuous–time signal*, often called an analog signal. Any signal value can be found at any arbitrary point in time. Mathematically, these signals can be described by functions of a continuous variable and they are related to operations with integrals. A simple example of a continuous–time signal is a sinusoidal function $u(t) = \sin(\omega t)$, where $t \in \mathbb{R}$ (*Figure 3.5*).

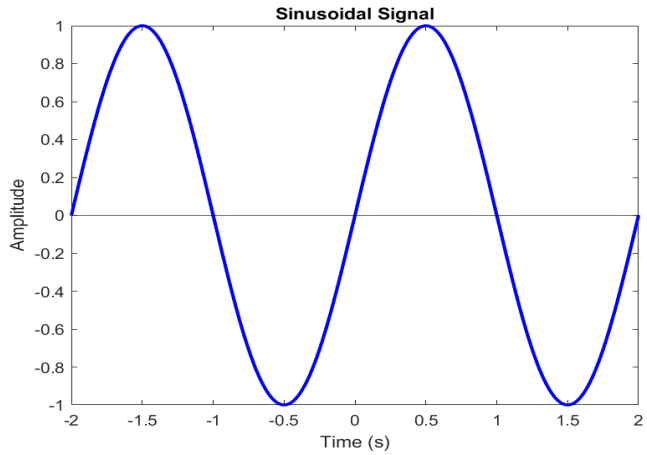

Figure 3.5: Example of a continuous−time signal: Sinusoidal signal $u(t) = \sin(\omega t)$, $t \in \mathbb{R}$, *with angular frequency* $\omega = \pi$ *rad/sec. [25]*

If the independent variable t takes on only discrete integer values, $t \in \mathbb{Z}$, for example $t = \pm 1$, ± 2, ± 3,..., then the corresponding signal is a discrete–time signal. A discrete time signal is not defined at instants between two successive points in time, therefore mathematically it can be represented by a sequence of real or complex numbers. To emphasize the discrete–time nature of these signals, they can be denoted as $u(n)$ instead of $u(t)$. A simple example of a discrete–time signal is a sinusoidal sequence $u(n) = \sin(\omega n)$, where $n \in \mathbb{Z}$ (*Figure 3.6*).

Generally, discrete–time signals may arise in two ways:

(1) By selecting values of a continuous–time signal at discrete−time instants. This process is called sampling and the values selected samples. As an example, *Figure 3.6* can be acquired by sampling the continuous−time signal of *Figure 3.5*. This is a fundamental process, as most signals of practical interest in nature (e.g. seismic signals, speech) are analog; consequently, they must be converted into a discrete–time form to be able to be processed by digital means (e.g. computers). More will be discussed in detail in section 3.7.

(2) By accumulating a variable's values over a period of time. For example, the daily rainfall data of a specific area or the hourly number of cars passing through a certain street result in discrete–time signals.

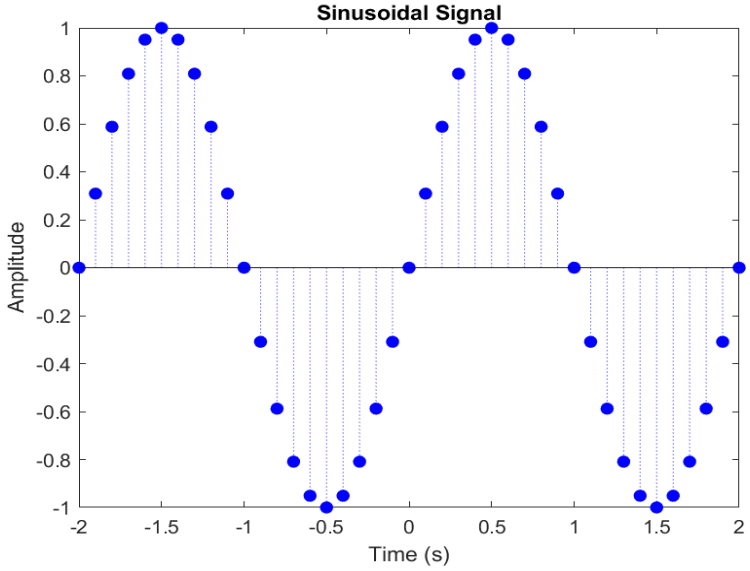

Figure 3.6: Example of a discete−time signal: Sinusoidal signal $u(n) = \sin(\omega n)$, $n \in \mathbb{Z}$, *with angular frequency* $\omega = \pi$ *rad/sec. [25]*

➢ *Deterministic and Random Signals*

Mathematical analysis and processing of signals demands the availability of a mathematical expression of the signal itself. This requirement leads to another important classification of signals, in relation to the existence or not of this formula: Deterministic signals are those whose values are predictable at any time and can be described exactly by a mathematical formula, a table of data, or a well–defined rule. It is worth mentioning that true deterministic signals are very rare in nature because unknown and uncontrollable factors (e.g. noise) usually influence the signal as well.

Random signals are signals that take on random values at any given time instant, therefore they are modeled stochastically, in probabilistic terms. Seismic signals and speech signals are examples of random signals.

➢ *Stationary and Non–stationary signals*

This classification results from the observation of the signal's frequency content over time:

Stationary signals are those whose frequency content remains unchanged in time. All frequency components exist at all times.

Non–stationary signals are those whose frequency content varies in time. These kinds of signals are the ones that are found in nature.

- *Periodic and aperiodic signals*

Periodic signals. These signals have waveforms whose pattern repeats at equal increments of time; this is expressed mathematically as: $u(t+T) = u(t)$, where T is the period of continuous–time signals, or $u(n+\mathrm{N}) = u(n)$, where N is the period for discrete–time signals.

Non−periodic or aperiodic signals, which are signals that are not periodic.

- *Energy signals and Power signals.*

This classification is based on the signal total energy E and signal average power P, definitions which are used to characterize a signal.

The total energy E of a signal is defined as:

For continuous–time signals $u(t)$:

$$E = \int_{-\infty}^{+\infty} |u(t)|^2 \, dt \tag{3.20}$$

For discrete–time signals $u(n)$:

$$E = \sum_{n=-\infty}^{+\infty} |u(n)|^2 \tag{3.21}$$

The average power P of a signal is defined as:

For continuous–time signals $u(t)$:

$$P = \lim_{T\to\infty} \frac{1}{2T} \int_{-T}^{+T} |u(t)|^2 \, dt \tag{3.22}$$

For discrete–time signals $u(n)$:

$$P = \lim_{\mathrm{N}\to\infty} \frac{1}{2\mathrm{N}+1} \sum_{n=-\mathrm{N}}^{+\mathrm{N}} |u(n)|^2 \tag{3.23}$$

Hence, the classification goes as follows:

Energy signals are those whose total energy is equal to a finite positive value, i.e. $0 < E < +\infty$, and their average power is zero ($P = 0$). Aperiodic signals are an example of energy signals.

Power signals are those whose average power P is finite, i.e. $0 < P < +\infty$, and their energy is infinite ($E = +\infty$). Periodic signals are examples of power signals.

- *Monocomponent and multicomponent signals*

A *monocomponent* signal is described in the time–frequency plane by a single "ridge" corresponding to an elongated region of energy concentration [1]. For example, the displacement response $u(t)$ of a SDOF system is a monocomponent signal (*Figure 3.7*).

A *multicomponent* signal may be described as the sum of two or more monocomponent signals. For example, the displacement response $u(t)$ of a MDOF system's d.o.f. is a multicomponent signal (*Figure 3.8*).

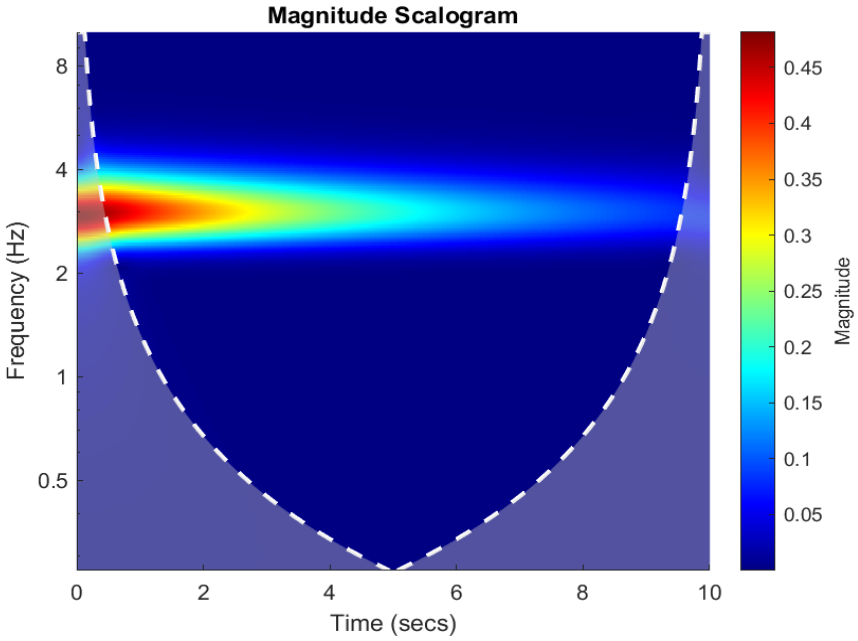

Figure 3.7: Example of time–frequency analysis of a monocomponent signal: Magnitude (Modulus) Scalogram of the CWT. [25]

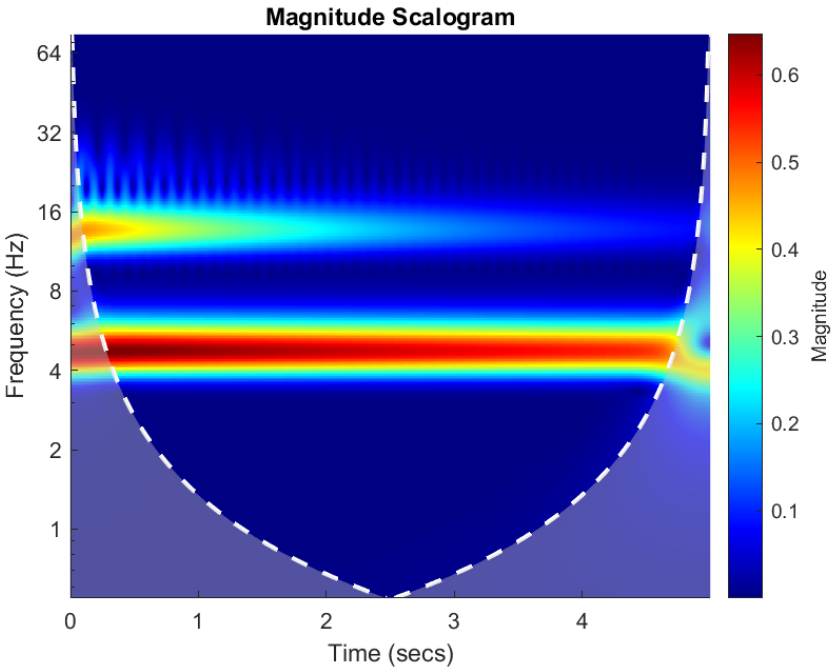

Figure 3.8: Example of time–frequency analysis of a multicomponent signal: Magnitude (Modulus) Scalogram of the CWT. [25]

➢ *Noise*

The term noise originates from radio engineering, where it describes the unwanted signal that it is heard when the radio is not tuned exactly to a radio station. In signal processing, noise is a general term for unwanted (and, in general, unknown) modifications that interfere and degrade the desirable information of a signal. This can happen during capture, storage, transmission, processing, or conversion of a signal [22]. Signals within which the presence of noise is insignificant, can be characterized as pure, while signals with significant noise present within them can be characterized as noisy. In real–life applications, signals are not "clean" in general and most often are embedded in noise. Noise can be eliminated by filtering of the signal. A filter is a system that removes unwanted components or features from a signal.

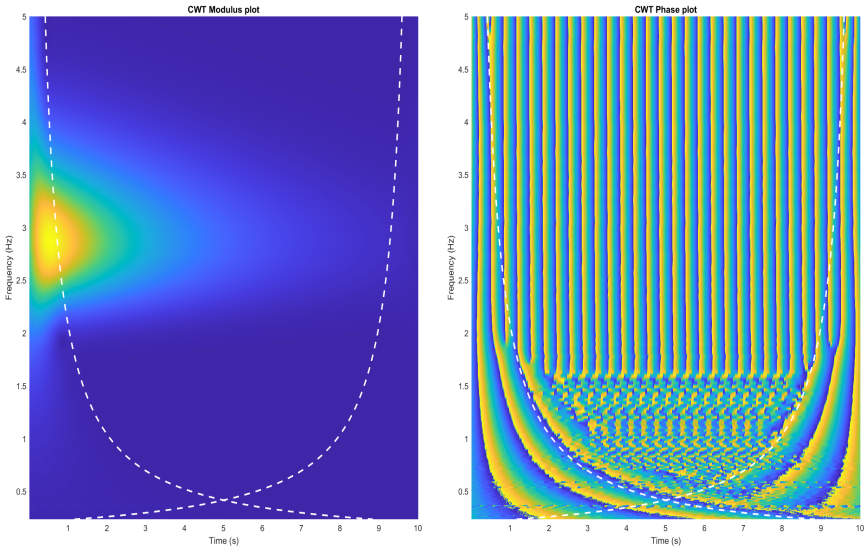

Figure 3.9:Time–frequency analysis of a monocomponent signal: Magnitude (Modulus) (left) and Phase Plot (right) of the CWT. [25]

3.6 The Time–Frequency Approach

The basic product of a time–frequency analysis is a set of data represented in the 2D time–frequency plane as in *Figures 3.7, 3.8* and *3.9*.

- *Instantaneous amplitude, phase and frequency*

As it was mentioned previously, time–frequency methods have the ability to analyze non−stationary signals efficiently. The frequency of a sinusoidal signal is a well defined quantity, as it was seen in section 3.4. However, often in practice, signals are not truly sinusoidal, or even aggregates of sinusoidal components. Non–stationary signals do not lend themselves well to decomposition into sinusoidal. For such signals, the notion of frequency loses its effectiveness, and one needs to use a parameter which accounts for the time–varying nature of the process [1]. Following the thought process of the simple harmonic motion in *equation 3.9* and *3.13*, such signals can be expressed as:

For monocomponent, frequency modulated (FM) signal:

$$u(t) = A(t)\cos\varphi(t) \tag{3.24}$$

For a multicomponent, frequency modulated (FM) signal:

$$u(t) = \sum_{j=1}^{N} A(t)\cos\varphi(t) \tag{3.25}$$

where $A(t)$ is the instantaneous amplitude and $\varphi(t)$ is the instantaneous phase of the signal.

Consequently, the instantaneous frequency (IF) is the temporal rate of the instantaneous phase and *equation 3.10* becomes:

$$\omega(t) = \frac{\varphi(t)}{dt} \tag{3.26}$$

- *Ridges*

The IF of a signal at time t_0 indicates the dominant frequency of the signal at that specific time, therefore it describes the frequency modulation law of the signal. For a monocomponent FM signal, the peak of the cross–sections parallel to the frequency axis of the time–frequency plane gives the IF law which describes the signal FM law, while for a multicomponent FM signal, the dominant peaks of the cross−sections parallel to the frequency axis of the time–frequency plane reflect the components' respective FM laws. Those peaks in the cross–sections parallel to the frequency axis correspond to elongated regions of energy concentration in the time–frequency plot, called ridges. [25]

- *Positive and negative frequencies*

Mathematically, the frequency f ranges from $-\infty$ to $+\infty$, yet in practice only the positive frequencies are used, as it can be seen from the plots shown in the previous figures. The intuitive explanation is that f represents the number of oscillations per second, therefore is expected to be positive. Mathematically, this is based on a property of the FT: if $u(t)$ is real, its FT $\hat{u}(\omega)$ has Hermitian symmetry (section 4.2.2), thus, the information contained in the negative frequencies is a duplication of the information contained in the positive frequencies. Therefore, in practice, negative frequencies are considered redundant and the analysis is done with positive frequencies. This is achieved by introducing a particular complex signal $Z(t)$ called the "analytic signal," which contains only positive frequencies.

3.7 Sampling and Aliasing – Nyquist's Theorem

As referred in the previous section, most signals of practical interest in nature are continuous–time signals, and therefore they must be converted into a discrete−time form to be able to be processed by digital means. This conversion of a continuous time signal to a discrete−time signal is done through a procedure called sampling.

The sampling type that is used most often in practice is the periodic (or uniform) sampling, where the discrete−time signal is obtained by "taking samples" of the continuous−time signal every T_s seconds. The time interval T_s between successive samples is called the sampling period. Its reciprocal $F_s = 1/T_s$ is called the sampling rate (how many samples per second are recorded) or the sampling frequency.

The sampling rate has a significant effect on the reconstruction of the continuous real signal in the time domain. Insufficient sampling frequency results to a phenomenon called aliasing. Aliasing is an effect that causes different signals to become indistinguishable (or aliases of one another) when sampled. It also often refers to the distortion or artifact that results when a signal reconstructed from samples is different from the original continuous−time signal. Generally, a high F_s is desired, because as F_s increases,

the effectiveness of sampling increases too, but after a certain value, no further improvement is achieved, and instead the computational time is increased.

- *Nyquist–Shannon sampling theorem*

To avoid the ambiguities resulting from aliasing, the sampling rate must be selected to be sufficiently high; this is solved by following the Nyquist–Shannon sampling theorem. Sampling frequency F_s must be at least two times greater than the signal's highest frequency F_{max}:

$$F_s \geq 2F_{max} \tag{3.27}$$

The theorem establishes a sufficient condition for a sample rate that permits a discrete sequence of samples to capture all the information from a continuous–time signal of finite bandwidth. Usually the general frequency content of the signal is known, thus the signal's highest frequency can be estimated.

- *Nyquist frequency*

The previous theorem leads to the definition of the Nyquist frequency as the maximum frequency in the frequency domain of the analysis:

$$F_{Nyquist} = \frac{F_s}{2} \tag{3.28}$$

4. Continuous Wavelet Transform (CWT)

The Wavelet Transform (WT) is one of the most important techniques in signal processing to build a framework in the identification of modal properties. It appeared in mathematics more than a century ago, starting with Haar who discovered in 1909 an orthonormal basis consisting of step functions. The Haar basis construction is a precursor of what is known today as the multi–resolution analysis [27] which refers to the expansion of a signal into components that can reproduce the original signal when added together. The principle of multi–resolution spaces is to decompose a signal of finite energy $L^2(\mathbb{R})$ to two complementary spaces: (i) a space of approximation; and (ii) a detail space that contains the approximation error. Multi–resolution analysis can be seen as a way to zoom into, or out of, the signal without losing information. From the beginning of 1980s, under the impetus of several French researchers, especially Grossmann and Morlet [28], wavelet research in mathematics has grown steadily with significant contributions from many authors.

As a time–frequency analysis tool, wavelet transform has the advantages of dealing with non–stationary, transient, and non–linear signals. The other very popular signal processing tool, Fourier analysis does not pave the path to study the nature of the time series in the time–frequency domain. Under the analysis of Fourier Transform, the time information along the time series is lost. Hence, it is difficult to distinguish transient relations and identify when the structural changes have exactly occurred. Further, these techniques are only appropriate for the time series with stable statistical properties. i.e. stationary time series (Conraria and Soares 2011).

Wavelet analysis allows studying the spectral characteristics of a time series as a function of time. It clearly illuminates the changes of different periodic components along the time series. One major advantage of wavelet transform is the ability to carry out natural local analysis of time series while the wavelet stretches into a long function to measure the low frequency movements, and it compresses into a short function in order to measure the high frequency movements. The Continuous Wavelet Transform is widely used as an analysis tool which provides highly redundant information in time–frequency domain. This has the ability to recover the original time series from its transform (Conraria and Soares 2011).

This chapter presents an overview of the background of the continuous wavelet transform. It provides the basic definitions and properties needed to understand the wavelet theory and its application to modal parameter identification.

4.1 Function Space

This section provides a brief description of the function spaces used in wavelet theory [5].

4.1.1 Normed Spaces

The concept of norm in a vector space is an abstract generalization of the length of a vector in the $\mathbb{R}^3$ set and is defined axiomatically; i.e. any real–valued function that satisfies some particular conditions can be defined as a norm.

A real–valued function $\|x\|$ defined on a vector space X, where $x \in X$, is called a norm on X if the following conditions are satisfied:

i. $\|x\| = 0$ if and only if $x = 0$,
ii. $\|ax\| = a\ \|x\|$ for every $a \in \mathbb{R}$ and $x \in X$,
iii. $\|x + y\| \leq \|x\| + \|y\|$ for all $x,y \in X$ (also known as the *triangle inequality*).

Combining i, ii, and iii, follows that: $0 = \|0\| = \|x - x\| \leq \|x\| + \|-x\| = 2\|x\|$, therefore $\|x\| \geq 0$ for every $x \in X$.

A normed space is a pair $(X, \|\cdot\|)$ where X is a vector space and $\|\cdot\|$ is a norm defined on X.
Note: It is possible to define different norms on the same vector space.

i. $\mathbb{R}$ is a real normed space with the norm defined by the absolute values: $\|x\| = |x|$.

ii. $\mathbb{C}$ is a complex normed space with the norm defined by the modulus: $\|z\| = |z|$.

The sequence space ℓ^p $(1 \leq p \leq +\infty)$ is the set of all sequences $\left[x_n\right]_{n=1}^{+\infty}$ of real (or complex) numbers such that $\left(\sum_{n=1}^{+\infty} |x_n|^p\right) < \infty$ is a normed space with a norm defined as:

$$\|x\|_p = \left[\sum_{n=1}^{+\infty} |x_n|^p\right]^{1/p} \tag{4.1}$$

For example, $\mathbb{R}^N = (x_1, x_2, \ldots, x_N)$: $x_1, x_2, \ldots, x_N \in \mathbb{R}$ is a vector space with norm defined by setting $p = 2$ at *equation 4.1*:

$$\|x\|_2 = \sqrt{(x_1^2 + x_2^2 + \ldots + x_N^2)} \tag{4.2}$$

where $x = (x_1, x_2, \ldots, x_N) \in \mathbb{R}$. This norm is called the *Euclidean Norm*.

L^p Spaces If $p \geq 1$ is any real number, the vector space of all complex−valued Lebesgue integrable functions f defined on $\mathbb{R}$ is denoted by $L^p(\mathbb{R})$ with a norm:

$$\|f\|_p = \left[\int_{-\infty}^{+\infty} |f(x)|^p \, dx\right]^{1/p} \tag{4.3}$$

where $\|f\|_p$ is the L^p−norm.

Remarks:

1. The range of p is $1 \leq p \leq +\infty$, as for values $0 < p < 1$ the function $\|\cdot\|_p$ does not satisfy the triangle inequality.

2. *Equation 4.1* is the discrete version of *equation 4.3*.

3. The case $p = 2$ warrants special attention: it is a Hilbert space, more will be discussed in subsection 4.3.

4. Elements of $L^2(\mathbb{R})$ are called square integrable functions.

5. The term "signal of finite energy" in the following, refers to a generic element of $L^2(\mathbb{R})$.

6. The equation of the total energy of a function (*equations 3.21* and *3.22*) can be defined as the square of the L^2 norm of the function.

4.1.3 The Complex Hardy Space

The Complex Hardy space $H^2(\mathbb{R})$ −sometimes called the space of analytic signals−, is made of signals which do not have negative frequency components, and is defined as:

$$\|H\|^2(\mathbb{R}) = [f \in L^2(\mathbb{R}); \widehat{f}(\omega) = 0 \text{ for } \omega \leq 0] \tag{4.4}$$

4.1.4 Convolution

Let f and g be functions in $L^1(\mathbb{R})$. Then the (continuous time) *convolution* of f and g is also an $L^1(\mathbb{R})$ function $h \in L^1(\mathbb{R})$ defined by:

$$h(x) = (f * g)(x) = \int_{-\infty}^{+\infty} f(x-y)\, g(y)\, dy \tag{4.5}$$

whenever the integral is well−defined. The convolution's properties are that it is commutative, associative and distributive.

If f and $g \in L^1(\mathbb{R})$, then the function $f(x-y)\, g(y) dy$ is integrable for almost all $x \in \mathbb{R}$. Furthermore, the convolution h is an integrable function and the following equality holds:

$$\| h \|_1 = \| f * g \|_1 \leq \| f \|_1 \| g \|_1 \tag{4.6}$$

4.1.5 Inner Product

Let f and $g \in L^2(\mathbb{R})$. The *inner product* and *norm* for the space $L^2(\mathbb{R})$ is given by:

$$\langle f, g \rangle = \int_{-\infty}^{+\infty} f(x)\, \overline{g(x)}\, dx \tag{4.7}$$

$$\| f \|_2 = \langle f , f \rangle^{1/2} \tag{4.8}$$

4.2 From Fourier analysis to Wavelet analysis

4.2.1 The Fourier Transform

As mentioned in the previous chapter, the Fourier Transform (FT) converts a signal from the time domain to the frequency domain by decomposing it into the sum of a (potentially infinite) number of sine wave frequency components.

For finite energy signals $u(t) \in L^1(\mathbb{R}) \cap L^2(\mathbb{R})$ the FT is defined as:

$$\hat{u}(\omega) = \mathscr{F}[u] = \int_{-\infty}^{+\infty} u(t) e^{-i\omega t} dt \tag{4.9}$$

And the inverse FT as:

$$u(t) = \mathscr{F}^{-1}[u] = \frac{1}{2\pi} \int_{-\infty}^{+\infty} \hat{u}(\omega) e^{i\omega t} d\omega \tag{4.10}$$

The function $\hat{u}(\omega)$ is complex, and can be expressed in polar form as $\hat{u}(\omega) = Ae^{i\varphi}$ to express the amplitude spectrum $A(\omega)$ (frequency−amplitude plot), and phase spectrum $\varphi(\omega)$ (frequency−phase angle plot).

It is important to mention that the Parseval identity allows the extension of the definition of FT from $L^1(\mathbb{R})$ to $L^2(\mathbb{R})$ to include finite energy signals. Let $f \in L^1(\mathbb{R}) \cap L^2(\mathbb{R})$. Then the FT $\widehat{f}$ of f is in $L^2(\mathbb{R})$, and satisfies the following Parseval's Identity:

$$\| f \|_2^2 = \frac{1}{2\pi} \| \widehat{f} \|_2^2 \tag{4.11}$$

which by substituting *equation 4.3* of norm, Parseval's Identity becomes:

$$\int_{-\infty}^{+\infty} |f(t)|^2 dt = \frac{1}{2\pi} \int_{-\infty}^{+\infty} |\widehat{f}(\omega)|^2 d\omega \tag{4.12}$$

It can be observed that the left hand side part of the equation is the energy of a signal (*equation 3.21*). Consequently, Parseval's Identity states a conservation of energy between the time and the frequency domains.

Then, for all f and $g \in L^1(\mathbb{R}) \cap L^2(\mathbb{R})$ (signals of finite energy), the following identity is easily obtained from Parseval's identity using the inner product definition (*equation 4.7*):

$$\int_{-\infty}^{+\infty} f(t)\overline{g(t)}dt = \frac{1}{2\pi}\int_{-\infty}^{+\infty} \hat{f}(\omega)\overline{\hat{g}(\omega)}d\omega \quad \text{or} \quad \langle f, g\rangle = \langle \hat{f}, \hat{g}\rangle \tag{4.13}$$

which emphasizes the fact that the Fourier transform preserves the Hilbert spaces inner products.

4.2.2 Properties of the Fourier Transform

Some basic properties of the FT are (mentioned because they will be extended to wavelet analysis):

- *Linearity*

$$\mathscr{F}\left[\sum_{j=1}^{N} u_j\right] = \sum_{j=1}^{N} \mathscr{F}[u_j] \tag{4.14}$$

- *Time scaling*

$$\mathscr{F}[u(at)](\omega) = \frac{1}{|a|}\hat{u}\left(\frac{\omega}{a}\right), \ a \neq 0 \tag{4.15}$$

- *Translation / time shifting*

For any real number $t_0 \in \mathbb{R}$:

$$\mathscr{F}[u(t-t_0)](\omega) = e^{-i\omega t_0}\hat{u}(\omega) \tag{4.16}$$

- *Modulation / frequency shifting*

For any real number $\omega_0 \in \mathbb{R}$:

$$\mathscr{F}[e^{-i\omega t_0}u(t)](\omega) = \hat{u}(\omega-\omega_0) \tag{4.17}$$

- *Hermitian symmetry*

For a real function $u(t) \in \mathbb{R}$:

$$\hat{u}(-\omega) = \overline{\hat{u}(\omega)} \tag{4.18}$$

- *Convolution*

$$(u_1 * u_2)(t) = \mathscr{F}^{-1}[\hat{u}_1(\omega)\hat{u}_2(\omega)] \tag{4.19}$$

4.2.3 The Fast Fourier Transform

FT is implemented in digital means by the discrete form of *equation 4.9*, the Discrete Fourier Transform (DFT). The DFT of a discrete−time signal $u(n)$ is:

$$\hat{u}(k) = \frac{1}{\mathrm{N}} \sum_{n=0}^{\mathrm{N}} u(n) e^{-i\left(\frac{2\pi kn}{\mathrm{N}}\right)} \tag{4.20}$$

where $k = 0, 1, \ldots, \mathrm{N} - 1$ is the frequency index.

However, the calculation of the DFT with *equation 4.20* requires performing approximately N^2 multiplications, which becomes impractical when large amounts of data (large values of N) are required for processing.

As it is implied by its name, the Fast Fourier Transform (FFT) is an algorithm that determines the DFT of a signal significantly faster than computing it directly, as it performs an N−term DFT in $2\mathrm{N}\log(\mathrm{N})$ calculations allowing the analysis of large data sets. FFT can be implemented in MATLAB using the *fft* command.

4.2.4 Spectral leakage

Signals that are used in practice are of finite length. Due to this finite duration, signals that are converted from the time domain to the frequency domain are subject to spectral leakage. When the DFT is applied to an aperiodic signal of finite length, it assumes that any existing frequency components are periodic and infinite, i.e the same finite signal is repeated infinite times. So, when a spectral component that is not a harmonic of the fundamental frequency for the observation window exists, the repetition of that finite component by the transform creates discontinuities at the boundaries of the iterations. Since that component is not a harmonic, and no longer a smooth wave due to the discontinuities, the energy of that component cannot be expressed on a single basis and instead is distributed among the other harmonic frequency bases. This “smearing” of energy manifests on the amplitude spectrum as low amplitude frequency components that are not actually present. Introducing a proper window function into the transform can reduce the degree of spectral leakage in the spectrum [8].

4.2.5 Window function

As it was mentioned, the problem of spectral leakage can be reduced with the use of a proper window function. Window functions operate by multiplying the time signal by a finite−length window with an amplitude that varies smoothly and gradually toward zero at the edges. In signal processing, a window function is a mathematical function that is zero−valued outside of some chosen interval, normally symmetric around the middle of the interval usually near a maximum in the middle, and usually tapering away from the middle.

A nontrivial function $\psi \in L^2(\mathbb{R})$ is called a window function if $x\psi(x)$ is also in $L^2(\mathbb{R})$. The center x_ψ and radius Δx_ψ of a window function w are defined respectively by:

$$x_\psi = \int_{-\infty}^{+\infty} x \frac{|\psi(x)|^2}{\|\psi\|_2^2} dx \tag{4.21}$$

and

$$\Delta x_\psi = \frac{1}{\|\psi\|_2} \sqrt{\int_{-\infty}^{+\infty} (x - x_\psi)^2 |\psi(x)|^2 dx} \tag{4.22}$$

Note that the radius Δx_ψ expression is equivalent to standard deviation in statistics. The width of the window function is defined as $2\Delta x_\psi$.

Most popular window functions are bell−shaped curves, for example the Hann window or a Gaussian window (*Figure 4.1*).

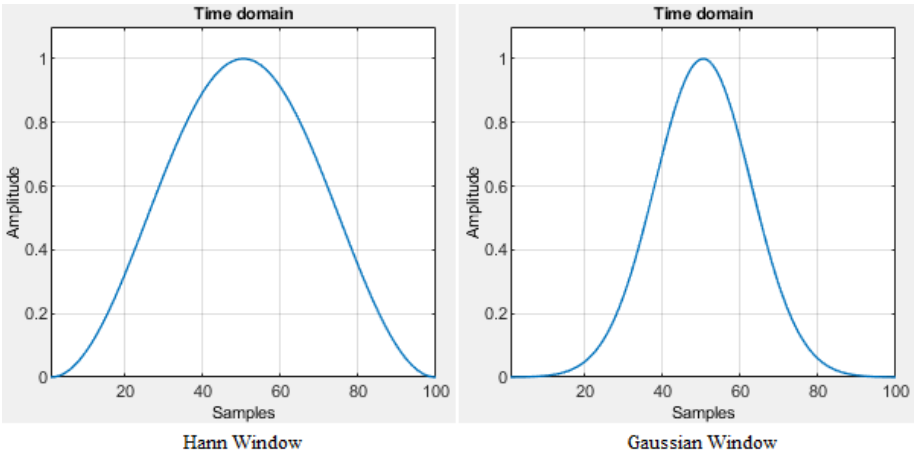

Figure 4.1: Example of two window functions in the time domain. [25]

4.2.6 Short Time Fourier Transform (or Windowed Fourier Transform)

As it presented in [25], the FT converts a signal from the time domain into the frequency domain and does not provide any information about the time localization of the frequency components. In Chapter 3, was mentioned that the need to overcome the inability of the frequency domain approach to capture time−varying features of a structure but retain the advantage of the frequency content information, plus the problem of spectral leakage, led to the development of the time–frequency domain methods.

Gabor in 1946 developed and introduced the Short Time Fourier Transform (STFT, otherwise known as the windowed Fourier transform, or Gabor transform). The STFT is nothing but a simple localization of the FT via the introduction of a sliding window function. The existence of this window makes this transform into a function of two parameters: a time parameter giving the location of the center of the window and a

frequency parameter for the computation of the Fourier transform of the windowed signal [2].

Introducing now the *time−frequency window* ψ, with time center and frequency center respectively defined as:

$$t_{\psi} = \int_{-\infty}^{+\infty} t \frac{|\psi(t)|^2}{\|\psi\|_2^2} dt \tag{4.23}$$

and

$$\omega_{\psi} = \int_{-\infty}^{+\infty} x \frac{|\hat{\psi}(\omega)|^2}{\|\hat{\psi}\|_2^2} d\omega \tag{4.24}$$

And with time radius and frequency radius respectively defined as:

$$\Delta t_{\psi} = \frac{1}{\|\psi\|_2} \sqrt{\int_{-\infty}^{+\infty} (t - t_{\psi})^2 |\psi(t)|^2 dt} \tag{4.25}$$

and

$$\Delta \omega_{\psi} = \frac{1}{\|\hat{\psi}\|_2} \sqrt{\int_{-\infty}^{+\infty} (\omega - \omega_{\psi})^2 |\hat{\psi}(\omega)|^2 d\omega} \tag{4.26}$$

The window function now is in the time−frequency plane and has dimensions $2\Delta t$ and $2\Delta\omega$.

The Heisenberg uncertainty principle states that:

$$\mu_{\psi} = \Delta t \, \Delta \omega \geq \frac{1}{2} \tag{4.27}$$

Consequently, an improvement of the time localization (i.e., a decrease of Δt) is accompanied by a deterioration in the frequency localization (i.e., an increase of $\Delta\omega$), thus it is not possible to achieve optimal localization simultaneously in the time and the frequency domains. Note that the inequality becomes an equality in the case of Gaussian (or modulated Gaussian) functions.

The STFT of a function $u(t)$, STFT_u consists of multiplying $u(t)$ by a (usually real) window function ψ shifted in time. If $\psi(t)$ is a prototype window, symmetric about $t = 0$, then STFT_u is calculated as:

$$STFT_u = \int_{-\infty}^{+\infty} u(t) \psi(t - b) e^{-i\omega t} dt \tag{4.28}$$

where the parameter b is used to translate the window in order to cover the whole time domain, for extracting local information of the Fourier transform of the signal.

Mother function Given a window function $g \in L^2(\mathbb{R})$ the corresponding family [$g_{b,\omega}$; $b \in \mathbb{R}$, $\omega \in \mathbb{R}$] of Gabor functions is obtained by shifting and modulating copies of g:

$$g_{b,\omega}(t) = g(t-b)e^{i\omega(t-b)} \tag{4.29}$$

Let $g \in L^2(\mathbb{R})$ a window function. The continuous Gabor Transform of a finite–energy signal $u(t) \in L^2(\mathbb{R})$ is defined by:

$$G_u(b,\omega) = \langle u, g_{b,\omega} \rangle = \int_{-\infty}^{+\infty} u(t)\overline{g}_{b,\omega}(t)dt \tag{4.30}$$

Consequently, the Gabor transform is essentially a STFT with a Gaussian window. As it can be observed by the previous definitions, changing the values of t simply corresponds to translating the window in time while its width is kept fixed. Similarly, as the modulation parameter ω varies, the transform translates in frequency, retaining a constant width. Thus, the resolution windows in the time–frequency plane have dimensions $2\Delta t$ and $2\Delta\omega$, which are fixed for all t and ω, thus, STFT and Gabor transform the fixed duration window function is accompanied by a fixed frequency resolution. Consequently, this transform allows only a fixed time–frequency resolution. This is shown in *Figure 4.2* in which the mother function is illustrated centered at (t_0, ω_0) and the sliding time window are centered at integral multiples of t_0 and the transforms are evaluated at frequencies centered at integral multiples of ω_0.

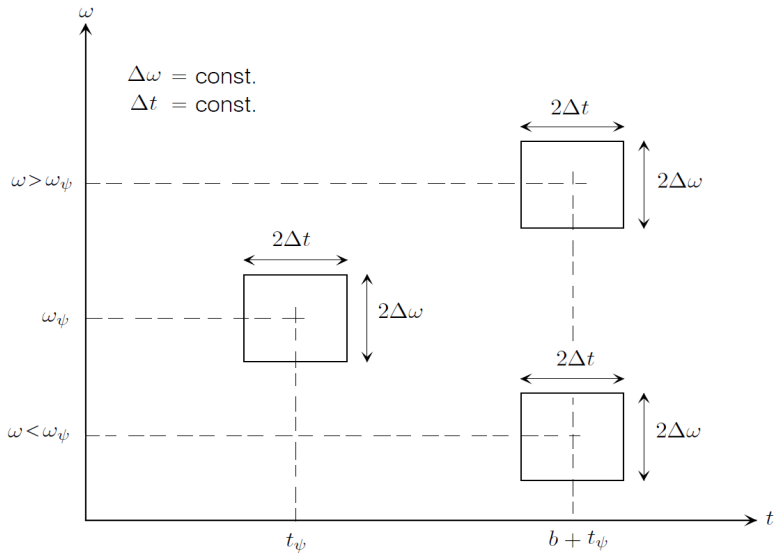

Figure 4.2: Fixed time–frequency resolution for the Gabor Transform.

However, the STFT represents an inaccurate and inefficient method of time–frequency localization, as it imposes a scale or "response interval" $2\Delta t$ into the analysis. The inaccuracy arises from the aliasing of high– and low–frequency components that do not fall within the frequency range of the window [21].

Since frequency is directly proportional to the number of cycles per unit time, it requires a narrow time–window to locate high frequency phenomena more precisely and a wide time–window to analyze low frequency behaviors more spectral information. In other words, it is important to have a flexible time–frequency window that automatically narrows at high *center–frequency* and widens at low *center–frequency*. Hence, the STFT is not suitable for analyzing signals with both very high and very low frequencies [3]. This constraint led to the development of the *Wavelet transform* where a dilation (or scale) parameter a is introduced to make the time–frequency window flexible.

Summarizing, the Gabor transform is based upon time and frequency translations, as opposed to time translations and scalings as in the case of the wavelet transform which is presented in the next section.

4.3 The Continuous Wavelet Transform

This section provides a presentation on the basic theory of the continuous wavelet transform. The main idea is that the wavelet transform is based on a set of basis functions (wavelet family) formed by dilation and translation of a prototype mother function (wavelet) $\psi(t)$ and is used to decompose a function (signal) $u(t)$ into the time–frequency domain.

Definitions in the literature vary slightly and depend on the choice of normalization of the wavelets. However, normalization is irrelevant to the basic theory [9], thus, in order to present the basic theory, the definition by Carmona et al. [2] is used for the wavelet definition; the differences and the influence of normalization are described in the "Normalization" section.

4.3.1 Definitions and basic properties

Mother wavelet Let $\psi \in L^1(\mathbb{R}) \cap L^2(\mathbb{R})$ be a window function. This function is called the mother (analyzing) wavelet, and the corresponding family of wavelets is the family $[\psi_{b,a};\ b \in \mathbb{R},\ a \in \mathbb{R}_+^*]$ of shifted and scaled (dilated) copies of ψ defined as:

$$\psi_{b,a}(t) = \frac{1}{a}\psi\left(\frac{t-b}{a}\right),\ t \in \mathbb{R} \tag{4.31}$$

where $a > 0$ is a scaling parameter that defines the dilation of the mother wavelet $\psi(t)$ and b is the translation parameter related to time. Scale factor $a > 1$ corresponds to dilation and $0 < a < 1$ corresponds to compression [25]. The mother wavelet is the member of the family where $b = 0$ and $a = 1$. Consequently, in terms of a window function, the $\psi_{b,a}(t)$ wavelet can be viewed as a copy of the original mother wavelet with center frequency rescaled by a, that is, ω_ψ/a and centered around the time $t_\psi + b$. Common mother wavelets are the Morlet wavelet, the Meyer wavelet, the Mexican Hat, the Paul wavelet, the Cauchy wavelet, the Daubechies wavelets, the Gaussian Derivative Family (DOG), the generalized Morse wavelets etc. (*Figure 4.3*).

For a window function $\psi(t)$ to be accepted as a mother wavelet, it must fulfill the admissibility condition:

Let $\psi \in L^1(\mathbb{R}) \cap L^2(\mathbb{R})$ be such that the number C_ψ defined by:

$$0 < C_\psi < \int_0^{+\infty} |\hat{\psi}(a\omega)|^2 \frac{da}{a} < +\infty \tag{4.32}$$

So, the constant C_ψ finite, non–zero and independent of $\omega \in \mathbb{R}$. The finiteness of this constant restricts the class of $L^2(\mathbb{R})$ functions that can be used as "mother wavelets" in the definition of the integral wavelet transform. In particular, if $\psi(t)$ must also be a window function, then is necessarily in $L^1(\mathbb{R})$ [3], meaning:

$$\int_{-\infty}^{+\infty} |\psi(t)|^2 \, dt < +\infty \tag{4.33}$$

and the integral of the mother wavelet $\psi(t)$ has to vanish, so that the graph in the time domain to be a small wave:

$$\int_{-\infty}^{+\infty} \psi(t) \, dt = 0 \tag{4.34}$$

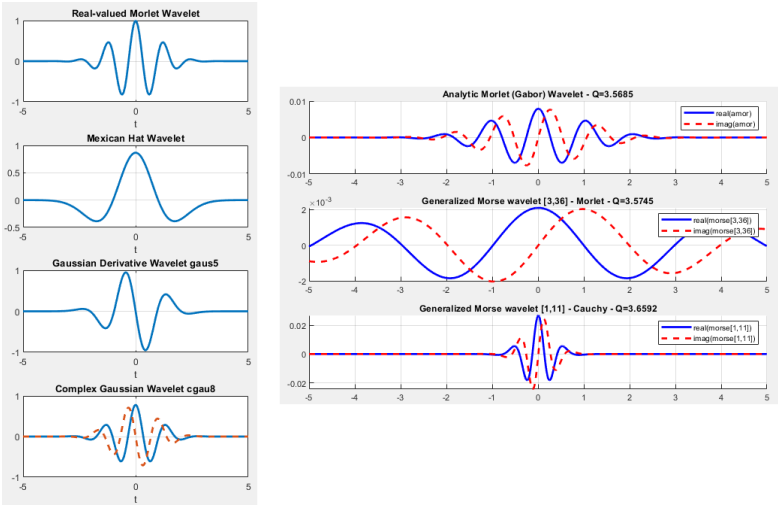

Figure 4.3: Example of different mother wavelets in the time domain, real and two complex. For the complex wavelets the plots illustrate the real part (solid) and imaginary part (dashed) for the wavelets. [25]

A wavelet $\psi(t)$ is progressive, when $\psi(t) \in H^2(\mathbb{R})$. That is, its FT $\hat{\psi}(t)$ vanishes for $\omega \leq 0$.

Let $u(t)$ be a signal that is of finite energy and a piece–wise continuous function of *t*. Given a mother wavelet $\psi(t)$, the continuous wavelet transform of this signal is given by the integral:

$$T_{\psi}[u](b,a) = \frac{1}{a}\int_{-\infty}^{+\infty} u(t)\bar{\psi}\left(\frac{t-b}{a}\right)dt \tag{4.35}$$

where a > 0 is a scaling parameter that defines the dilation of the mother wavelet $\psi(t)$ and *b* is the translation parameter related to time. As it can be observed by the *equation 4.35*, CWT transforms a one–dimensional (time domain) signal $u(t)$ to a two–dimensional representation: the time–scale plane. Scales are directly linked with frequencies: a scale *a* corresponds to a scaled version of the mother wavelet with center frequency ω_{ψ}/a, thus bringing the CWT on the time–frequency plane.

The CWT, as defined by *equation 4.35*, can be interpreted as:

- The convolution of $u(t)$ with $\frac{1}{a}\bar{\psi}\left(-\frac{b-t}{a}\right)$, based on *equation 4.5*.
- The inner product of of $u(t)$ with the shifted and scaled copies of the mother wavelet $\psi_{b,a} = \frac{1}{a}\bar{\psi}\left(\frac{t-b}{a}\right)$, based on *equation 4.7*.

Consequently, the CWT can be viewed as a tool that measures the similarity between a signal $u(t)$ and the shifted and scaled copies $\psi_{b,a}$ of a mother wavelet $\psi(t)$. A general illustration of how the CWT works can be seen in *Figure 4.4*. This concept now allows for a more simple definition of the ridges as the region where the frequency of the scaled mother wavelet is equal to the instantaneous frequency of the signal. Thus, in the ridges' regions of the TF plane, the CWT coefficients have (locally) relatively larger values, as the level of similitude is high, creating peaks in the TF representation as it can be see in *Figure 4.5*.

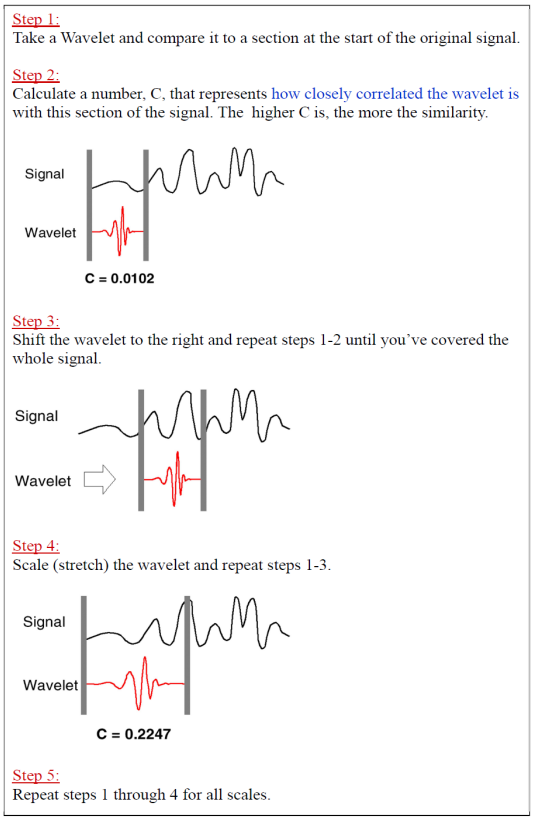

Figure 4.4: General illustration of how the CWT works. Source, class notes from [18].

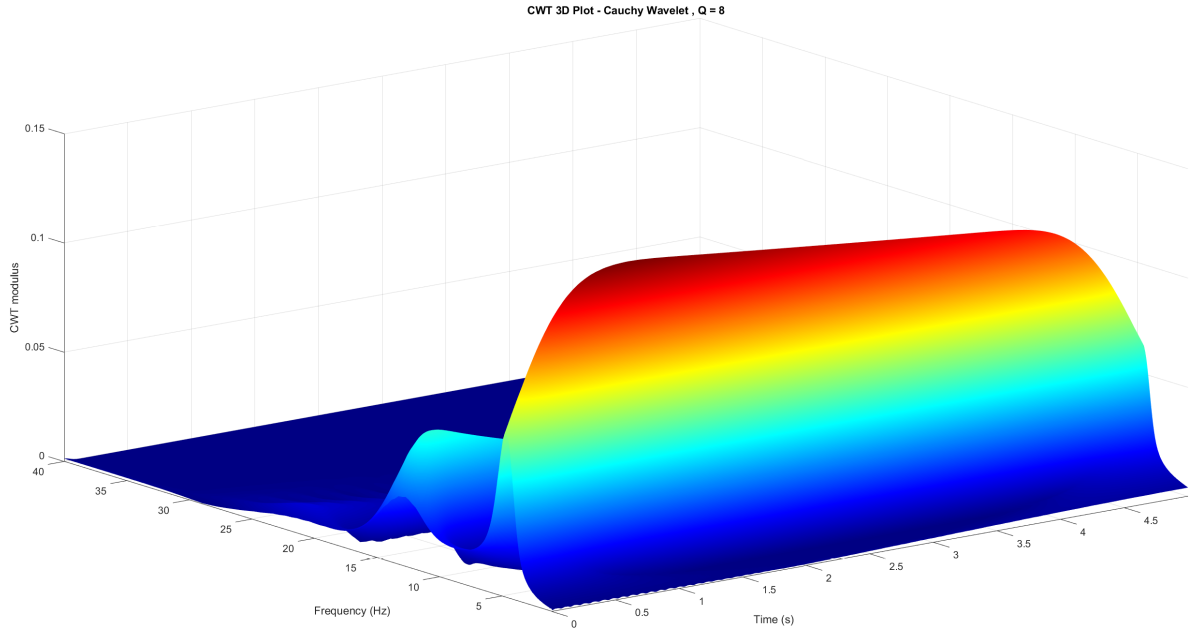

Figure 4.5: 3D representation of the TF plane to observe the ridges. [25]

Inverse Continuous wavelet transform When the admissibility condition is fulfilled, the signal $u(t)$ can be reconstructed as:

$$u(t) = \frac{1}{C_\psi} \int_{-\infty}^{+\infty} \int_{0}^{+\infty} T_\psi[u](b,a)\bar{\psi}\left(\frac{t-b}{a}\right)\frac{da}{a}db \tag{4.36}$$

Remark: A simple application of Parseval's relation gives the wavelet coefficients in terms of the Fourier transforms of the signal and the mother wavelet using the definition of the inverse Fourier transform:

$$T_\psi[u](b,a) = \frac{1}{2\pi}\int_{-\infty}^{+\infty} \hat{u}(\omega)\bar{\hat{\psi}}(a\omega)e^{i\omega b}d\omega \tag{4.37}$$

4.3.2 CWT Properties

- *Linearity*

$$T_\psi\left[\sum_{j=1}^{N} u_j\right](b,a) = \sum_{j=1}^{N} T_\psi[u_j](b,a) \tag{4.38}$$

Consequently, multicomponent signals can be processed and a particular component $u_j(t)$ can be extracted by using the localization properties of the mother wavelets, in both time and frequency domains.

- *CWT of $u(t)$, $\dot{u}(t)$, $\ddot{u}(t)$ relations*

Generally, the free responses that are recorded are displacement, velocity or acceleration, so the relation between their CWT can be useful. If $\psi(t)$ and $u(t)$ are continuous and piece–wise differentiable, the integration by parts theorem allows *equation 4.35* to be rewritten as:

$$T_\psi[\dot{u}](b,a) = \frac{1}{a}\left[u(t)\bar{\psi}\left(\frac{t-b}{a}\right)\Big|_{-\infty}^{+\infty} - \frac{1}{a}\int_{-\infty}^{+\infty} u(t)\bar{\dot{\psi}}\left(\frac{t-b}{a}\right)dt\right] \tag{4.39}$$

$\psi(t)$ is a window function, so:

$$\lim_{t\to+\infty}|\psi(t)| = \lim_{t\to-\infty}|\psi(t)| = 0 \tag{4.40}$$

Consequently, it follows that:

$$\lim_{t\to+\infty}\left|u(t)\bar{\psi}\left(\frac{t-b}{a}\right)\right| = \lim_{t\to-\infty}\left|u(t)\bar{\psi}\left(\frac{t-b}{a}\right)\right| = 0\,, \tag{4.41}$$

$$\lim_{t\to+\infty} u(t)\bar{\psi}\left(\frac{t-b}{a}\right) = \lim_{t\to-\infty} u(t)\bar{\psi}\left(\frac{t-b}{a}\right) = 0 \tag{4.42}$$

Therefore,

$$\lim_{t\to+\infty} u(t)\bar{\psi}\left(\frac{t-b}{a}\right) - \lim_{t\to-\infty} u(t)\bar{\psi}\left(\frac{t-b}{a}\right) = u(t)\bar{\psi}\left(\frac{t-b}{a}\right)\Big|_{-\infty}^{+\infty} = 0 \tag{4.43}$$

So, when $\dot{\psi}(t)$ is square and absolutely integrable and $\dot{u}(t)$ is of finite energy, the CWT of $\dot{u}(t)$ with $\psi(t)$ is then related to the CWT of $u(t)$ with $\dot{\psi}(t)$:

$$T_{\psi}[\dot{u}](b,a) = -\frac{1}{a}T_{\dot{\psi}}[u](b,a) \tag{4.44}$$

This relation can be easily extended to the finite energy signal $\ddot{u}(t)$ when $\ddot{\psi}(t)$ is square and absolutely integrable:

$$T_{\psi}[\ddot{u}](b,a) = -\frac{1}{a}T_{\dot{\psi}}[u](b,a) = \frac{1}{a^2}T_{\ddot{\psi}}[u](b,a) \tag{4.45}$$

4.3.3 Resolution

The value $T_{\psi}[u](b,a)$ of contains the information of the level of similitude of the signal $u(t)$ with the scaled wavelet at scale *a* around the time point *b*. The scaled wavelet at scale *a* has a duration Δt and frequency bandwidth $\Delta\omega$, thus the local resolution of the CWT in time and in frequency depends on the scale parameter *a* and is determined, respectively, by the duration Δt_{ψ} and bandwidth $\Delta\omega_{\psi}$ of the mother wavelet.
The resolution of the time−frequency window can be constructed by considering:

Time localization: Considering the time shifting property, *equation 4.16*:

$$\psi_b(t) = \psi(t-b) \text{ and } \widehat{\psi_b}(\omega) = e^{-i\omega t}\hat{\psi}(\omega) \tag{4.46}$$

Consequently, if the mother wavelet is localized around the time $t = t_{\psi}$, with temporal resolution Δt_{ψ}, the translation property gives the temporal localization of $\psi_b(t)$ around $t = b + t_{\psi}$ with the same time resolution Δt_{ψ}.

Frequency localization: In the STFT, the frequency localization of the analyzing wavelet was changing by translating the value of the frequency in the frequency axis. In CWT, where the concept of scale is applied, the frequency localization of the mother wavelet is obtained considering the time scaling property, *equation 4.15*:

$$\psi_a(\cdot) = \frac{1}{a}\left(\frac{\cdot}{a}\right) \text{ and } \hat{\psi}_a(\omega) = \psi(a\omega) \tag{4.47}$$

Consequently, if the mother wavelet is localized around t_ψ and ω_ψ with time and frequency resolution Δt_ψ and $\Delta\omega_\psi$ respectively, the scaled copy $\psi_{b,a}$ is localized around:

$$t = b + at_\psi \,,\, \omega = \frac{\omega_\psi}{a} \tag{4.48}$$

with time and frequency resolution Δt_ψ and $\Delta\omega_\psi$ respectively:

$$\Delta t = a\,\Delta t_\psi \,,\, \Delta\omega = \frac{\Delta\omega_\psi}{a} \tag{4.49}$$

Thus, looking ω_ψ/a as the frequency variable ω, then the $t - \omega$ plane can be considered as the time−frequency plane. The localization domain for the CWT at point ($b + at_\psi$, ω_ψ/a) is the time−frequency window (*Figure 4.6*):

$$[b + at_\psi - a\,\Delta t_\psi \,,\, b + at_\psi + a\,\Delta t_\psi] \times \left[\frac{\omega_\psi}{a} - \frac{\Delta\omega_\psi}{a} \,,\, \frac{\omega_\psi}{a} + \frac{\Delta\omega_\psi}{a}\right] \tag{4.50}$$

where

$$[b + at_\psi - a\,\Delta t_\psi \,,\, b + at_\psi + a\,\Delta t_\psi] \tag{4.51}$$

is the time−window, which narrows for small values of a and widens for large values of a, and

$$\left[\frac{\omega_\psi}{a} - \frac{\Delta\omega_\psi}{a} \,,\, \frac{\omega_\psi}{a} + \frac{\Delta\omega_\psi}{a}\right] \tag{4.52}$$

is the frequency−window, which widens for small values of a and narrows for large values of a.

Hence, this window automatically narrows for detecting rapidly changing details, i.e. high frequency phenomena (small a), and widens for investigating slowly changing details, i.e. low−frequency behavior (large a). This is exactly what is most desirable in time−frequency analysis, and makes the use of the CWT appropriate for analyzing non–stationary signals. This can be observed clearly in *Figure 4.6*.

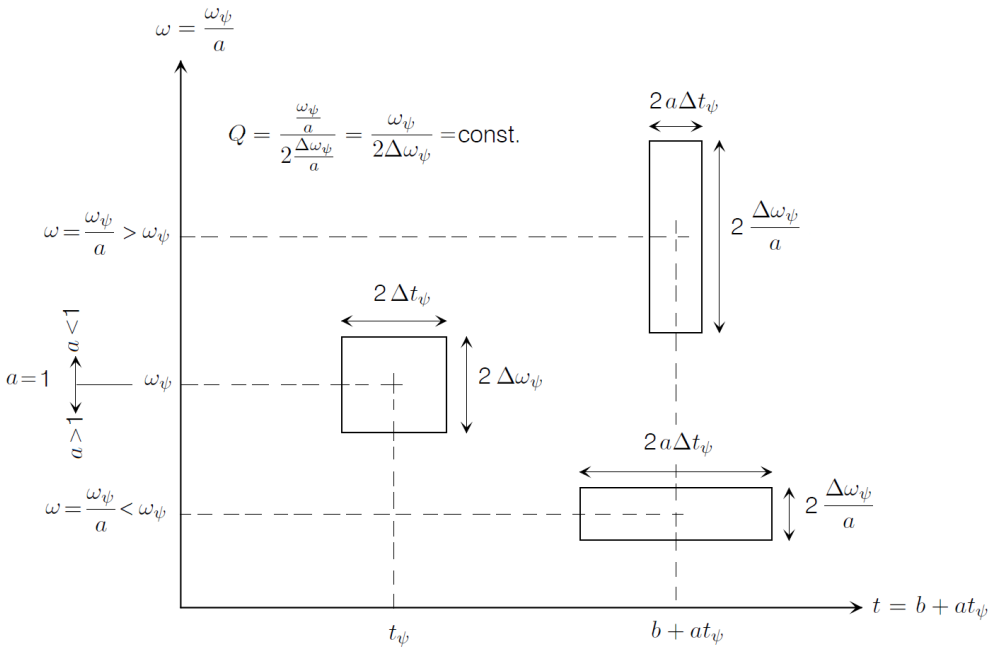

Figure 4.6: Time–frequency resolution for the CWT. The mother wavelet is illustrated at (t_ψ, ω_ψ) , as a = 1 and b = 0 by definition. Scaled wavelets at points ($b + at_\psi$, ω_ψ/a) for scales a > 1 and scales 0 < a < 1.

4.3.4 Normalization

To ensure that the wavelet transforms at each scale *a* are directly comparable to each other and to the transforms of other time series, the wavelet function at each scale a is normalized.

Different normalizations can be found in the literature. Attempting now to give a general definition in order to explore the choice of normalization, let the mother wavelet $\psi(t)$ and an arbitrary number $q \geq 0$. The corresponding family of wavelets is the family $[\psi_{b,a};\ b \in \mathbb{R},\ a \in \mathbb{R}_+^*]$ of shifted and scaled (dilated) copies of ψ defined as:

$$\psi_{b,a}(t) = |a|^{-q}\psi\left(\frac{t-b}{a}\right) \ ,\ t \in \mathbb{R} \tag{4.53}$$

where *a* is the scaling parameter and *b* is the translation parameter. This definition associates the normalization choice with the just the value of *q*. Different values have been selected in the literature, for example, Carmona et al. [2], Delprat et al. [6] use $q = 1$. Chui [3] and Daubechies [4] use $q = 1/2$. When dealing with orthonormal bases of wavelets, the choice $q = 0$ is sometimes convenient [9]. Thus, these three values will be explored and presented in the next.

Starting with $q = 1$, *equation 4.53* becomes:

$$\psi_{b,a}(t) = \frac{1}{a}\psi\left(\frac{t-b}{a}\right) \ ,\ t \in \mathbb{R} \tag{4.54}$$

The scaled wavelets $\psi_{a,b}(t)$ have been normalized in such a way that:

$$\|\psi_{b,a}(t)\|_1 = \int_{-\infty}^{+\infty} |\psi_{b,a}(t)| = \|\psi(t)\|_1 = constant \tag{4.55}$$

Thus, all the scaled wavelets, $\psi_{a,b}(t)$, at every scale *a* enclose the same area.

For $q = 1/2$, *equation 4.53* becomes:

$$\psi_{b,a}(t) = \frac{1}{\sqrt{a}}\psi\left(\frac{t-b}{a}\right) \ , \ t \in \mathbb{R} \tag{4.56}$$

The scaled wavelets $\psi_{a,b}(t)$ have been normalized in such a way that:

$$\|\psi_{b,a}(t)\|_2 = \int_{-\infty}^{+\infty} |\psi_{b,a}(t)|^2 = \|\psi(t)\|_2 = constant \tag{4.57}$$

Thus, all the scaled wavelets, $\psi_{a,b}(t)$, at every scale *a* have the same energy.

For $q = 0$, *equation 4.53* becomes:

$$\psi_{b,a}(t) = \psi\left(\frac{t-b}{a}\right) \ , \ t \in \mathbb{R} \tag{4.58}$$

The scaled wavelets $\psi_{a,b}(t)$ have been normalized in such a way that:

$$\|\psi_{b,a}(t)\|_\infty = constant \tag{4.59}$$

Thus, all the scaled wavelets, $\psi_{a,b}(t)$, at every scale, *a*, have merely the same maximum value.

4.3.5 Choice of mother wavelets

There are a lot of mother wavelets in the literature, some examples are shown in *Figure 4.3*. The choice of the mother wavelet is dictated by the characteristics of the signal under study and the nature of the application. It is important to use a wavelet that is the best fit for the analysis that will follow. Consequently, there are several factors which should be considered in the choice of the mother wavelet [21]:

(1) **Complex or Real.** A complex wavelet function will return information about both amplitude and phase and is better adapted for capturing oscillatory behavior. A real mother wavelet returns only a single component and can be used to isolate peaks or discontinuities.

(2) **Shape.** The wavelet function should reflect the type of features present in the time series. For example, in the analysis of free responses of structures, wave–like mother

wavelets with an increased number of oscillations such as the Morlet wavelet and the Cauchy wavelet are preferred. For time series with sharp jumps or steps, one would choose a boxcar–like function such as the Harr, while for smoothly varying time series one would choose a smooth function such as a damped cosine. If one is primarily interested in wavelet power spectra, then the choice of wavelet function is not critical, and one function will give the same qualitative results as another. Conversely, the wavelet function can also be chosen to uncover specific signal features that are hypothesized to exist in the signal but may not be directly evident upon initial inspection.

(3) **Width.** The resolution of a wavelet function is determined by the balance between the width in real space and the width in Fourier space. A narrow (in time) function will have good time resolution but poor frequency resolution, while a broad function will have poor time resolution, yet good frequency resolution.

(4) **Orthogonal or nonorthogonal.** This refers to the DWT. In orthogonal wavelet analysis, the number of convolutions at each scale is proportional to the width of the wavelet basis at that scale. This produces a wavelet spectrum that contains discrete "blocks" of wavelet power and is useful for signal processing as it gives the most compact representation of the signal. Unfortunately for time series analysis, an aperiodic shift in the time series produces a different wavelet spectrum. Conversely, a nonorthogonal analysis is highly redundant at large scales, where the wavelet spectrum at adjacent times is highly correlated. The nonorthogonal transform is useful for time series analysis, where smooth, continuous variations in wavelet amplitude are expected.

The optimal mother wavelet ψ for modal identification purposes using the free responses of a MDOF system should satisfy the following conditions [10]:

(1) ψ is admissible. Obvious, required by definition.

(2) ψ is progressive. Several reasons suggest the use of progressive wavelets instead of real ones for the analysis of real signals:

i. It allows the direct connection between a real signal and its associated analytic signal.

ii. The wavelet transform of real signals using real wavelets yields real wavelet coefficients, and there is no natural way of making a connection with some "local spectrum" which one would like associate with a given signal.

(3) ψ has good time and frequency localization properties. This condition is very important in the context of time–frequency analysis as presented in the section of resolution.

(4) The first and the second derivatives of ψ satisfy the three previous conditions. This condition makes the processing by CWT of displacement, velocity and acceleration easier without differential and integral operations

Two important complex mother wavelets are *Complex Morlet wavelet and Cauchy wavelet of order n* and their properties are presented in *Table 4.1*.

Table 4.1: Definition and main properties of the Complex Morlet wavelet and the Cauchy wavelet of order n.

	Morlet wavelet	Cauchy wavelet
$\psi(t)$	$e^{-t^2/(2\delta^2)}e^{i\beta t}$	$\left(\frac{i}{t+i}\right)^{n+1}$
$\hat{\psi}(\omega)$	$\delta\sqrt{2\pi}e^{-(\omega-\beta)^2\delta^2/2}$	$\frac{2\pi\omega^n e^{-\omega}}{n!}\Theta(\omega)$
C_ψ:	∞	$4\pi^2\frac{1}{2^{2n}}\frac{(2n-1)!}{(n!)^2}$
t_ψ	0	0
ω_ψ	β	$n+\frac{1}{2}$
$\Delta\omega_\psi$:	$\frac{1}{\delta\sqrt{2}}$	$\frac{\sqrt{2n+1}}{2}$
Δt_ψ:	$\frac{\delta}{\sqrt{2}}$	$\frac{1}{\sqrt{2n-1}}$
μ_ψ:	$\frac{1}{2}$	$\frac{1}{2}\sqrt{1+\frac{2}{2n-1}}$
$Q=\frac{\omega_\psi}{2\Delta\omega_\psi}$	$\frac{\beta\delta}{\sqrt{2}}$	$\frac{n+\frac{1}{2}}{\sqrt{2n+1}}$

where n is the order of Cauchy wavelet, β is a frequency parameter controlling the number of oscillations of the wavelet and δ is a parameter that controls the spread of the wavelet (see more in [25]).

For the needs of the current thesis, the Cauchy wavelet is used.

4.3.6 Scales and Converting scale to frequency

By definition the CWT decomposes signals based on time and scale parameters. However in many applications, including the modal parameter identification, the results are preferred to be on the time–frequency plane. Therefore, it is important to define a relationship between scale and frequency. As it was presented in the Resolution section a scaled wavelet's frequency is $\omega = \frac{\omega_\psi}{a}$, thus scale and frequency are inversely proportional and related through the center frequency ω_ψ, and can be theoretically computed as:

$$f = \frac{f_\psi}{a} \tag{4.60}$$

where f_ψ is the center frequency of the mother wavelet, and a the scale.

In a more intuitive sense, the center frequency of a wavelet is a simplified approximation of the dominant frequency component contained in the function. The center frequency can be determined and visualized by superimposing a sine wave onto the wavelet and determining the frequency value for which the sinusoid best parallels the wavelet's main oscillation. MATLAB, in the built in cwt command, determines the center frequency

by this approximation and makes a slight variation of the theoretical equation, adding the sampling period *dt*:

$$f = \frac{f_\psi}{a}\frac{1}{dt} \tag{4.61}$$

As the frequency variable is identified as a constant multiple of $1/a$, then the mother wavelet ψ can be considered as an adaptive bandpass filter, with pass–band given by 4.52. Thus, the series of the scaled copies of ψ can be viewed as a bandpass filterbank. The number of scales used in an analysis defines the number of scaled copies of the mother wavelet that will be generated; the finer the scales, the finer the frequency resolution.

Octave is a notion from acoustics and refers to a duplication of frequency, e.g. a frequency range [10 20] Hz is one octave, as $\log_2(f_{max}/f_{min}) = \log_2(20/10) = 1$. Number of Voices per Octave is a term commonly used to designate the number of scaled wavelets per octave, i.e. the number of scales per octave. Therefore, number of voices per octave determines the number of scales between a frequency duplication.

Summarizing, the number of octaves determines the span of frequencies being analyzed, while the number of voices per octave determines the number of scales (i.e. samples) across this span. The appropriate range of octaves and scales depends on the spectral content of the data, and the highest requested frequency in the CWT [12].

4.3.7 Edge effect–Cone of influence

The CWT works as described in *Figure 4.4*, i.e, the mother wavelet is scaled, then translated in time and covers the whole signal. Inevitably, when the wavelets are near the beginning or end of the data "catch" data outside the observation interval, thus the computed wavelet coefficients near the beginning and end of the data are affected by the fact that there are wavelets extending outside the boundary. This is called the *edge effect problem*, which arises due to the finite length and to the discretization of measured data record and to the nature of the CWT [10]. Furthermore, the extent of the wavelet coefficients affected by data outside the observation interval depends on the scale (frequency). Low frequencies correspond to wavelets of larger scale, while higher frequencies correspond to wavelets of smaller scale. The edge effect persists longer in time with large scaled wavelets, that is why the affected area takes the shape of a cone [14]. Various techniques have been developed to remedy the edge effect, however it cannot be removed and the interpretation of wavelet coefficients near the boundaries must be handled with great caution. Thus, a domain *D* in the TF plane, must be determined, where the edge effect can be neglected. The *cone of influence* (COI) is the region of the wavelet spectrum in which edge effects become important.

However, there is no closed mathematical formula to determine the extent of the cone of influence at each scale. Nobach et al. [17] define the extent of the cone of influence at each scale as the point where the wavelet transform magnitude decays to 2% of its peak value. Because many of the wavelets used in continuous wavelet analysis decay exponentially in time, Torrence and Compo [21] use the time constant 1/e to delineate the borders of the cone of influence at each scale. For Morse wavelets, Lilly [11] uses the concept of the "wavelet footprint", which is the time interval that encompasses approximately 95% of the wavelet's energy. Lilly delineates the COI by adding 1/2 the

wavelet footprint to the beginning of the observation interval and subtracting 1/2 the footprint from the end of the interval at each scale.

Le and Argoul [10] introduced two real coefficients $c_t \geq 1$ and $c_f \geq 1$ that have the property that:
when t is outside the interval $I_{ct} = [t_\psi - c_t\Delta t_\psi \, , \, t_\psi + c_t\Delta t_\psi]$
and when ω is outside the interval $I_{cf} = [\omega_\psi - c_f\Delta\omega_\psi \, , \, \omega_\psi + c_f\Delta\omega_\psi]$,

$\psi(t)$ and $\hat{\psi}(t)$ have good decreasing properties, i.e. have null or very "small" values.

They explored the effect of the different values of c_t and c_f and concluded that the choice of $c_t = 5$ and $c_f = 5$ seem to yield good results. Consequently, they proposed to define the domain D as an "extended" time–frequency localization domain for the CWT as expressed in *equation 4.50* around the point b_j , $\omega_j = \omega_\psi/a_j$: Using the coefficients c_t and c_f and the progressive property of the mother wavelet, D becomes:

$$\left[b_j + \frac{\omega_\psi}{\omega_j} t_\psi - \frac{\omega_\psi}{\omega_j} c_t \Delta t_\psi \; , \; b_j + \frac{\omega_\psi}{\omega_j} + \frac{\omega_\psi}{\omega_j} c_t \Delta t_\psi \right] \times \left[max\left(0 \; , \; \omega_j \left(1 - c_f \frac{\Delta\omega_\psi}{\omega_\psi} \right) \right) \; , \; \omega_j \left(1 + c_f \frac{\Delta\omega_\psi}{\omega_\psi} \right) \right] \tag{4.62}$$

The domain D must be included into $[0, L]\times[2\pi f_{\text{Nyquist}}]$, this leads to the following system of inequalities:

$$\begin{cases} \dfrac{\omega_\psi}{\omega_j} c_t \Delta t_\psi - \dfrac{\omega_\psi}{\omega_j} t_\psi \; \leq \; b_j \; \leq \; L - \dfrac{\omega_\psi}{\omega_j} c_t \Delta t_\psi - \dfrac{\omega_\psi}{\omega_j} t_\psi \\ 0 < \omega_j \; \leq \; \dfrac{2\pi f_{Nyquist}}{1 + c_f \dfrac{\Delta\omega_\psi}{\omega_\psi}} \end{cases} \tag{4.63}$$

where L is the signal's duration.

As mentioned in *Table 4.1*, $t_\psi = 0$ for both the complex Morlet and the Cauchy wavelets, thus the domain D becomes:

$$\begin{cases} \dfrac{\omega_\psi}{\omega_j} c_t \Delta t_\psi \; \leq \; b_j \; \leq \; L - \dfrac{\omega_\psi}{\omega_j} c_t \Delta t_\psi \\ 0 < \omega_j \; \leq \; \dfrac{2\pi f_{Nyquist}}{1 + c_f \dfrac{\Delta\omega_\psi}{\omega_\psi}} \end{cases} \tag{4.64}$$

Solving for ω, four equations are obtained, which delimit the useful domain D:

$$\begin{cases} \omega_1 = \dfrac{\omega_\psi}{b} c_t \Delta t_\psi \\ \omega_2 = \dfrac{\omega_\psi}{L-b} c_t \Delta t_\psi \\ \omega_3 = 0 \\ \omega_4 = \dfrac{2\pi f_{Nyquist}}{1 + c_f \dfrac{\Delta \omega_\psi}{\omega_\psi}} \end{cases} \tag{4.65}$$

ω_1 and ω_2 are two hyperbolae and ω_3 and ω_4 are two horizontal lines (*Figure 4.7*). Due to the introduction of the two parameters $c_t \geq 1$ and $c_f \geq 1$, the useful time interval is smaller than L and the maximum usefull frequency is smaller than f_{Nyquist}.

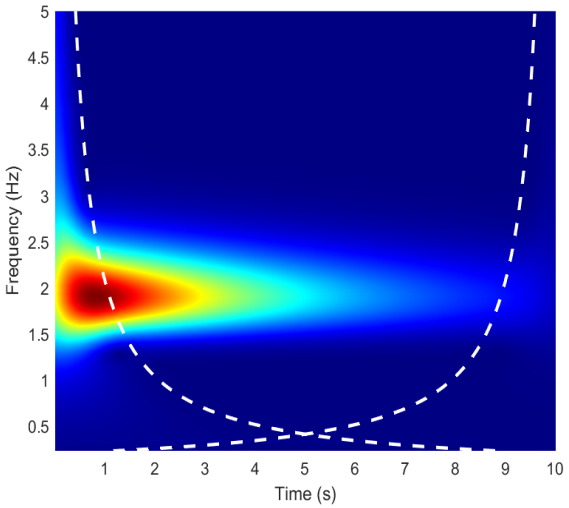

Figure 4.7: CWT modulus Scalogram. Illustration of edge effects, $c_t = 3$ and $c_f = 3$. [25]

Figure 4.7 illustrates the modulus scalogram of a SDOF system with natural period $T = 0.5$ sec. The white lines are the ω_1 and ω_2 hyperbolae limits. Notice the cone of influence on the region where the data begins that manifests as a spread of energy along the frequency axis. Observe that the white line follows that shape.

4.3.8 Q factor and its influence

In *Figure 4.6*, a parameter Q is presented and stated that it remains constant. As it was mentioned in the previous, the center frequency ω_ψ is assumed to be positive. This enables the consideration on the frequency window of *4.52* as a frequency band (or octave) with center–frequency ω_ψ/a and bandwidth $2\Delta\omega_\psi/a$. The importance of this identification is that it allows the introduction of the following ratio (Q factor):

$$Q = \frac{\frac{\omega_\psi}{a}}{2\frac{\Delta\omega_\psi}{a}} = \frac{\omega_\psi}{2\Delta\omega_\psi} \tag{4.66}$$

Q is independent of the scaling a. Hence, if the frequency variable is identified as a constant multiple of $1/a$, then an adaptive band–pass filter, with pass–band given by *4.52*, has the property that the center–frequency to bandwidth ratio is independent of the location of the center–frequency, thus it remains constant. This is called constant–Q filtering, where Q, once set in the beginning of the analysis, remains the same for all scaled and shifted wavelets. Q depends only at the mother wavelet choice. [25]

Gram–Hansen and Dorize [7] associate this Q value to the filterbank of a (1/N)*th* octave as:

$$Q = \frac{1}{2^{1/2N} - 2^{-1/2N}} \tag{4.67}$$

where an (1/N)*th* of center frequency ω_ψ is a band $[\omega_1, \omega_2]$ with $\omega_1 = 2^{-1/(2N)}$ and $\omega_2 = 2^{1/(2N)}$.

As it follows by it's definition in *4.66*, the Q factor can be associated with the mother wavelet parameters and define their tuning. Higher Q produce narrower wavelets, with more oscillations within their waveform. Consequently applying the CWT with a high Q factor allows a multi–scale analysis with high frequency resolution (at the expense of a lower time resolution), making it appropriate for analyzing oscillatory signals such as the displacement response of a structure. Therefore, the choice of Q depends on the spectral components contained in the signal as well as the sampling frequency F_s and the duration of the signal. [25]

The Q factor value has also another significant property, it can be used to correctly extract two close ridges corresponding to two coupled modes, which is of great importance in the modal parameter identification of MDOF systems. Continuing with the method proposed by Le and Argoul [10], the problem is set as: ω_j the angular eigen−frequency and $d\omega_j$ the frequency discrepancy from which the effect of the modal coupling must be avoided. In order to solve this problem, the frequency localization domain of the CWT along a ridge, as modified to take into account the edge effects in relation *4.62* is assumed to be included into a bandwidth $[\omega_j - d\omega_j, \omega_j + d\omega_j]$. This leads to bounding the Q as:

$$Q \geq c_f \frac{\omega_j}{2\, d\omega_j} \tag{4.68}$$

Let $d\omega_j = min[(\omega_j - \omega_{j-1}), (\omega_{j+1} - \omega_j)]$ for $1 \leq j \leq N$ with $\omega_0 = 0$, $\omega_{N+1} = 2\pi f_{Nyquist}$.

Consequently, the edge effect delimiting inequality

$$0 \leq \omega_j \leq \frac{2\pi f_{Nyquist}}{1 + c_f \frac{1}{2Q}} \tag{4.69}$$

is immediately checked, since $d\omega_j < \pi f_{\text{Nyquist}}$. Then, the edge effect delimiting inequality

$$\frac{1}{\omega_j} 2 c_t Q \mu_\psi \leq b_j \leq L - \frac{1}{\omega_j} 2 c_t Q \mu_\psi \tag{4.70}$$

combined with the Heisenberg's inequality gives:

$$Q \leq \frac{L \omega_j}{2 c_t} \tag{4.71}$$

Concluding, the parameter Q can be bounded as:

$$c_f \frac{\omega_j}{2 d\omega_j} \leq Q \leq \frac{L \omega_j}{2 c_t} \tag{4.72}$$

where L is the signal's length and the contained $\omega_j s$ in a signal can be obtained by applying FFT, then classified in an increasing order. Finally, c_t and c_f must fulfill the following inequality:

$$c_t c_f \leq L d\omega_j \tag{4.73}$$

Le and Argoul propose to start with $c_t = c_f = 5$. When the *inequality 4.73* is not satisfied, c_t and c_f should be reduced until it becomes true. Then the value of Q can be chosen between the limits posed in *4.72*.

5. Structural Dynamics

This Chapter provides a basic theoretical background on structural dynamics. It presents the well−known differential equations of motion in structural dynamics and describes the procedure of the extraction of the displacement, velocity and acceleration responses for MDOF and SDOF. The systems considered are linear, with viscous proportional damping.

5.1 Single Degree of Freedom (SDOF) systems

5.1.1 Equation of motion

Let $u(t)$, $\dot{u}(t)$, $\ddot{u}(t)$ denote respectively the displacement, velocity, and acceleration of a SDOF. system. The equation of motion then is given by:

$$m\,\ddot{u}(t) + c\,\dot{u}(t) + k\,u(t) = p(t) \tag{5.1}$$

where m is the system's mass, c is the damping constant, k is the stiffness and $p(t)$ is the externally applied dynamic force.

5.1.2 Viscoulsy damped free vibration of SDOF systems

Free vibration is initiated by displacing the system from its static equilibrium position via imparting the mass an initial displacement $u(0)$ and velocity $\dot{u}(0)$ at time zero $t = 0$. If there is no externally applied dynamic force, then the free motion depends only on these initial conditions $u(0)$ and $\dot{u}(0)$. Setting $p(t) = 0$ in *equation 5.1* gives the differential equation governing free vibration of SDOF systems with damping:

$$m\,\ddot{u}(t) + c\,\dot{u}(t) + k\,u(t) = 0 \tag{5.2a}$$

Dividing by the mass m gives:

$$\ddot{u}(t) + 2\,\xi\omega\,\dot{u}(t) + \omega^2 u(t) = 0 \tag{5.2b}$$

where, ω is the undamped angular natural frequency of the system, given by:

$$\omega = \sqrt{\frac{k}{m}} \tag{5.3}$$

and ξ is the damping ratio or fraction of critical damping of the system, defined as:

$$\xi = \frac{c}{2m\omega} = \frac{c}{c_{cr}} \tag{5.4}$$

where, c, the damping constant, is a measure of the energy dissipated in a cycle of free vibration or in a cycle of forced harmonic vibration. c_{cr} refers to the critical damping coefficient; it is the smallest value of c that inhibits oscillation completely, i.e. it is the dividing line between oscillatory and non−oscillatory motion and vise−versa. Consequently, c_{cr} defines the type of the system as:

i. Under−damped systems, where $c < c_{cr}$ or $\xi < 1$: the system oscillates about its equilibrium position with a progressively decreasing amplitude.

ii. Critically damped systems, where $c = c_{cr}$ or $\xi = 1$: the system returns to its equilibrium position without oscillating.

iii. Over−damped systems, where $c > c_{cr}$ or $\xi > 1$: the system does not oscillate and returns to its equilibrium position, as in the $\xi = 1$ case, but at a slower rate.

As mentioned, for the associated analytic signal to be approximated as $Z_u(t) \approx A_u(t)e^{i\varphi_u(t)}$, the assumption of weak damping $\xi \ll 1/\sqrt{2}$ is made, therefore the solution of the *equation 5.2* that is presented in the following is for underdamped systems.

5.1.3 Free response of under−damped SDOF system

For under−damped systems where c < c_{cr} or $\xi < 1$ the solution to the *equation 5.2* subject to the initial conditions $u(0)$ and $\dot{u}(0)$ is:

$$u(t) = e^{-\xi\omega t}\left[u(0)\cos(\widetilde{\omega}t) + \frac{\dot{u}(0) + u(0)\xi\omega}{\widetilde{\omega}}\sin(\widetilde{\omega}t)\right] \tag{5.5}$$

where $\widetilde{\omega}$ is the damped angular natural frequency of the system, given by:

$$\widetilde{\omega} = \omega\sqrt{1-\xi^2} \tag{5.6}$$

Setting

$$\rho = \sqrt{[u(0)]^2 + \left[\frac{\dot{u}(0) + u(0)\xi\omega}{\widetilde{\omega}}\right]^2} \tag{5.7}$$

and

$$\varphi = \arctan\left(\frac{\dot{u}(0) + u(0)\xi\omega}{u(0)\widetilde{\omega}}\right) \tag{5.8}$$

the *equation 5.5* of displacement becomes:

$$u(t) = \rho e^{-\xi\omega t}\cos(\widetilde{\omega}t-\varphi) \tag{5.9}$$

The velocity and the acceleration are obtained by successively deriving the displacement $u(t)$:

The velocity is calculated as:

$$\begin{aligned}\dot{u}(t) &= \rho\omega e^{-\xi\omega t}[-\xi\cos(\widetilde{\omega}t-\varphi)-\sqrt{1-\xi^2}\sin(\widetilde{\omega}t-\varphi)] \\ &= -\rho\omega e^{-\xi\omega t}\cos(\widetilde{\omega}t-\varphi-\delta)\end{aligned} \tag{5.10}$$

where

$$\delta = \arctan\left(\frac{\sqrt{1-\xi^2}}{\xi}\right) \tag{5.11}$$

and the acceleration is calculated as:

$$\begin{aligned}\ddot{u}(t) &= \rho\omega e^{-\xi\omega t}(-\xi\omega)[-\xi\cos(\widetilde{\omega}t-\varphi)-\sqrt{1-\xi^2}\sin(\widetilde{\omega}t-\varphi)] \\ &+ \rho\omega e^{-\xi\omega t}[\xi\widetilde{\omega}\sin(\widetilde{\omega}t-\varphi)-\sqrt{1-\xi^2}\widetilde{\omega}\cos(\widetilde{\omega}t-\varphi)] \\ &= \rho\omega^2 e^{-\xi\omega t}(-\xi\omega)[(\xi^2-(1-\xi^2))\cos(\widetilde{\omega}t-\varphi) + 2\xi\sqrt{1-\xi^2}\sin(\widetilde{\omega}t-\varphi)] \\ &= -\rho\omega^2 e^{-\xi\omega t}\cos(\widetilde{\omega}t-\varphi+\theta)\end{aligned} \tag{5.12}$$

where

$$\theta = \arctan\left(\frac{2\xi\sqrt{1-\xi^2}}{1-2\xi^2}\right) \tag{5.13}$$

It can be noted that the phase of the velocity and the phase of the acceleration are differentiated from the phase of the displacement by a quantity depending on the damping ratio ξ.

5.2 Multi Degree of Freedom (MDOF) systems

5.2.1 Equation of motion

Let $\boldsymbol{u}(t)$, $\dot{\boldsymbol{u}}(t)$, $\ddot{\boldsymbol{u}}(t)$ denote respectively the displacement, velocity, and acceleration vectors of a MDOF system with N degrees of freedom. The equation of motion then is given by:

$$\mathbf{M}\ddot{\boldsymbol{u}}(t) + \mathbf{C}\dot{\boldsymbol{u}}(t) + \mathbf{K}\boldsymbol{u}(t) = \mathbf{P}(t) \tag{5.14}$$

where **M** is the system's mass matrix, **C** is the damping matrix, **K** is the stiffness matrix and **P**(*t*) is the externally applied dynamic force vector.

5.2.2 Modal superposition

Let **Φ** be the modal matrix made of eigen−vectors $\boldsymbol{\Phi}_j = [\Phi_{1j}, \Phi_{2j}, ..., \Phi_{Nj}]^T$. By definition, the mode shape vector Φ_j describes the shape of the j^{th} mode corresponding to the natural frequency ω_j. Then, the vector of displacements can be described mathematically by:

$$\boldsymbol{u}(t) = \sum_{j=1}^{N} \boldsymbol{\Phi}_j y_j(t) = \boldsymbol{\Phi}\mathbf{Y}(t) \tag{5.15}$$

The coupled equation of motion of *equation 5.14* can be uncoupled after substituting $\boldsymbol{u}(t)$ using *equation 5.15* and left multiplying it with $\boldsymbol{\Phi}^T$. This is achieved with the aid of the orthogonality condition, which makes **M**, **K** and **C** diagonal, and is defined as:

$$\boldsymbol{\Phi}_j \mathbf{M} \boldsymbol{\Phi}_i = \begin{cases} M_j & , \text{if } j = i \\ 0 & , \text{if } j \neq i \end{cases} \tag{5.16}$$

$$\boldsymbol{\Phi}_j \mathbf{C} \boldsymbol{\Phi}_i = \begin{cases} C_j & , \text{if } j = i \\ 0 & , \text{if } j \neq i \end{cases} \tag{5.17}$$

$$\boldsymbol{\Phi}_j \mathbf{K} \boldsymbol{\Phi}_i = \begin{cases} K_j & , \text{if } j = i \\ 0 & , \text{if } j \neq i \end{cases} \tag{5.18}$$

5.2.3 Viscoulsy damped free vibration of MDOF systems

Considering again damped free vibration with initial conditions $\boldsymbol{u}(0)$, $\dot{\boldsymbol{u}}(0)$ at $t = 0$, then $\boldsymbol{P}(t) = 0$, the equation of motion becomes:

$$\mathbf{M}\ddot{\boldsymbol{u}}(t) + \mathbf{C}\dot{\boldsymbol{u}}(t) + \mathbf{K}\boldsymbol{u}(t) = 0 \tag{5.19}$$

Procedures to obtain the desired solution differ depending on the form of damping. The damping matrix **C** generally is not easy to calculate in practice. However, with condition 5.17, the transformation that diagonalizes both **M** and **K** will also diagonalize **C**. So, by applying *equation 5.15*, *equation 5.19* becomes:

$$\mathbf{M\Phi}\ddot{\boldsymbol{Y}} + \mathbf{C\Phi}\dot{\boldsymbol{Y}} + \mathbf{K\Phi}\boldsymbol{Y} = 0 \tag{5.20}$$

Left multiplying by $\mathbf{\Phi}^{\mathrm{T}}$ gives:

$$\mathbf{\Phi}^{\mathrm{T}}\mathbf{M\Phi}\ddot{\boldsymbol{Y}} + \mathbf{\Phi}^{\mathrm{T}}\mathbf{C\Phi}\dot{\boldsymbol{Y}} + \mathbf{\Phi}^{\mathrm{T}}\mathbf{K\Phi}\boldsymbol{Y} = 0 \tag{5.21}$$

Thus, the equations of motion can then be expressed as a N set of uncoupled SDOF. equations:

$$M_j\ddot{y}_j + C_j\dot{y}_j + K_j y_j = 0 \qquad , \quad j = 1, 2, \ldots \mathrm{N} \tag{5.22}$$

Considering $C_j = 2\xi_j M_j \omega_j$ and $K_j = M_j\omega_j^2$, and dividing by M_j , the equations can be further simplified to:

$$\ddot{y}_j + 2\xi_j\omega_j\dot{y}_j + \omega_j^2 y_j = 0 \qquad , \quad j = 1, 2, \ldots \mathrm{N} \tag{5.23}$$

5.2.4 Free response of under−damped MDOF system

Consequently, the *equations 5.23* are of the same form as *equation 5.2b* governing the free vibration of a SDOF system with viscous proportional damping. Adapting this result, the solution for *equations 5.23* becomes:

$$\ddot{y}_j(t) = \rho_j e^{-2\xi_j\omega_j t}\cos(\widetilde{\omega}_j t - \varphi_j) \tag{5.24}$$

$$\dot{y}_j(t) = -\rho_j\omega_j e^{-2\xi_j\omega_j t}\cos(\widetilde{\omega}_j t - \varphi_j - \delta_j) \tag{5.25}$$

$$y_j(t) = -\rho_j\omega_j^2 e^{-2\xi_j\omega_j t}\cos(\widetilde{\omega}_j t - \varphi_j + \theta_j) \tag{5.26}$$

where

$$\omega_j^2 = \frac{k_j}{m_j} \tag{5.27}$$

$$\widetilde{\omega}_j = \omega_j\sqrt{1-\xi_j^2} \tag{5.28}$$

Therefore, for any degree of freedom k = 1, 2, ...,N, the MDOF system's responses can be expressed as:

$$u_k(t) = \sum_{j=1}^{\mathrm{N}} u_{kj}(t) = \Phi_{kj}\rho_j e^{-2\xi_j\omega_j t}\cos(\widetilde{\omega}_j t - \varphi_j) \tag{5.29}$$

$$\dot{u}_k(t) = \sum_{j=1}^{N} \dot{u}_{kj}(t) = -\sum_{j=1}^{N} \Phi_{kj}\rho_j\omega_j e^{-2\xi_j\omega_j t}\cos(\widetilde{\omega}_j t - \varphi_j - \delta_j) \tag{5.30}$$

$$\ddot{u}_k(t) = \sum_{j=1}^{N} \ddot{u}_{kj}(t) = -\sum_{j=1}^{N} \Phi_{kj}\rho_j\omega_j^2 e^{-2\xi_j\omega_j t}\cos(\widetilde{\omega}_j t - \varphi_j + \theta_j) \tag{5.31}$$

6. Modal Parameters Identification

As referred in Chapter 4, if the Fourier transform of a mother wavelet $\psi(t)$ is sharply concentrated near a fixed value $\omega = \omega_j$ of frequency, the continuous wavelet transform tends to "concentrate" near a series of curves in the time–frequency domain, called the ridges of the transform. The ridge, let it be referred to as $a_r(b)$, has an interesting property: it describes the frequency modulation law of the signal. This property can be utilized to extract important features of the original signal which can be associated with the modal parameters of the under study system.

6.1 Canonical representation of a real signal

Physical signals $u(t)$ obtained from vibration measurement are real valued and in the time domain. Following the concepts presented in Chapter 3 and since by definition the instantaneous angular frequency is the derivative of phase with respect to time [25], there is a need for the signal to be expressed by canonical representation. An arbitrary real monocomponent signal $u(t)$ can always be represented in terms of instantaneous modulus $\mathrm{A}_u(t)$ and instantaneous phase $\varphi_u(t)$, in the form:

$$u(t) = A_u(t)\cos[\varphi_u(t)] \tag{6.1}$$

where $\mathrm{A}_u(t) \geq 0$, and $\varphi_u(t) \in [0, 2\pi)$

Multicomponent signals then may be expressed canonically as the sum of two or more monocomponent signals:

$$u(t) = \sum_{j=1}^{\mathrm{N}} A_u(t)\cos[\varphi_u(t)] \tag{6.2}$$

As referred in section 4.3.8, choosing an appropriate value of Q allows to isolate coupled modes, therefore it can be assumed that multicomponent signals have components which do not interact. Consequently, the analysis can be restricted to a domain where the wavelet coefficients of all but one component are negligible, allowing to treat each component as a monocomponent signal (which is one of the advantages of employing a time–frequency analysis). That being the case, the following theory focuses on monocomponent signals.

Continuing with *equation 6.1*, differentiating the phase $\varphi_u(t)$ with respect to time gives the instantaneous angular frequency:

$$\omega_u(t) = \frac{d\varphi_u(t)}{dt} = \dot{\varphi}_u(t) \tag{6.3}$$

However, there is a problem with this representation: the pair of $[A_u(t), \varphi_u(t)]$ is far from unique since there are infinite such pairs that can be associated with the real signal $u(t)$. This obstacle can be overcome with the use of the Hilbert Transform, which can be utilized as described in the following sub–chapter.

6.2 Hilbert Transform

The Hilbert transform of u can be considered as the convolution of the function (or signal) $u(t)$ with the function $h(t) = \frac{1}{\pi t}$, known as the Cauchy kernel. Because $\frac{1}{t}$ is not integrable across $t = 0$, the integral defining the convolution does not always converge. Therefore, the Hilbert transform is given by:

$$H_u(t) = u(t) * \frac{1}{\pi} = \frac{1}{\pi} p.v. \int_{-\infty}^{+\infty} \frac{u(\tau)}{t-\tau} d\tau, \quad t \in \mathbb{R} \tag{6.4}$$

where p.v.[·] denotes the Cauchy principal value of the improper integral (i.e., to account for the $t = \tau$ situation).

In the frequency domain, the Hilbert transform has a very useful form:

$$\widehat{H_u}(\omega) = -isgn(\omega)\hat{u}(\omega), \quad \omega \in \mathbb{R} \tag{6.5}$$

where $sgn(\omega)$ is the sign function of a real number.

6.3 Analytic Signals and Instantaneous Frequency

An analytic signal is defined as a complex–valued function that has no negative frequency components, therefore, the analytic signal $Z_u(t)$ associated with a real–valued signal of finite energy $u(t)$ is obtained by a linear filtering of $u(t)$ canceling its negative frequencies. By using the Hilbert transform, $Z_u(t)$ can be defined (up to a factor 2) as $u(t)$ signal's orthogonal projection onto the subspace $H^2(\mathbb{R})$ of $L^2(\mathbb{R})$:

$$Z_u(t) = u(t) + iH_u(t) \tag{6.6}$$

Note that $\mathrm{Re}[Z_u(t)] = u(t)$. It should be mentioned also that, although an analytic signal contains no negative frequencies, it may have a spectral component at zero frequency. Considering the previous sub–chapter's observation, the Fourier Transform of an analytic signal is given by:

$$\widehat{Z_u}(\omega) = \hat{u}(\omega) + i\widehat{H_u}(\omega) =$$

$$= \hat{u}(\omega) - i^2 sgn(\omega)\hat{u}(\omega)\hat{u}(\omega) =$$

$$= \hat{u}(\omega) + sgn(\omega) =$$
$$= \begin{cases} 2\hat{u}(\omega), & \text{if } \omega \geq 0 \\ 0, & \text{if } \omega = 0 \end{cases}$$

$$= 2\hat{u}(\omega)\Theta(\omega) \tag{6.7}$$

where $\Theta(\omega)$ denotes the Heaviside step function.

By definition, $Z_u(t)$ is an analytic function in the upper half complex plane (hence the term analytic). If one assumes a pair $[A_u(t), \varphi_u(t)]$, where $A_u(t) = |Z_u(t)| \geq 0$ and $\varphi_u(t) = \angle [Z_u(t)] \in [0, 2\pi)$, the function $Z_u(t)$ has a unique polar coordinate representation:

$$Z_u(t) = A_u(t)e^{i\varphi_u(t)} \tag{6.8}$$

where

$$A_u(t) = |Z_u(t)| = \sqrt{\left[\mathrm{Re}(Z_u(t))\right]^2 + \left[\mathrm{Im}(Z_u(t))\right]^2} \tag{6.9}$$

and

$$\varphi_u(t) = \angle(Z_u(t)) = \arctan\left(\frac{\mathrm{Im}(Z_u(t))}{\mathrm{Re}(Z_u(t))}\right) \tag{6.10}$$

Applying this canonical pair $[A_u(t), \varphi_u(t)]$ to *equation 6.1*, a unique representation of the form can be determined and it is defined as the canonical representation of a real signal. The instantaneous angular frequency then can be defined by setting $\varphi_u(t) = \angle[Z_u(t)]$ in *equation 6.3* as:

$$\omega_u(t) = \frac{d\varphi_u(t)}{dt} = \frac{d\angle(Z_u(t))}{dt} \tag{6.11}$$

This is the most direct method for determination of instantaneous frequency, and is easy to implement. However it is important to note that although this definition of the instantaneous frequency is always valid mathematically, its physical meaning can be doubtful in some particular situations, especially when the signal $u(t)$ is not oscillating enough, i.e. when $\varphi_u(t)$ varies slowly compared to $A_u(t)$, or when the frequency $\omega_u(t)$ itself has fast variations [2],[20].

6.4 Ridge definition and extraction

6.4.1 One component signal

As it has been shown the CWT of an asymptotic signal will tend to "concentrate" in the neighborhood of a curve $a_r(t)$ called "ridge" that consists of an aggregation of points called ridge points. The ridge points are commonly obtained either from the CWT modulus of the signal, or from its phase, and are called amplitude ridge points and phase ridge points, respectively [33].
In the time–scale map, a ridge can be defined (reference [32]) from its canonical phase $\varphi_u(t)$ by:

$$a_r(t) = \frac{2\pi f_\psi^*}{\dot{\varphi}_u(t)} \tag{6.12}$$

where f_ψ^* appears in the chosen mapping between scale and frequency (see more in [40]).

The restriction of the CWT to the ridge $a_r(t)$, is called the "skeleton" of the wavelet transform.

From the skeleton, it is possible to reproduce the signal, or more precisely, what is associated with the analytical signal $Z_u(b)$, while it behaves like the product of $Z_u(b)$ by a multiplicative factor entirely characterized by the mother wavelet and the ridge $a_r(b)$:

$$T_\psi[u](a_r(b),b) = \frac{1}{2}\bar{\hat{\psi}}(a_r(b)\dot{\varphi}_u(b))Z_u(b) = \frac{1}{2}\bar{\hat{\psi}}(2\pi f_\psi^*)Z_u(b) \tag{6.13}$$

The process of estimating the ridge from the absolute value and/or from the phase information of the CWT of the signal is called "ridge extraction". Different techniques for extracting ridges exist [2] and can be classified into two categories: the "differential" and the "global" methods [31].

Differential methods rely on local properties of the CWT of the signal $u(t)$, they are verified theoretically on the ridge curve and they are based on the partial differential equations of the CWT. The differential method used here is based on the modulus of $T_\psi[u](a,b)$, which is maximum at b in the vicinity of the ridge, and therefore verifies a cancellation of its partial derivative at a. This definition is given in [33] and its implementation has the advantage that it is particularly simple and stable since it is a simple search for maxima.

The global methods, introduced in reference [34], are based on the search for curves that maximize the energy of the CWT while maintaining a certain regularity of the solution. When the considered frequency and amplitude modulated signal is embedded in noise and near the ridges, the contribution of the signal is much larger than that of the noise, while the wavelet transform of the noise spreads in the whole time–frequency plane. Several algorithms for global ridge extraction are detailed in the book by Carmona et al. [2] and are discussed with reference to their robustness to noise.

Once the ridge extraction method has been chosen and the ridge has been determined, the analytical signal $Z_u(b)$ can be obtained. Its real and imaginary parts give the signal and its Hilbert transform, respectively. The final goal of ridge extraction is to get an estimate of $\dot{\varphi}_u(t)$ from *equation 6.12* and then of $Z_u(b)$ feeding it back into *equation 6.13*.

6.4.2 Multicomponent signals

The analytical expression of the structural responses of linear systems is well–known, even in the case of non–proportionally damped systems [35]. The aim of this section is to characterize the behavior of structures from multi–channel dynamic signals obtained from measurements made by a set of N sensors, typically accelerometers. The set of displacement measurements at these sensor points is grouped into the vector: $\boldsymbol{u} = [u_1, u_2, \ldots, u_N]^T$. Note that this notation is generic and can also be used when the signal is an acceleration. The modal decomposition expresses the state equation as a linear combination of the various modes of the system. Thanks to the modal decomposition approach for linear systems, every signal can be expanded as a linear combination of the different modes of the system, e.g. *M* components, each corresponding to a different eigen−mode of the structure [35]. The CWT of each component of $\boldsymbol{u}$ is also grouped in the vector $\boldsymbol{T}_\psi[\boldsymbol{u}]$, as follows:

$$\boldsymbol{T}_\psi[\boldsymbol{u}](a,t) = [T_\psi[u_1](a,t),\ T_\psi[u_2](a,t),\ \ldots, T_\psi[u_N](a,t)]^T \tag{6.14}$$

Therefore, the displacement $u_k(t)$, taking into account the *M* modes, can be obtained as:

$$u_k(t) = \Re \sum_{l=1}^{M} \left\{ A_l^{u_k}(t)\, e^{i\theta_l^{u_k}(t)} \Phi_k^{(l)} \right\} \tag{6.15}$$

where $A_l^{u_k}(t)e^{i\theta_l^{u_k}(t)}$ is the analytical modal participation factor of the *l*–th complex mode being its *k*–th component) to the structural response $u_k(t)$, while its real part are assumed to be asymptotic. The real part of u_k is $A_l^{u_k}(t)\cos(\theta_l^{u_k}(t))$.

The vector φ is the complex *l*–th mode, which we have chosen to normalize as $(\varphi^{(l)})^T \varphi^{(l)} = 1$, based on the generalisation of a criterion usually used for real modal deformations: $\|\varphi^{(l)}\|^2 = 1$ (cf. Carpine [30]). In the case of free responses, the dynamic signals contain the vibrations of each mode of the structure, associated with an exponentially damped sinusoidal component. Thus, *equation 6.15* becomes:

$$u_k(t) = \Re \sum_{l=1}^{M} \left\{ A_l^{u_k}(t)\, e^{i\theta_l^{u_k}(t)} \Phi_k^{(l)} \right\} = \Re \sum_{l=1}^{M} \left\{ Z_l^{u_k}\, e^{i\lambda_l t} \Phi_k^{(l)} \right\} \tag{6.16}$$

where $Z_l^{u_k}$ is a complex constant, $\lambda_l = 2\pi i f_l \sqrt{1-\xi_l^2} - \xi_l 2\pi f_l$ is the *l*–th pole and f_l, ξ_l are the eigen–frequency and the modal damping ratio associated with mode *l*, respectively.

With the aid of the above form, which is a sum of asymptotic amplitude and frequency modulated components, in the case of a single asymptotic amplitude and frequency modulated signal, the absolute value of its CWT tends to concentrate near the "ridges" of the transform [2]. In the time–frequency plane, the ridge is a well–defined region, but most importantly, the wavelet transform acts as a "regularizing" filter that concentrates the information that is carried within the signal and hence allows to characterize the instantaneous frequencies.

Based on the discussion above, the linearity of the CWT and a good choice of the mother wavelet ψ can allow to separate these different components and extract the ridge for each of them. There are several approaches for detecting multiple ridges, the final choice depends on their interaction, or their independence. When these ridges do not interact and are located at distinct regions of the time–frequency plane, a frequently encountered case in the analysis of dynamic signals for which each instantaneous frequency remains in the vicinity of a horizontal straight line, the methods previously mentioned can be implemented as in [31], [36].

As previously discussed, the ridges can then be deduced using *equation 6.12*. A common problem is when there are two close eigen–frequencies, f_j and f_k. The possibility of extracting the ridges is guaranteed if the following condition is satisfied:

$$\xi_j \leq \frac{\sqrt{2}}{c_f}\frac{|f_j - f_k|}{f_j} \tag{6.17}$$

,where c_f is a constant related to edge effects [37], ξ_j is the modal damping ratio of the j–th mode and the j and k indexes correspond to two neighboring modes j and k, respectively. If the condition of *equation 6.17* is not met, the extraction of accurate ridges is not guaranteed and may even not be possible since the modes are too close and they cannot be separated in the case that they are heavily damped. This tells us that two close modes cannot be well separated from each other if they are damped too much. *Figure 6.1* plots the ξ_j values as function of f_j and $\Delta f = |f_j - f_k|$ for $c_f = 3$.

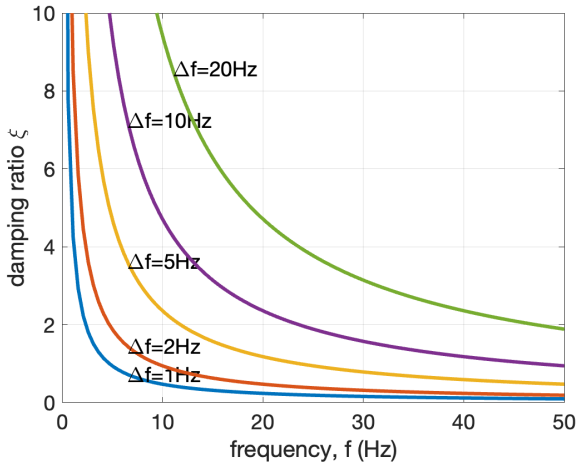

Figure 6.1: Relationship between damping ration and frequency for ridge identification according to equation 6.17 ($c_f = 3$).

As already discussed, at each measurement point u_k, $k \in [1, N]$, a set of ridges $a_k^{(l)}(t)$ can be extracted from the time–frequency plot, for the l–th mode excited by the shock, where $l = 1, 2, \ldots, M$. For the extraction of ridges, differential methods based on a local analysis of the extrema of the CWT modulus are here preferred. Thus the ridges, or the instantaneous frequencies $a_l^{(k)}(t)$, are extracted by the computation of local maxima of $|T_\psi[u_k](a,t)|$ as function of time t and for the l–th mode excited by the shock:

$$a_l^{(k)}(t) = arg_a max |T_\psi[u_k](a,t)| \tag{6.18}$$

So, for a mode l, a set of $k = 1, 2, \ldots, M$, ridges $a_l^{(k)}(t)$ is obtained, and a procedure to retain only one ridge for the instantaneous frequency must be then made, in [31], for example assuming the average of the k signals:

$$a_l^{mean}(t) = \frac{1}{N} \sum_{k=1}^{N} a_l^k(t) \tag{6.19}$$

An alternative way of obtaining a single ridge a for mode l instead of several ridges (one for each measurement point) was recently been proposed by the authors in [29]. This new procedure is based on the computation of the Averaged Continuous Wavelet Transform (ACWT) $\widetilde{T}_\psi[\boldsymbol{u}](a,b)$, which combines the CWTs of each measurement point $u_k(k \in [1, N])$, as follows:

$$\widetilde{T}_\psi[\boldsymbol{u}](a,b) = \sum_{k=1}^{N} [T_\psi[u_k](a,b)]^2 \tag{6.20}$$

Equation 6.20 is suitable for ridge extraction in the case of free responses of systems whose eigen−vectors are real or with a negligible imaginary part, which is the case of weakly damped systems [35] and practically refers to all civil engineering structures. In fact, the use of the squares of the transforms makes it possible to orient the contributions of the useful signal in each measurement channel according to the same orientation in the complex plane, while those of noise remain a priori randomly distributed. Therefore, *equation 6.20* allows to obtain a single ridge a for mode l as follows:

$$a_\Sigma^{(l)}(t) = arg_a max \left| [\widetilde{T}_\psi[\boldsymbol{u}](a,b)] \right|^{\frac{1}{2}} = arg_a max \left| \sum_{k=1}^{N} [T_\psi[u_k](a,b)]^2 \right|^{\frac{1}{2}} \tag{6.21}$$

Finally, for both definitions of the ridges, i.e., $a_l^{mean}(t)$ *equation 6.18*, or $a_\Sigma^{(l)}(t)$ *equation 6.21* a procedure has been proposed in [29] to smooth the result of the maxima obtained for each time t; for two neighboring points in frequency of a maximum to the right and to the left make it possible to perform a parabolic interpolation from which we obtain the coordinates of a new ridge in the time scale plane for the mode l under consideration $(t, \breve{a}_k^{(l)}(t))$, or $(t, \breve{a}_\Sigma^{(l)}(t))$. A procedure for chaining the discrete points of the time–frequency plane to transform them into ridges is finally performed [2]. The set of maxima of the absolute value of the CWT along the ridges present in the signal forms the skeleton of the CWT of the signal. According to the definition chosen for a ridge l in *equation 6.18* or in

equation 6.21, the absolute value of the CWT along each ridge $T_\psi[u](\breve{a}_k^{(l)}(t),t)$ or the ACWT along the single ridge $\widetilde{T}_\psi[\boldsymbol{u}](\breve{a}_\Sigma^{(l)}(t),t)$ is preferred.

6.5 System Dynamic Characterization

The modal parameters of a system under transient vibrations can be identified by extracting the ridges and the skeleton of the CWT time–frequency representation. Once the ridges of the CWT have been extracted, the instantaneous frequencies, the modal damping ratio and the modal shapes can be estimated. If the system is purely linear, the shape of the ridges associated with the eigen–frequencies will be a straight horizontal line. Furthermore, the damping ratio of the modes of interest can be estimated from the exponential decrease in amplitude associated with these ridges, and finally the modal shapes can be obtained from the relative amplitudes and phase shifts between the channels corresponding to the different sensors.

Therefore, the extraction of the "ridges" is a critical aspect for the successful application of the CWT for modal identification in the case of transient structural responses. Among the authors who have used the CWT for modal identification from transient structural responses, we can cite two references published in 1997: Staszewski [49] and Ruzzene *et* al. [38]. Staszewski [49] proposed several CWT–based methods for estimating damping ratios and applied them to simulated multi Degree–of–freedom (DOF) systems. Ruzzene *et* al. [38] showed that the CWT analysis of the free response of a system allows the estimation of its natural frequencies and viscous damping ratios. A more complete procedure, which also gives access to frequencies and modal shapes, can be found in Lardies & Gouttebroze [39]. In Le & Argoul [31], the authors propose a more precise and complete method where the choice of the mother wavelet, its quality factor and the management of the edge effects of the TOC are studied in depth. The subsequent article by Erlicher & Argoul [36] discusses the use of this procedure in the case of systems with non–proportional damping, and therefore in the presence of complex deformations.

For amplitude and phase modulated signals of the form: $u(t) = A(t)\cos(\varphi(t))$, the restriction of the wavelet transform to its ridge behaves mainly as the associated complex signal of $u(t)$: $A(t)\exp[i\varphi(t)]$. This representation also allows the reconstruction of such original signals in non–significant noise situations [2]. If the system behavior is close to be linear, from the CWT (or the ACWT) of its transient responses, the extracted ridges are similar to horizontal lines and the associated skeleton has an exponential decrease [31]. The logarithm $\log\left|T_\psi[u](\breve{a}_k^{(l)}(t),t)\right|$ for the CWT, or $\log\left|\widetilde{T}_\psi[\boldsymbol{u}](\breve{a}_\Sigma^{(l)}(t),t)\right|$ for the ACWT can be then deduced and the calculation of the slope of the "straight lines" for each mode l can be performed in order to estimate the corresponding modal damping ratio of the l–th mode. The slope allows to get an estimate to the near sign of the product $2\pi f_l\xi_l$ that is the reciprocal of the time constant characterizing the exponential decay of the l–th mode.

The calculation of the eigen–shapes requires a set of measurements grouped in the vector: $\boldsymbol{u} = [u_1, u_2,\ldots, u_N]^T$. The CWT of each component of $\boldsymbol{u}$ along the smoothed ridge $\breve{a}_\Sigma^{(l)}(t)$ mode l are also grouped in the vector $\boldsymbol{T}_\psi[\boldsymbol{u}]$, as follows:

$$\boldsymbol{T}_\psi[\boldsymbol{u}](\breve{a}_\Sigma^{(l)}(t),t) = [T_\psi[u_1](\breve{a}_\Sigma^{(l)}(t),t), T_\psi[u_2](\breve{a}_\Sigma^{(l)}(t),t),\ldots, T_\psi[u_N](\breve{a}_\Sigma^{(l)}(t),t)]^T \tag{6.22}$$

Depending on the choice made for the definition of the ridge, i.e. either *equation 6.18*, or *equation 6.21*, the instantaneous complex modal shapes $\varphi^{(l)}(t)$ can be derived from the relative amplitude and phase of the CWT calculated along each ridge. There are several ways to normalise the modal vector. One way is to choose the unit amplitude for the measurement point u_{max}, where the max index corresponds to the measurement point where the modal amplitude is greatest [31]. The k–th component $\varphi_k^{(l)}(t)$ of the "instantaneous" complex mode can be expressed as follows:

$$\varphi_k^{(l)}(t) = \frac{T_\psi[u_k](\breve{a}_k^{(l)}(t), t)}{T_\psi[u_{max}](\breve{a}_l^{(l)}(t), t)} \tag{6.23}$$

As already discussed above, in this work we prefer the following scaling condition: $(\varphi^{(l)}(t))^{\mathrm{T}}\varphi^{(l)}(t) = 1$ for instantaneous mode shape $\varphi^{(l)}(t)$ [29], [30]. This definition results to:

$$\varphi_k^{(l)}(t) = \pm\frac{\boldsymbol{T}_\psi[u_k](\breve{a}_\Sigma^{(l)}(t), t)}{[\boldsymbol{T}_\psi[\boldsymbol{u}](\breve{a}_\Sigma^{(l)}(t), t)^{\mathrm{T}}\boldsymbol{T}_\psi[\boldsymbol{u}](\breve{a}_\Sigma^{(l)}(t), t)]^{\frac{1}{2}}} \tag{6.24}$$

where the sign follows the continuity of $\varphi_k^{(l)}(t)$ over time. The amplitude of mode l is then equal to:

$$A_l(t) = \left|[\boldsymbol{T}_\psi[\boldsymbol{u}](\breve{a}_\Sigma^{(l)}(t), t)^{\mathrm{T}}\boldsymbol{T}_\psi[\boldsymbol{u}](\breve{a}_\Sigma^{(l)}(t), t)]^{\frac{1}{2}}\right| \tag{6.25}$$

To obtain a "constant" mode, especially in the case of linear behavior, the mean value over time, denoted $\bar{\varphi}$, can be calculated for each component k of the l–th mode:

$$\bar{\varphi_k}^{(l)}(t) = \frac{1}{t_f - t_i}\int_{t_i}^{t_f}\varphi_k^{(l)}(t)\,dt \tag{6.26}$$

The ACWT method is chosen for the numerical applications of the following chapters.

7. Applications of CWT

In this chapter the CWT method is tested on three structures. A 4–storey 2–d frame, an 8–storey 2–d frame and EuroProteas, a real–scale model structure. Also, the RDT Method is presented in order to calculate the damping ratios using ambient vibration measurements. Furthermore the function signal–to–noise ratio (SNR) and its influence are presented. The analyzed signals are imported into modal analysis software "ARTeMIS Modal" and the results are compared with the ones from the CWT.

7.1 Random Decrement Technique

The Random Decrement Technique (RDT) is a method used to estimate the damping ratio of a structure. This method is using the ambient vibration measurement of the structure and is extracting a RDT signature which represents the response equivalent to the damped free vibration response. This method is based on that the response of a dynamic system is composed of three response components. That is initial displacement, velocity and the force vibration response.

The intention of using the sampling technique is that averaging time segments of the ambient vibration measurement of a structure with a common triggering condition is to reduce the initial velocity response and the forced vibration response to zero. As number of segments increases the ensemble average of the forced vibration response tends to zero. If all segments in the average begin at the same threshold level and alternating positive and negative slope, then the response due to initial velocity is averaged out while the response due to initial displacement remains. Based on this explanation, the RDT signature is equivalent to a damped free vibration response of a structure to an initial displacement equivalent to the selection amplitude. The RDT signature δ is expressed by:

$$\delta_t = \frac{1}{\mathrm{N}} \sum_{i=1}^{\mathrm{N}} \left(x_{i,(t_i+r)} \right) \tag{7.1}$$

7.2 Signal–to–Noise Ratio

Signal–to–Noise Ratio (SNR or S/N) is a measure used in science and engineering that compares the level of a desired signal to the level of background noise. SNR is defined as the ratio of signal power to noise power, often expressed in decibels. A ratio higher than 1:1 (greater than 0 dB) indicates more signal than noise. [43]

SNR is an important parameter that affects the performance and quality of systems that process or transmit signals, such as communication systems, audio systems, radar systems, imaging systems, and data acquisition systems. A high SNR means that the signal is clear and easy to detect or interpret, while a low SNR means that the signal is corrupted or obscured by noise and may be difficult to distinguish or recover. SNR can be improved by various methods, such as increasing the signal strength, reducing the noise level, filtering out unwanted noise, or using error correction techniques. [43]

SNR also determines the maximum possible amount of data that can be transmitted reliably over a given channel, which depends on its bandwidth and SNR. This relationship is described by the Shannon–Hartley theorem, which is a fundamental law of information theory. [43]

SNR can be calculated using different formulas depending on how the signal and noise are measured and defined. The most common way to express SNR is in decibels, which is a logarithmic scale that makes it easier to compare large or small values. Other definitions of SNR may use different factors or bases for the logarithm, depending on the context and application. [43]

In this thesis, the SNR is applied in order to investigate how adding noise influences the modal parameter identification. This was made possible by using the Matlab toolbox.

7.3 4–storey 2d frame

The present system was modeled with 4 springs in series. Each spring represents one storey. Its stiffness was given directly. This means that there is no columns, beams, cross sections defined. The height of each storey can be assumed to be 3 meters high. The acting load, a white noise produced by Matlab's *randn* command, is performed on the structure's base. The load is applied with a time step of $T_Q = 0.001$ sec (sampling frequency $f_8 = 1000$ Hz) for a total duration of of 100 sec. The ambient vibration responses for each storey were extracted from OpenSees and then they were analyzed with CWT.

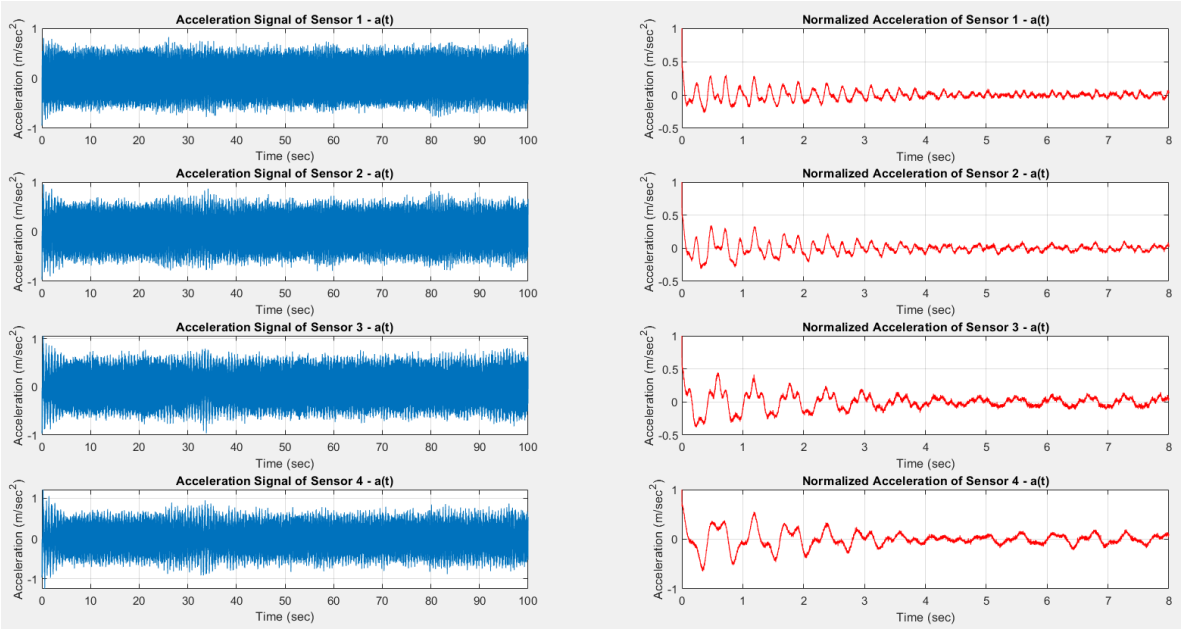

(a) *(b)*

Figure 7.1: Accelerograms (a) Ambient vibrations, (b) Normalized accelerations –free decay responses– after the application of RDT Method.

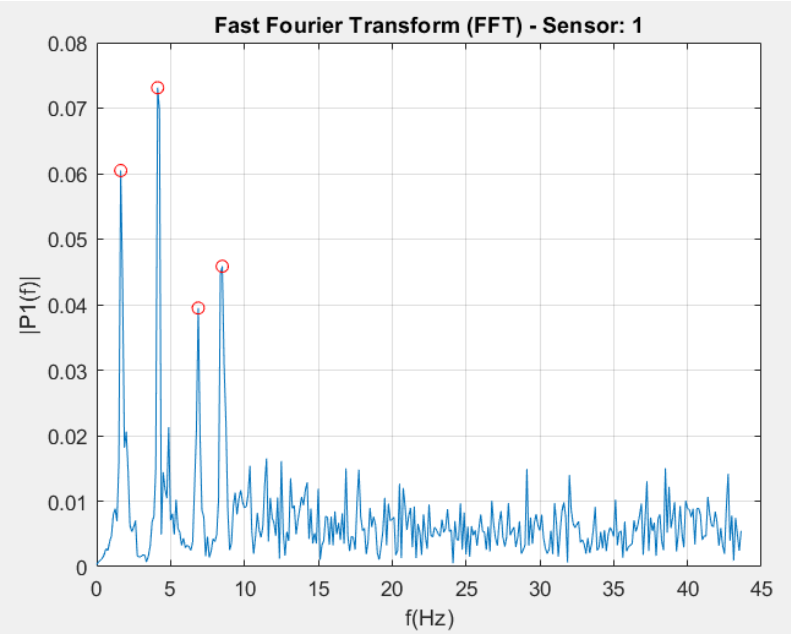

Figure 7.2: Fast Fourier Transform – FFT.

- *Ridges estimation with ACWT*

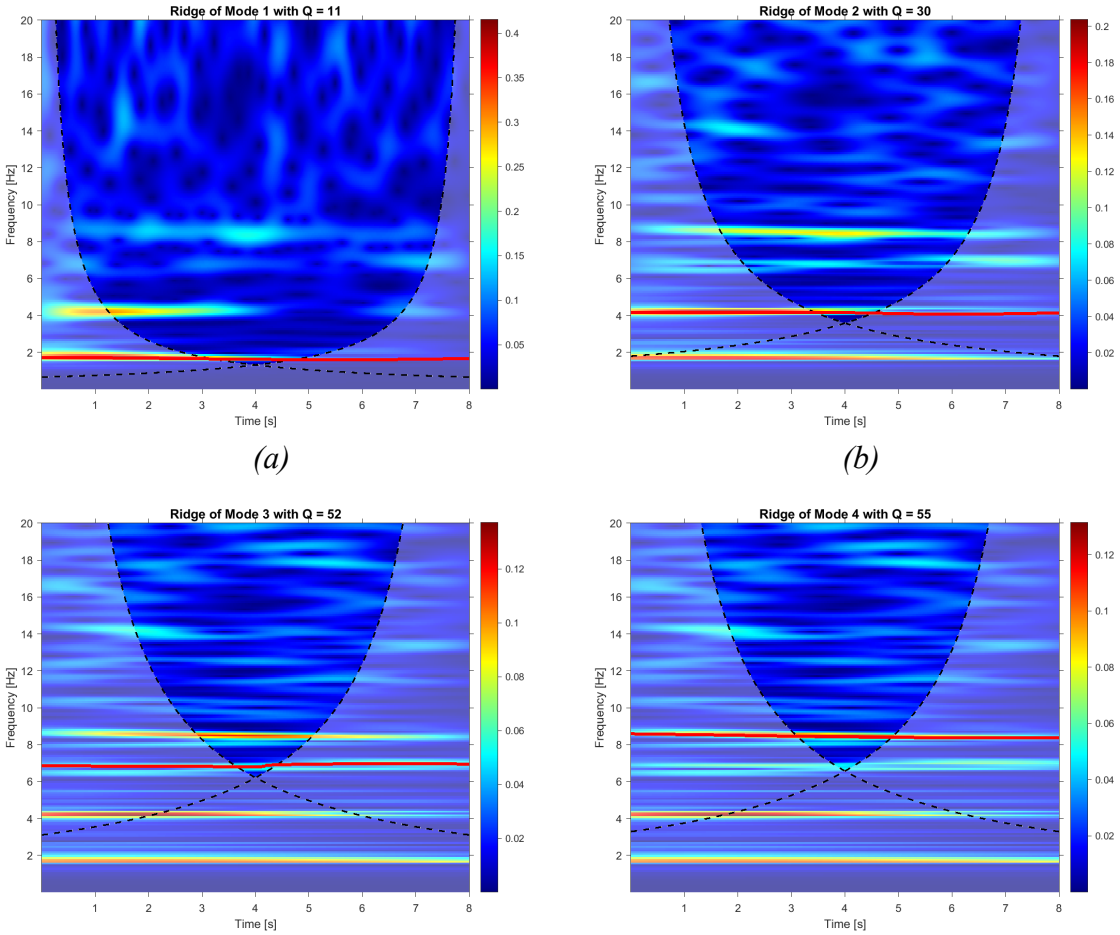

(a) *(b)*

(c) *(d)*

Figure 7.3: Time–frequency domain using ambient vibrations. Ridge extraction for each mode.

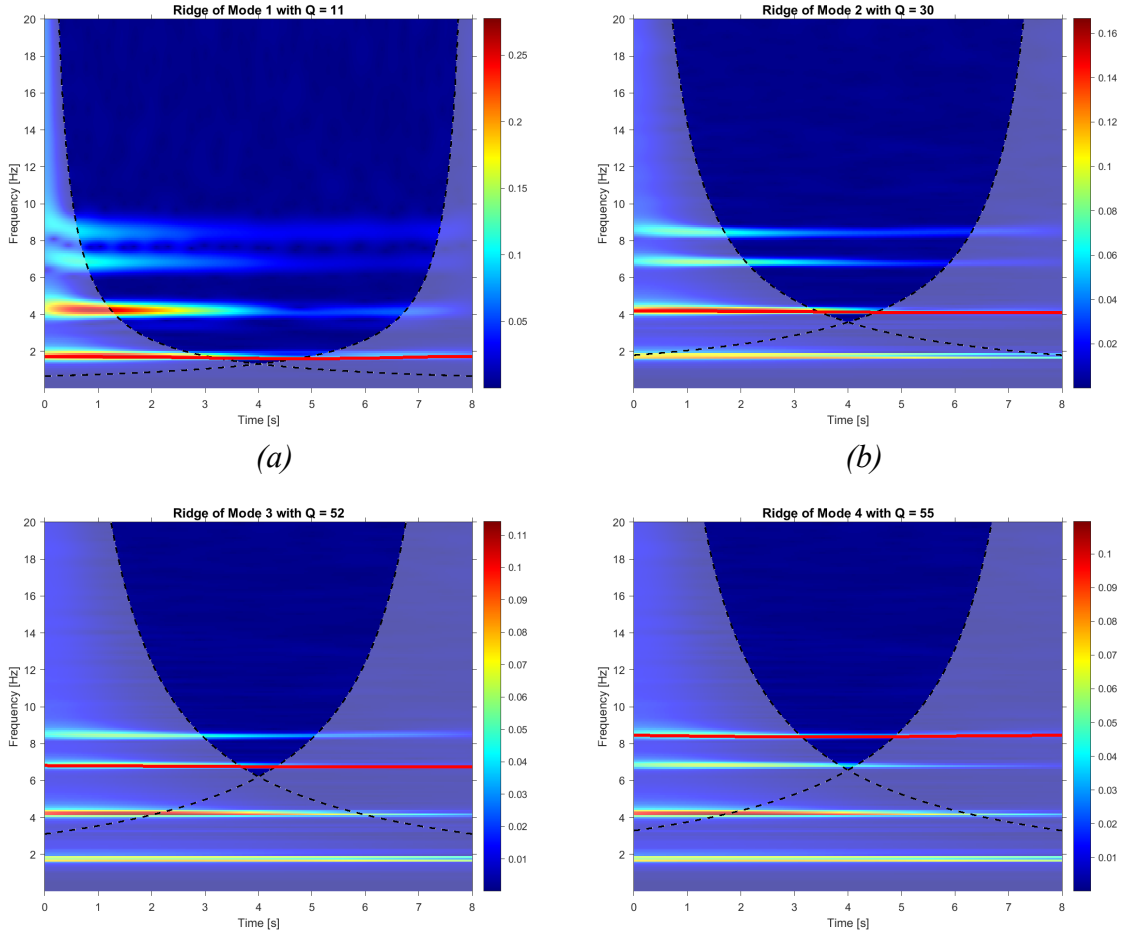

(a) *(b)*

(c) *(d)*

Figure 7.4: Time–frequency domain using free–decay responses. Ridge extraction for each mode.

- *Eigen–modes estimation*

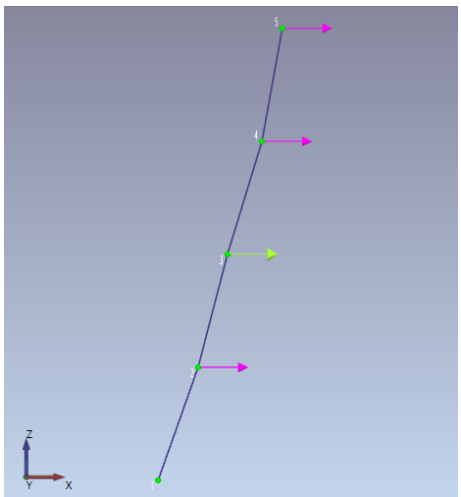

(a) 1st Eigen–mode

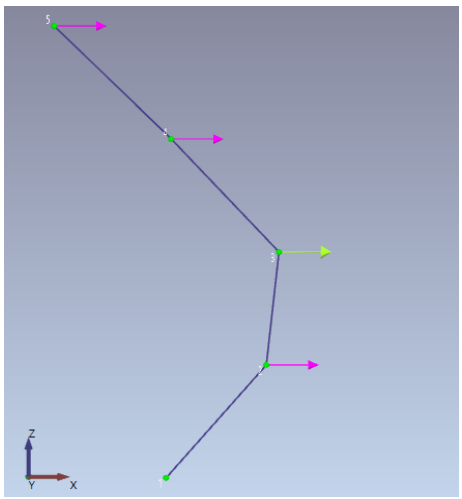

(b) 2nd Eigen–mode

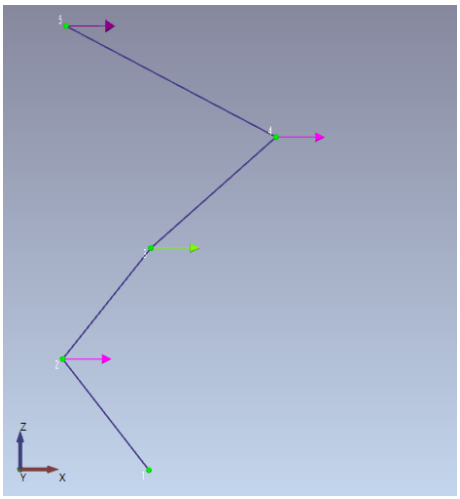

(c) 3rd Eigen–mode

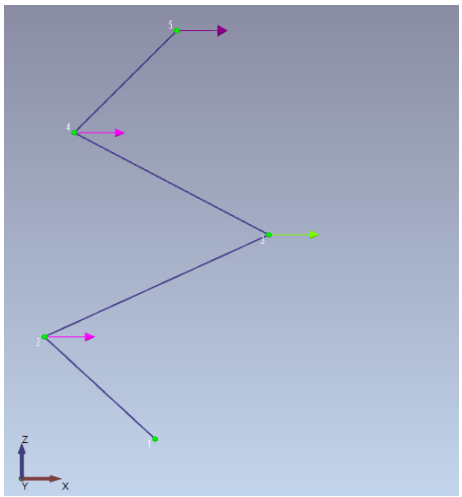

(d) 4th Eigen–mode

Figure 7.5: Eigen–modes estimation from ARTeMIS Modal.

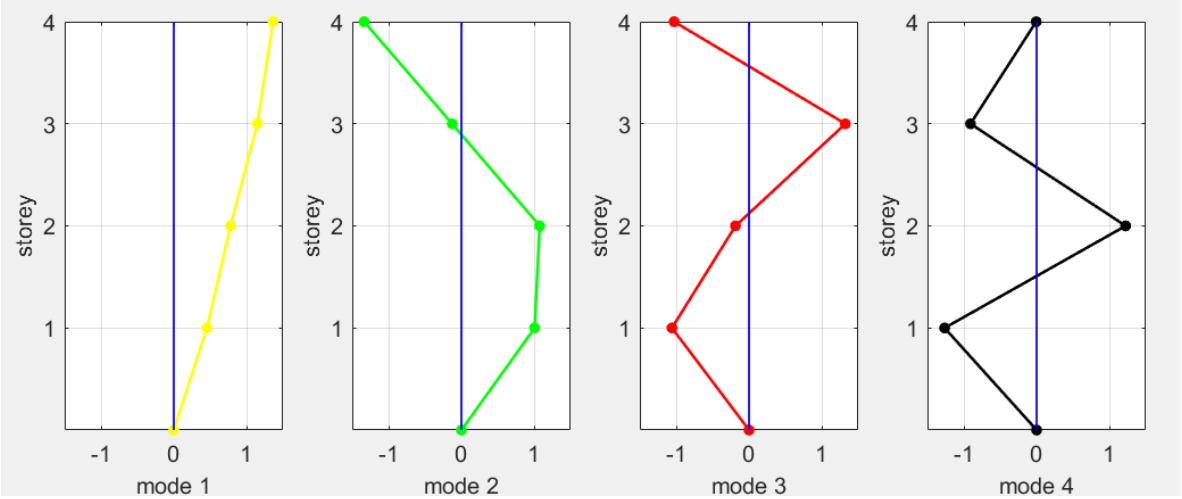

Figure 7.6: Eigen–modes estimation from ACWT.

- *Signal Reconstruction*

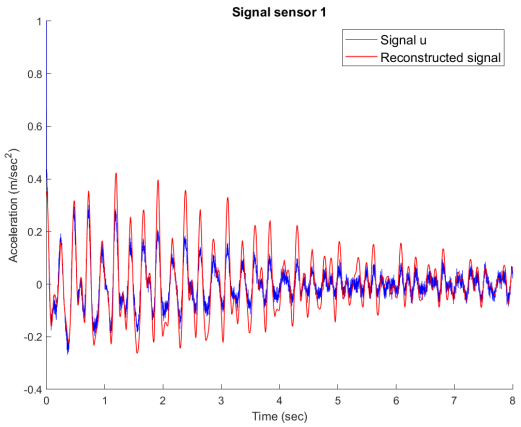

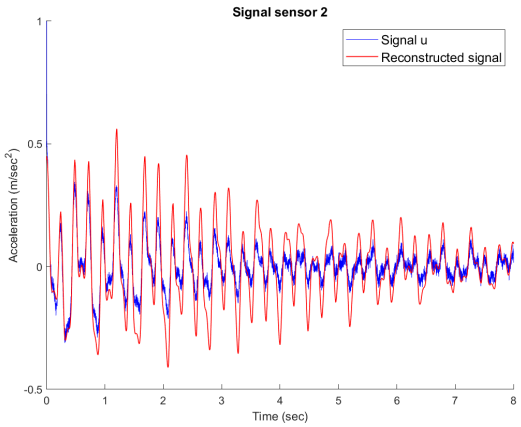

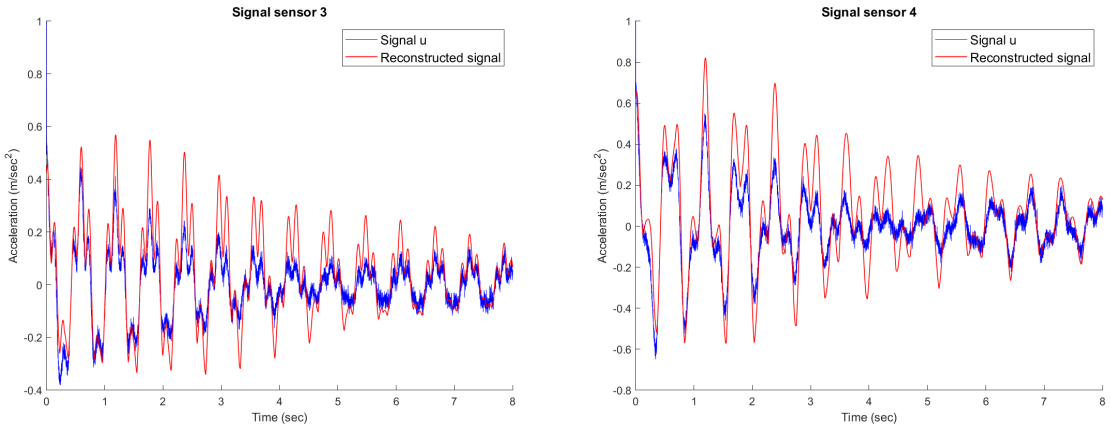

Figure 7.7: Reconstructed signals compared to the normalized signals

- *Eigen–frequencies*

Mode	OpenSees	ACWT	FFT	SSI–COV (ARTeMIS Modal–Automatic estimation)
1	1.69	1.62	1.625	(–)
2	4.17	4.15	4.125	4.172
3	6.78	6.85	6.875	6.79
4	8.40	8.42	8.5	8.39

- *Damping ratios*

Mode	OpenSees	ACWT (linFit)	expoFit	SSI–COV (ARTeMIS Modal–Automatic estimation)
1	0.0500	0.02626	0.0262	(–)
2	0.0497	0.012482	0.0118	0.02345
3	0.0663	0.005584	0.005835	0.00782
4	0.0783	0.004128	0.004832	0.00708

Addition of noise and comparison of the eigen−values using the signal–to–noise ratio.

- *Eigen–frequencies*

	SNR = ∞ (no additional noise)	**SNR = 49.7**		
Mode	**ACWT**	**FFT**	**ACWT**	**SSI–COV (ARTeMIS Modal)**
1	1.62	1.625	1.623	(–)
2	4.15	4.125	4.147	4.093
3	6.85	6.875	6.85	6.783
4	8.42	8.5	8.42	8.41

	SNR = 23.86			**SNR = 2.16**		
Mode	**FFT**	**ACWT**	**SSI–COV (ARTeMIS Modal)**	**FFT**	**ACWT**	**SSI–COV (ARTeMIS Modal)**
1	1.625	1.623	(–)	1.625	1.627	(–)
2	4.125	4.148	4.071	4.125	4.14	4.063
3	6.875	6.85	6.778	6.875	6.84	6.834
4	8.5	8.42	8.442	8.5	8.43	8.414

	SNR = 0.4			**SNR ≈ 0**		
Mode	**FFT**	**ACWT**	**SSI–COV (ARTeMIS Modal)**	**FFT**	**ACWT**	**SSI–COV (ARTeMIS Modal)**
1	(–)	1.64	(–)	(–)	(–)	(–)
2	4.25	4.17	(–)	(–)	(–)	(–)
3	(–)	6.72	6.809	(–)	(–)	(–)
4	(–)	8.427	8.41	(–)	(–)	(–)

- *Damping ratios*

	SNR = ∞ (no additional noise)	**SNR = 49.7**		**SNR = 23.86**	
Mode	**ACWT**	**ACWT**	**SSI–COV (ARTeMIS Modal)**	**ACWT**	**SSI–COV (ARTeMIS Modal)**
1	0.02626	0.0262	(–)	0.0262	(–)
2	0.012482	0.01255	0.03421	0.01294	0.04013
3	0.005584	0.00554	0.01801	0.005409	0.01736
4	0.004128	0.0041	0.00856	0.00412	0.00883

	SNR = 2.16		**SNR = 0.4**		**SNR ≈ 0**	
Mode	**ACWT**	**SSI–COV (ARTeMIS Modal)**	**ACWT**	**SSI–COV (ARTeMIS Modal)**	**ACWT**	**SSI–COV (ARTeMIS Modal)**
1	0.033	(–)	0.0354	(–)	(–)	(–)
2	0.011	0.03381	0.00137	(–)	(–)	(–)
3	0.01158	0.01941	0.02537	0.01678	(–)	(–)
4	0.00277	0.00792	0.0008	0.0087	(–)	(–)

7.4 8–storey 2d frame

The present system was modelled with 8 springs in series, similarily with the previous model. The white noise load is applied with a time step of T_Q = 0.001 sec (sampling frequency f_8 = 1000 Hz) for a total duration of of 100 sec.

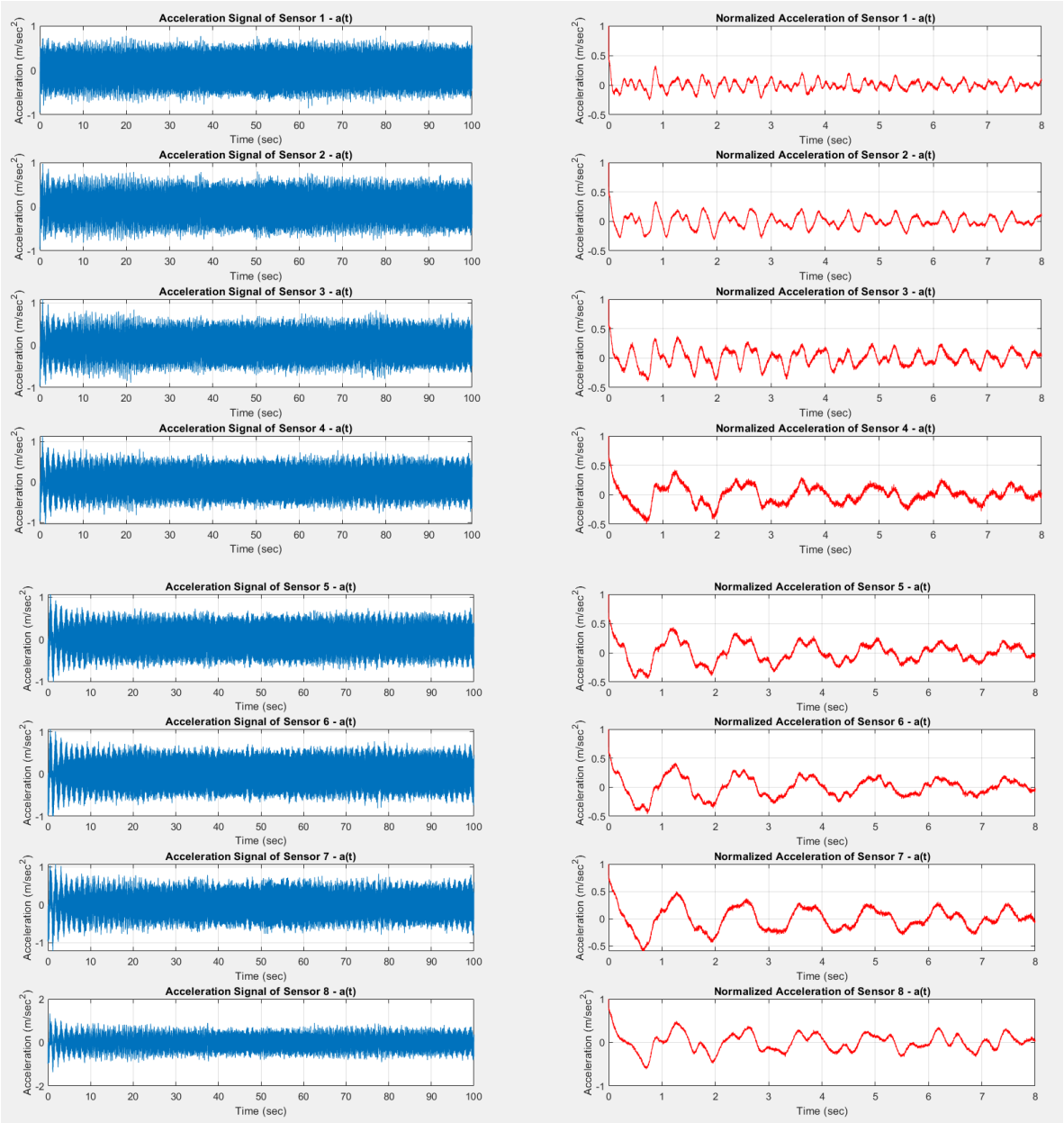

(a) *(b)*

Figure 7.8: Accelerograms (a) Ambient vibrations, (b) Normalized accelerations –free decay responses– after the application of RDT Method.

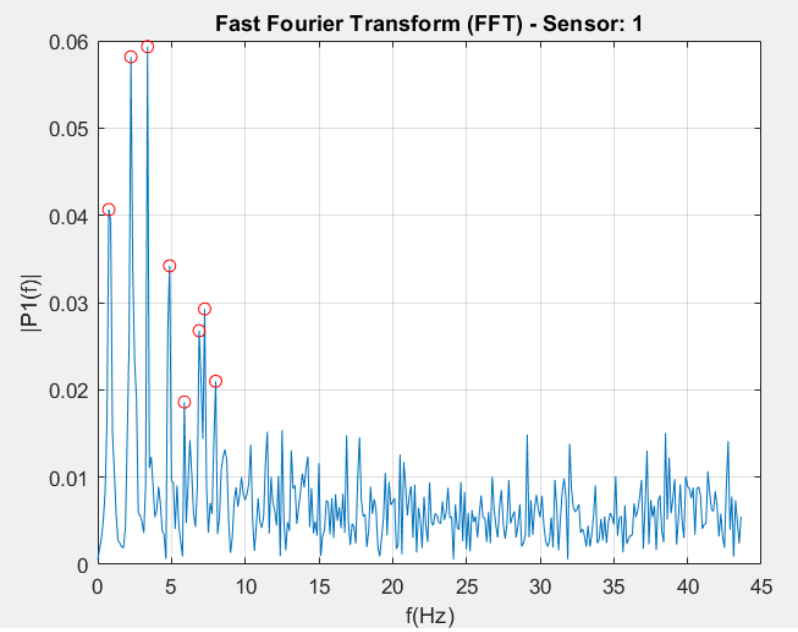

Figure 7.9: Fast Fourier Transform – FFT.

- *Ridges estimation with ACWT*

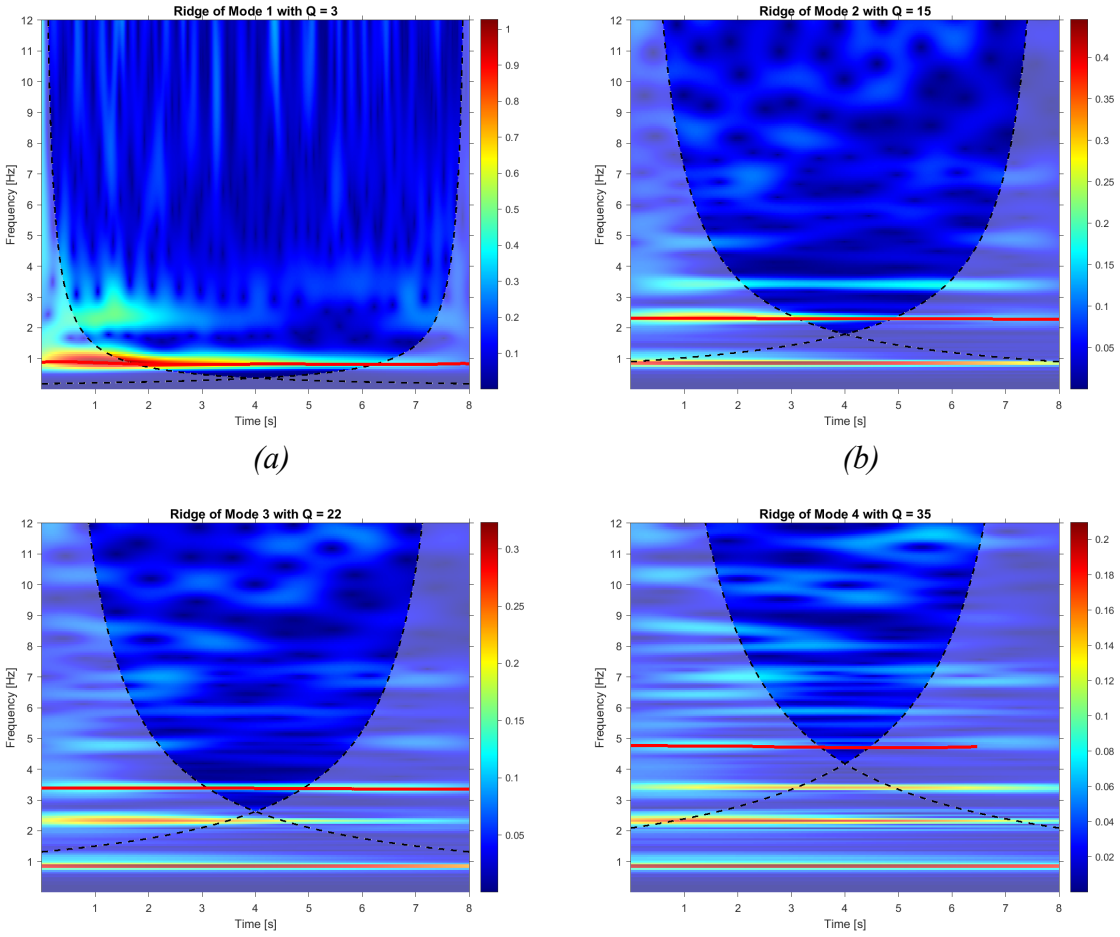

(a) *(b)*

(c) *(d)*

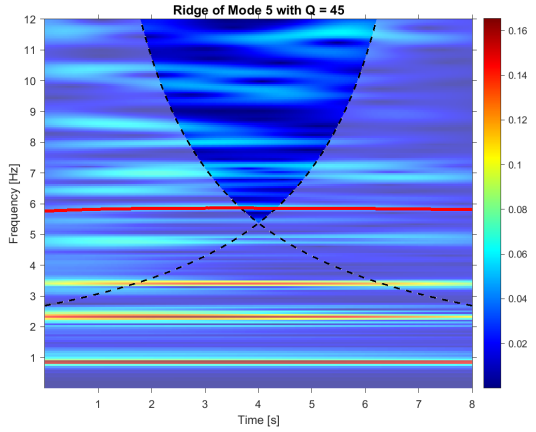

(e)

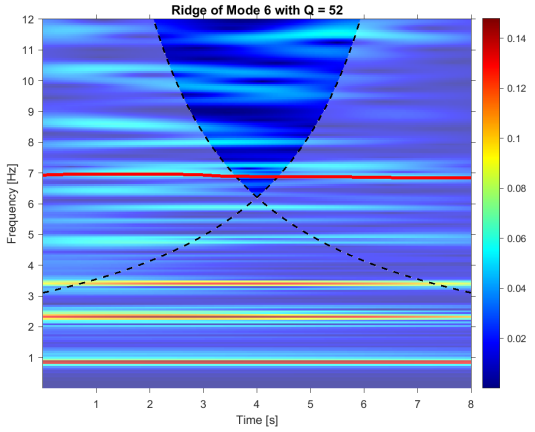

(f)

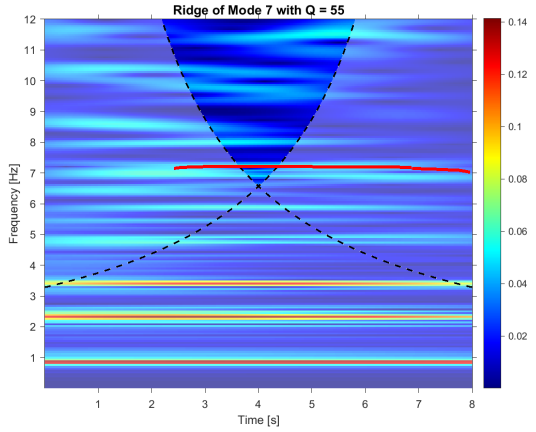

(g)

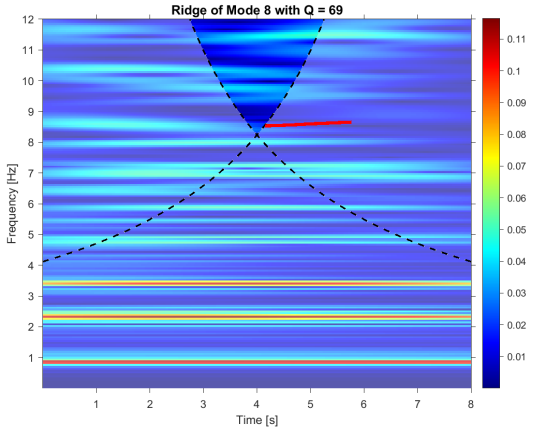

(h)

Figure 7.10: Time–frequency domain using ambient vibrations. Ridge extraction for each mode.

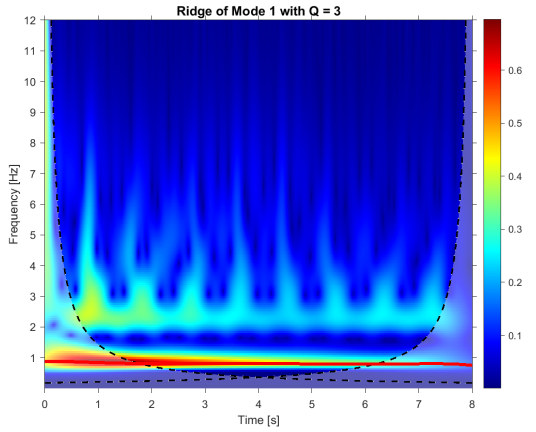

(a)

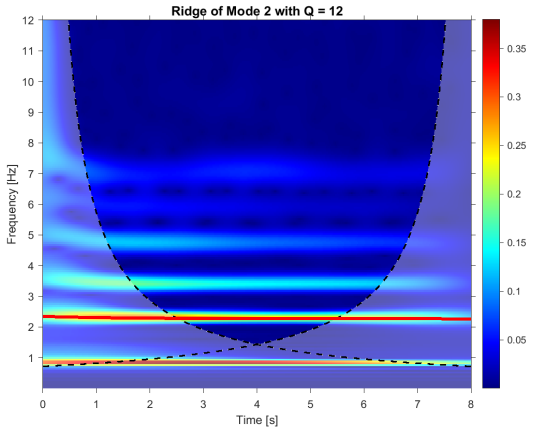

(b)

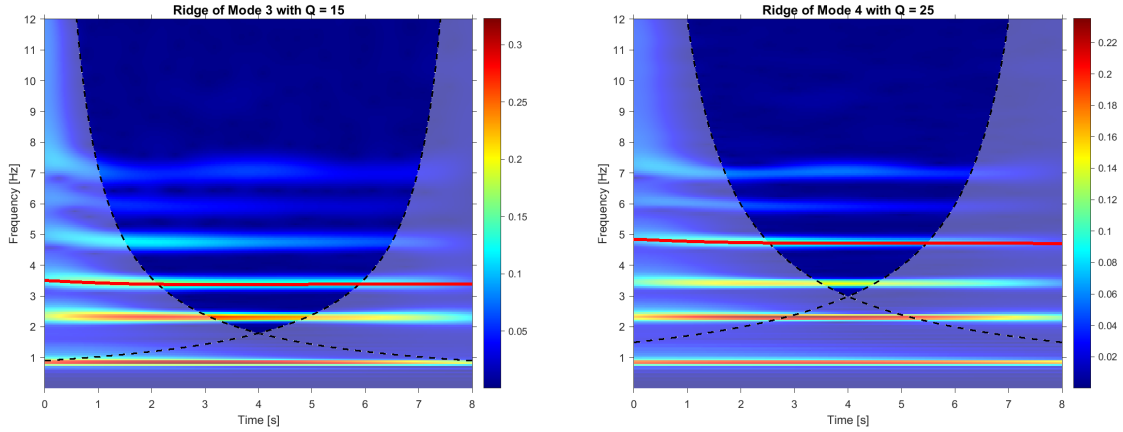

(c)

(d)

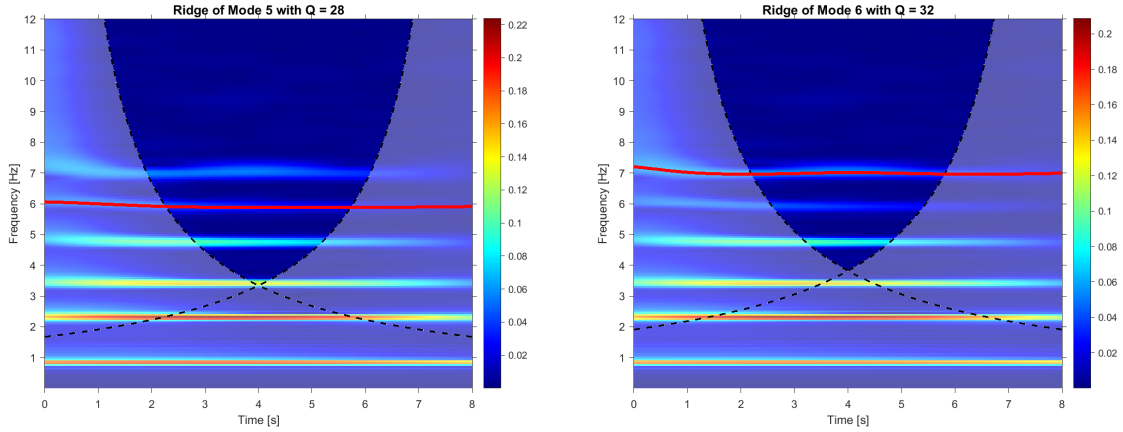

(e)

(f)

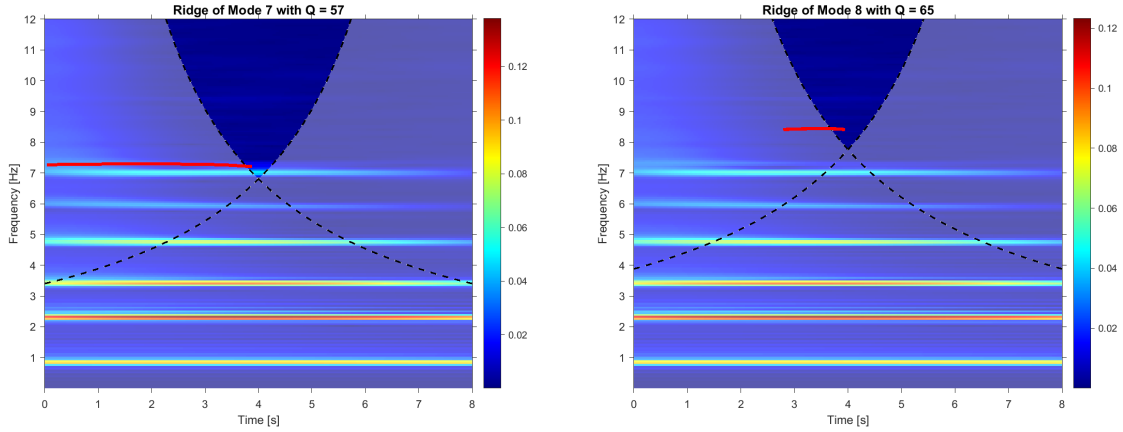

(g)

(h)

Figure 7.11: Time–frequency domain using free–decay responses. Ridge extraction for each mode.

➢ *Eigen–modes estimation*

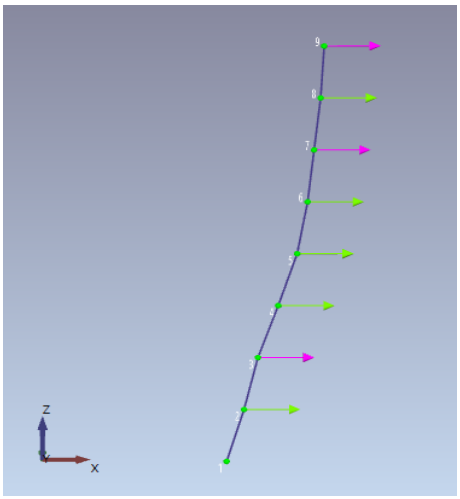

(a) 1st Eigen–mode

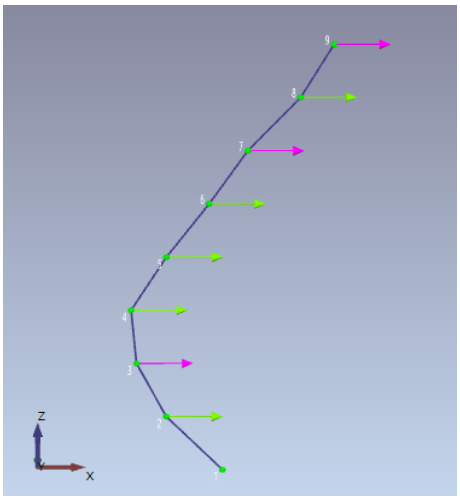

(b) 2nd Eigen–mode

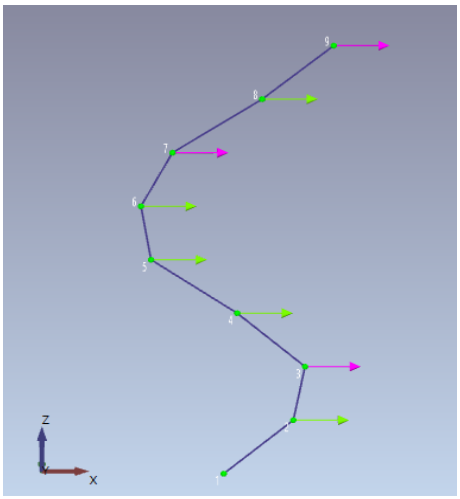

(c) 3rd Eigen–mode

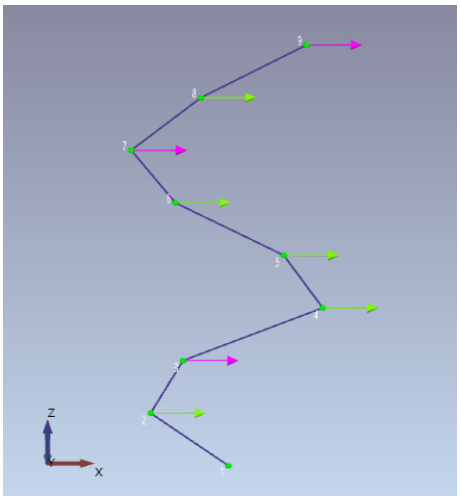

(d) 4th Eigen–mode

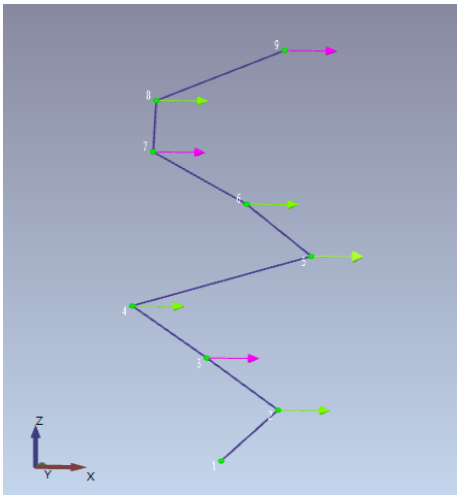

(e) 5th Eigen–mode

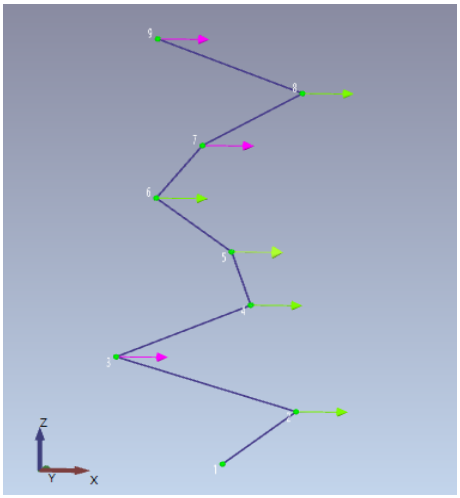

(f) 6th Eigen–mode

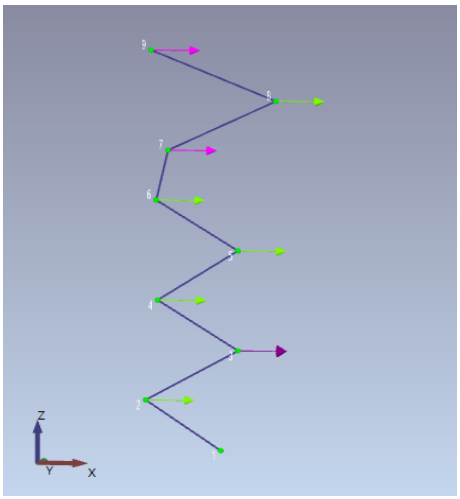

(–)

(g) 7th Eigen–mode

Figure 7.12: Eigen–modes estimation from ARTeMIS Modal.

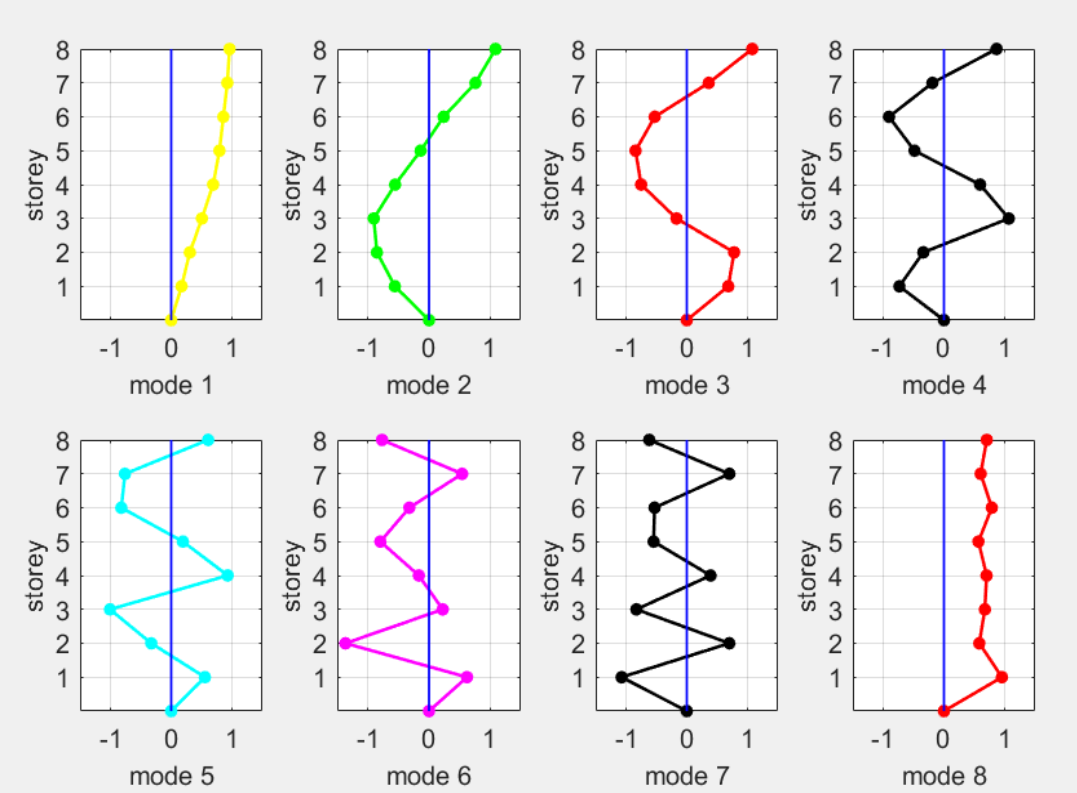

Figure 7.13: Eigen–modes estimation from ACWT.

➢ *Signal Reconstruction*

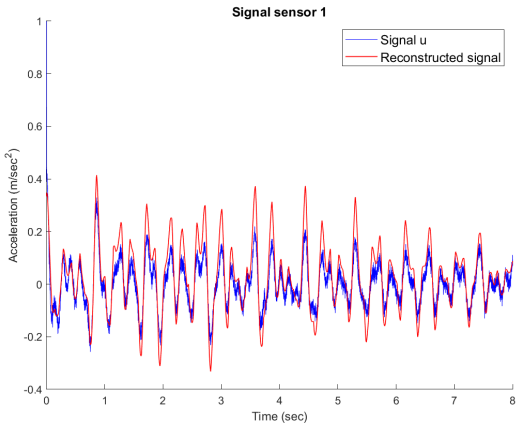

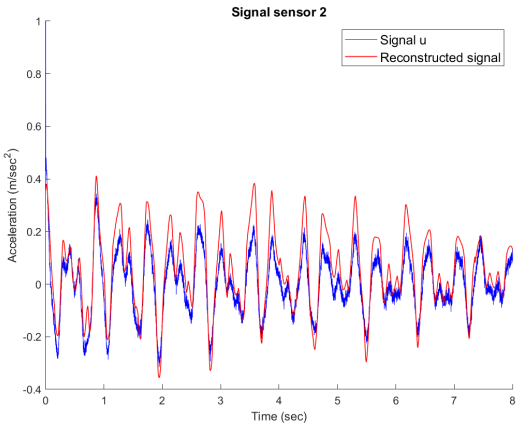

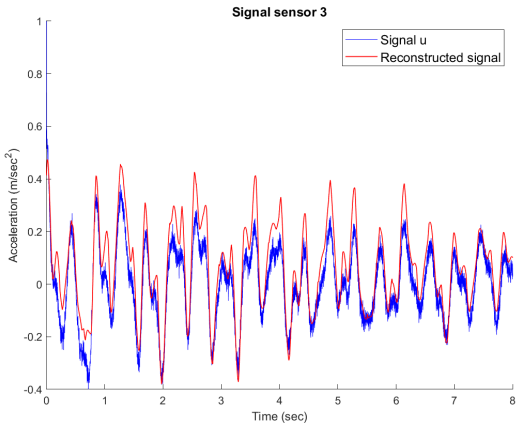

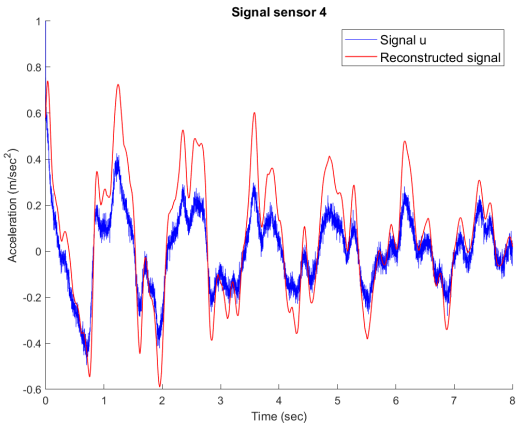

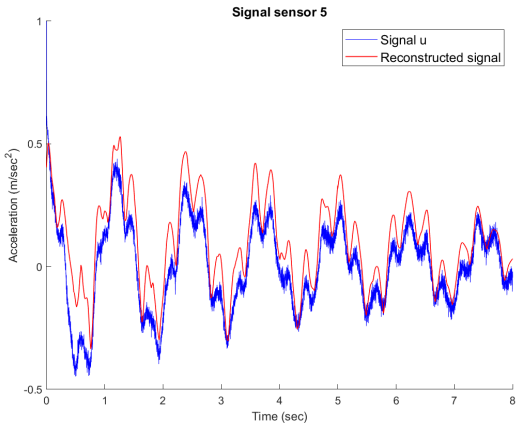

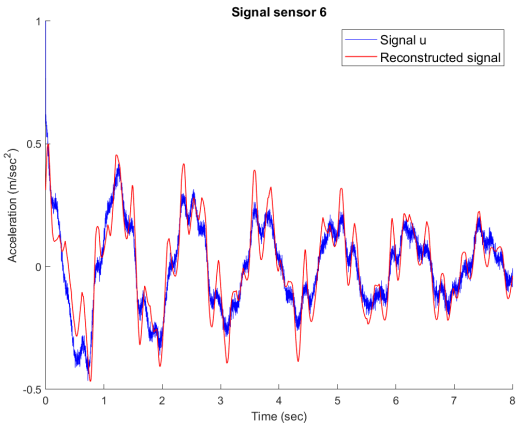

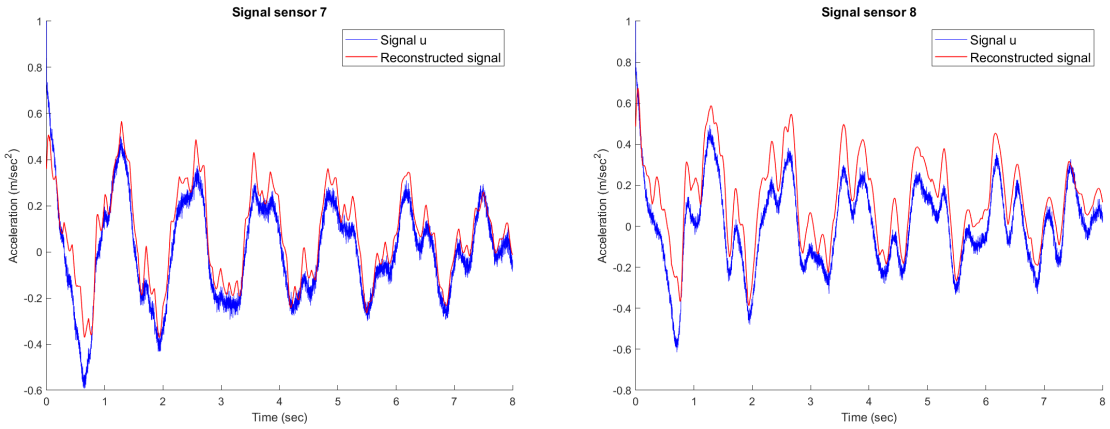

Figure 7.14: Reconstructed signals compared to the normalized signals

- *Eigen–frequencies*

Mode	OpenSees	ACWT	FFT	SSI–COV (ARTeMIS Modal–Automatic estimation)
1	0.81	0.817	1.625	0.78
2	2.29	2.29	2.25	2.93
3	3.39	3.38	3.375	3.45
4	4.74	4.72	4.875	4.883
5	5.88	5.856	5.875	5.31
6	6.97	6.886	6.875	6.42
7	7.19	7.2	7.25	7.095
8	8.59	(–)	8	(–)

- *Damping ratios*

Mode	OpenSees	ACWT (linFit)	expoFit	SSI–COV (ARTeMIS Modal–Automatic estimation)
1	0.0500	0.0307	0.0072	0.415
2	0.0497	0.0052	0.00363	0.1873
3	0.0630	0.0035	0.00364	0.04556
4	0.0821	0.0044	0.0035	(–)
5	0.0993	0.0051	0.00253	0.01921
6	0.1159	0.0021	0.0022	(–)
7	0.1192	0.00054	0.00333	0.01109

Addition of noise and comparison of the eigen−values using the signal–to–noise ratio.

- *Eigen–frequencies*

	SNR = ∞ (no additional noise)	**SNR = 49.7**		
Mode	**ACWT**	**FFT**	**ACWT**	**SSI–COV (ARTeMIS Modal)**
1	0.817	0.75	0.817	0.977
2	2.29	2.25	2.29	2.441
3	3.38	3.375	3.38	3.441
4	4.72	4.875	4.72	4.883
5	5.856	5.875	5.856	(–)
6	6.886	6.875	6.886	6.836
7	7.2	7.25	7.2	7.135

	SNR = 23.86			**SNR = 2.16**		
Mode	**FFT**	**ACWT**	**SSI–COV (ARTeMIS Modal)**	**FFT**	**ACWT**	**SSI–COV (ARTeMIS Modal)**
1	0.75	0.817	0.98	0.875	0.817	(–)
2	2.25	2.29	2.441	2.25	2.29	2.219
3	3.375	3.38	3.418	3.375	3.38	(–)
4	4.875	4.716	4.883	4.75	4.715	(–)
5	(–)	5.856	(–)	(–)	5.91	(–)
6	6.875	6.885	6.905	(–)	6.89	(–)
7	7.25	7.2	7.132	7.25	7.2	(–)

	SNR = 0.4			**SNR ≈ 0**		
Mode	**FFT**	**ACWT**	**SSI–COV (ARTeMIS Modal)**	**FFT**	**ACWT**	**SSI–COV (ARTeMIS Modal)**
1	(–)	0.827	(–)	(–)	(–)	(–)
2	(–)	2.29	(–)	(–)	(–)	(–)

3	(–)	3.386	(–)	(–)	(–)	(–)
4	(–)	4.73	(–)	(–)	(–)	(–)
5	(–)	5.853	(–)	(–)	(–)	(–)
6	(–)	6.89	(–)	(–)	(–)	(–)
7	(–)	7.22	(–)	(–)	(–)	(–)

- *Damping ratios*

	SNR = ∞ (no additional noise)	**SNR = 49.7**		**SNR = 23.86**	
Mode	**ACWT**	**ACWT**	**SSI–COV (ARTeMIS Modal)**	**ACWT**	**SSI–COV (ARTeMIS Modal)**
1	0.0307	0.0306	(–)	0.0305	(–)
2	0.0052	0.0058	0.05872	0.0051	0.05553
3	0.0035	0.0035	0.0265	0.00338	0.02144
4	0.0044	0.00439	(–)	0.0045	(–)
5	0.0051	0.00512	(–)	0.0049	(–)
6	0.0021	0.00207	0.0041	0.00202	0.0088
7	0.00054	0.00225	0.00373	0.001	0.0086

	SNR = 2.16		**SNR = 0.4**		**SNR ≈ 0**	
Mode	**ACWT**	**SSI–COV (ARTeMIS Modal)**	**ACWT**	**SSI–COV (ARTeMIS Modal)**	**ACWT**	**SSI–COV (ARTeMIS Modal)**
1	0.0323	(–)	0.029	(–)	(–)	(–)
2	0.0078	0.05516	0.012	(–)	(–)	(–)
3	0.00556	(–)	0.0034	(–)	(–)	(–)
4	0.00406	(–)	0.002	(–)	(–)	(–)
5	0.0032	(–)	0.00224	(–)	(–)	(–)
6	0.00272	(–)	0.00028	(–)	(–)	(–)
7	0.00126	(–)	0.00042	(–)	(–)	(–)

7.5 EuroProteas

EuroProteas is a real–scale simplified model structure built in Euroseistest site in the framework of the European project "Seismic Engineering Research Infrastructures for European Synergies, SERIES". It is a project ([42]), conducted by Dimitris Pitilakis, Despina Lamprou, Maria Manakou, Emmanuil Rovithis and Anastasios Anastasiadis, aiming to identify the soil–foundation system of a structure founded on soft soil. The structure consists of a steel frame on a reinforced concrete (RC) of 0.40 m thickness. Two similar RC slabs of 9 Mg mass are placed on top of the frame. EuroProteas was instrumented with a large amount (> 70). Its response to ambient noise, forced–vibration tests and free–vibration tests was recorded for multiple long hour sessions in different days and seasons. The paper results are based on total of 277 sec recordings on 6 accelerometers of the instrumentation form shown in *Figure 7.15*. The sampling rate is 0.005 sec (f_8 = 200 Hz).

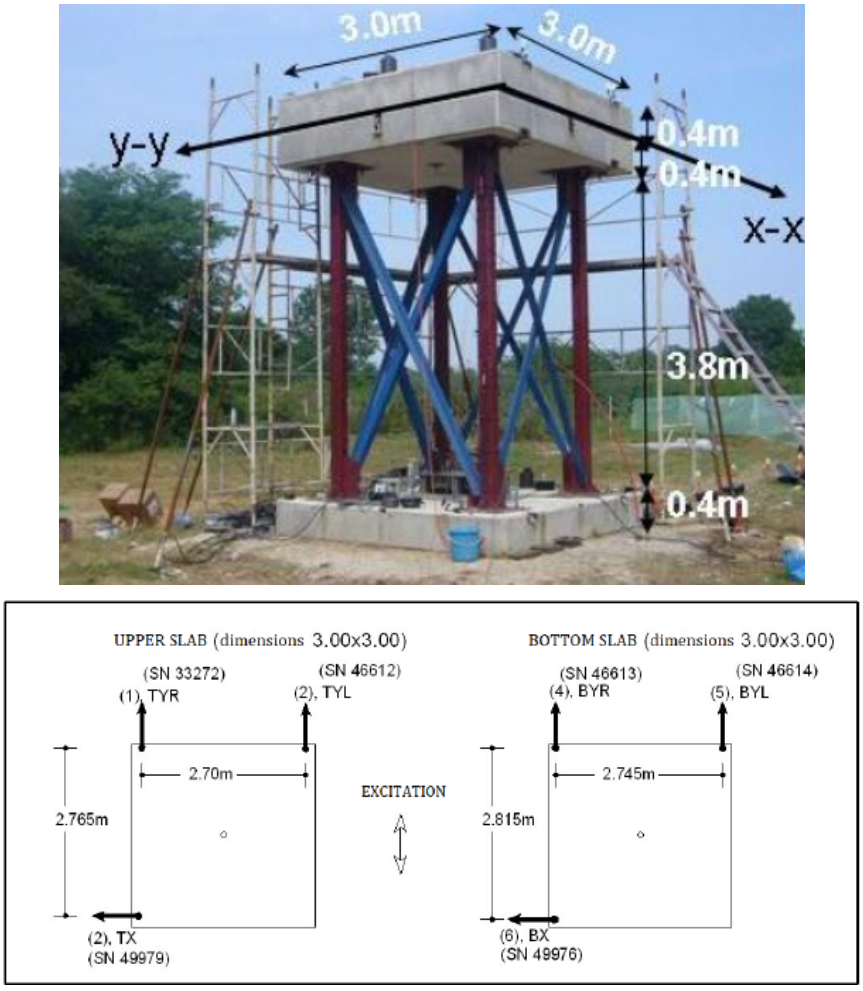

Figure 7.15: The structure and the 6 accelerometers configuration used in this example. [42]

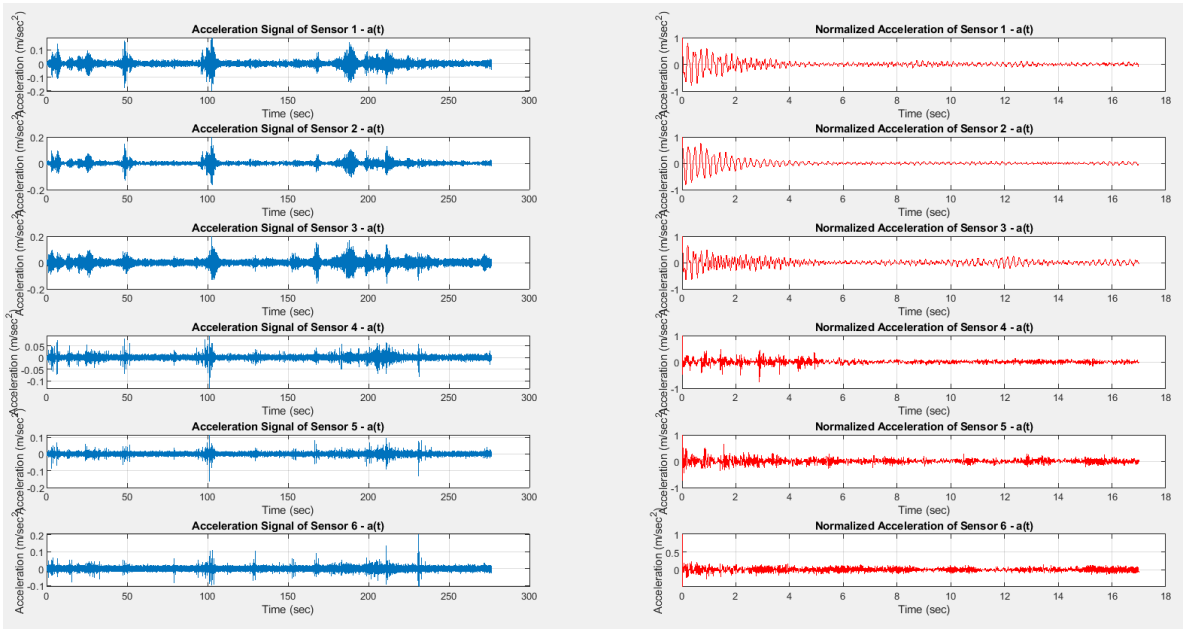

(a) *(b)*

Figure 7.16: Accelerograms (a) Ambient vibrations, (b) Normalized accelerations –free decay responses– after the application of RDT Method.

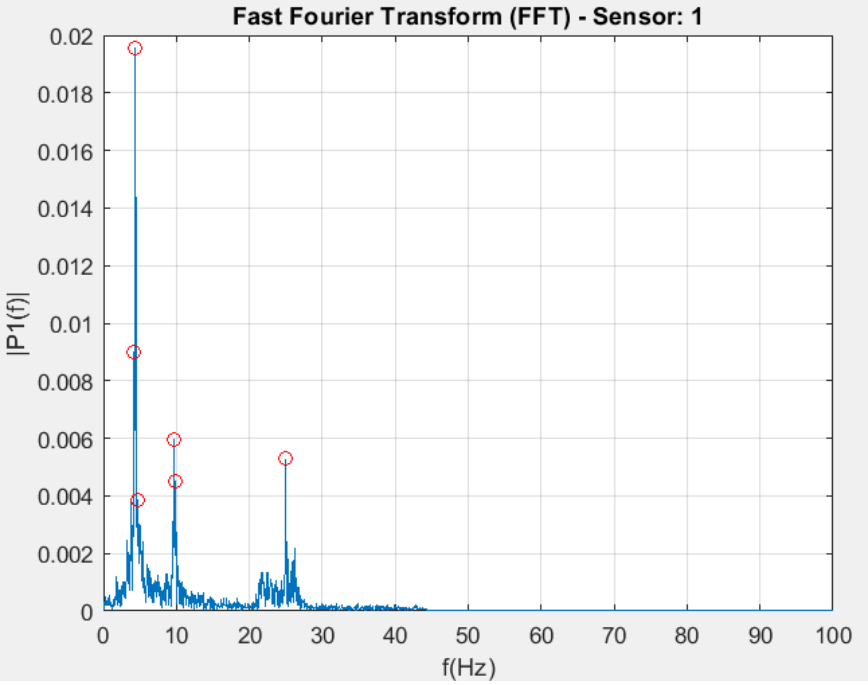

Figure 7.17: Fast Fourier Transform – FFT.

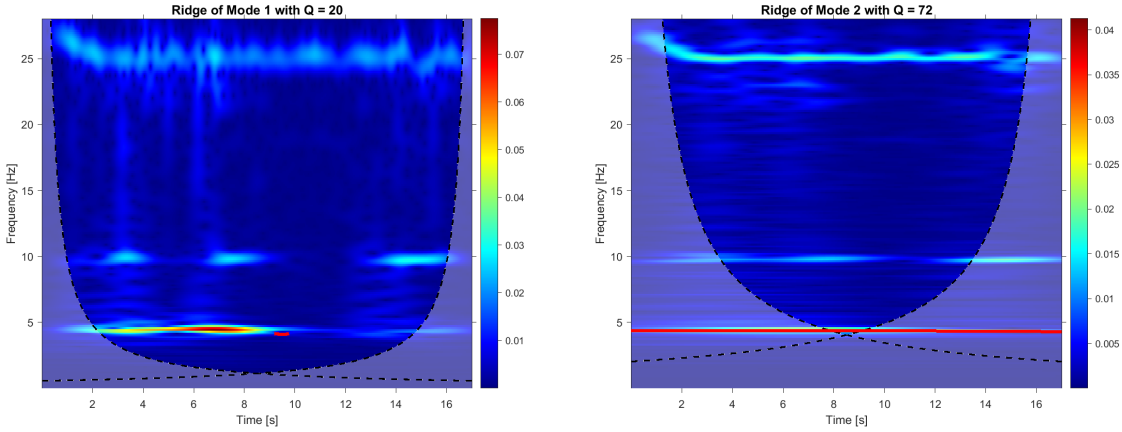

(a)

(b)

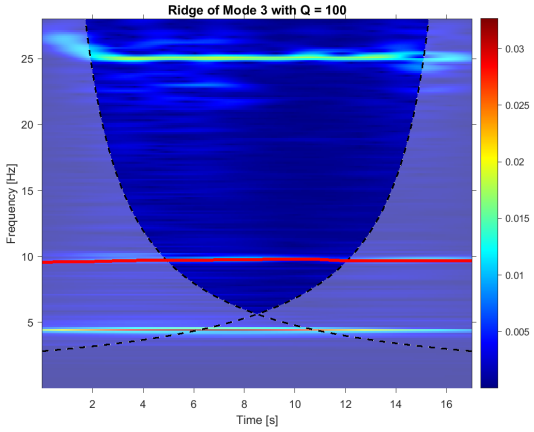

(c)

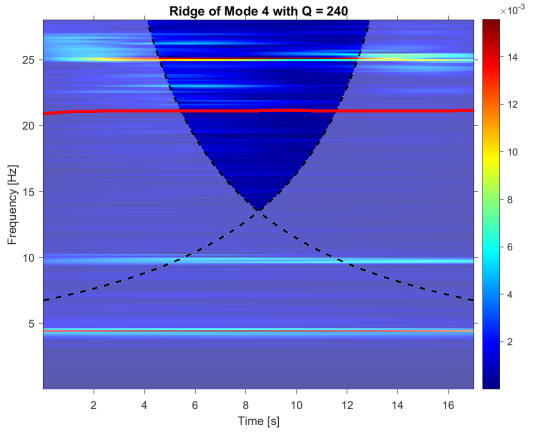

(d)

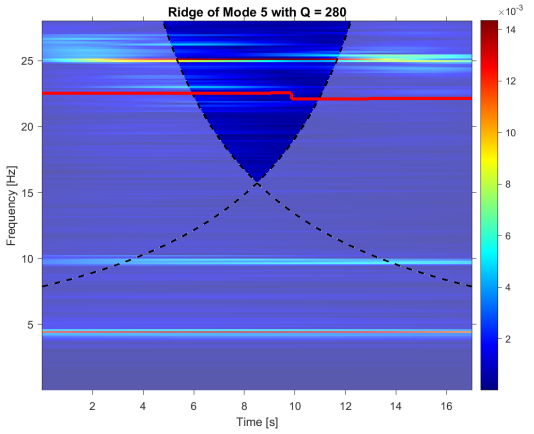

(e)

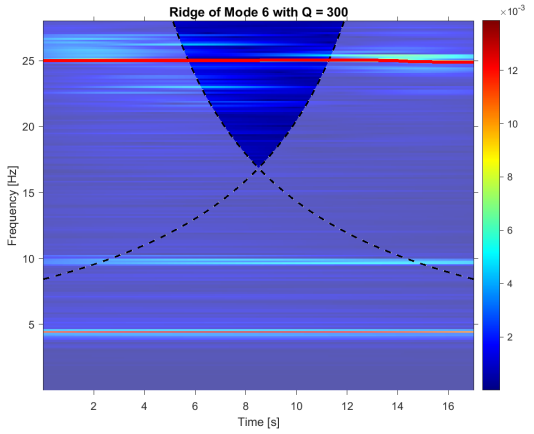

(f)

Figure 7.18: Time–frequency domain using ambient vibrations. Ridge extraction for each mode.

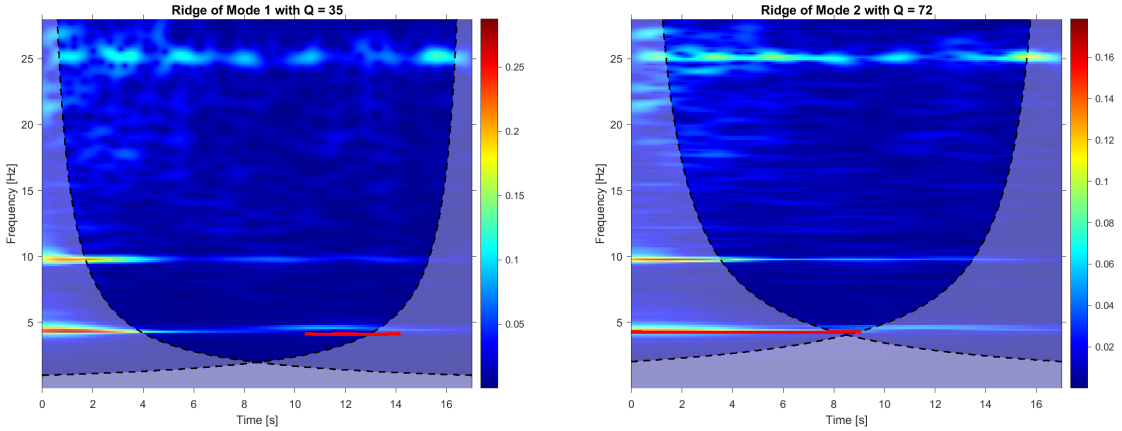

(a)

(b)

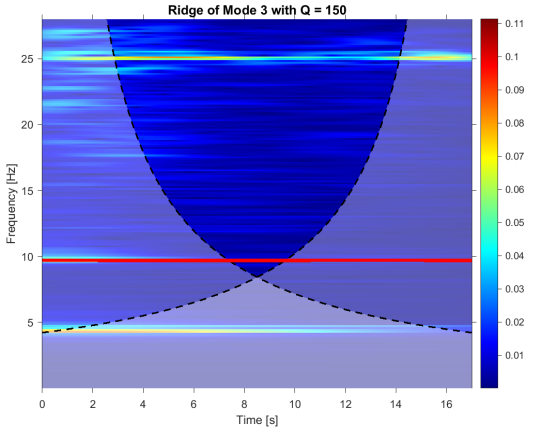

(c)

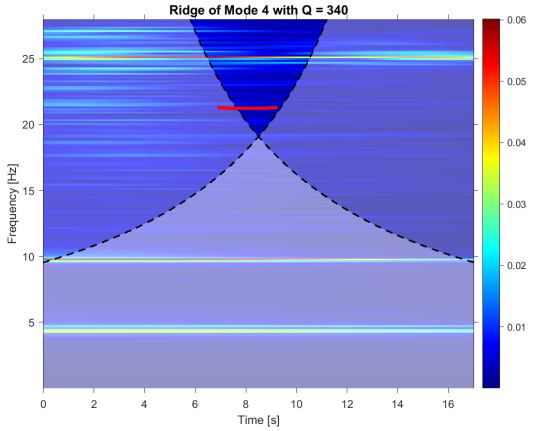

(d)

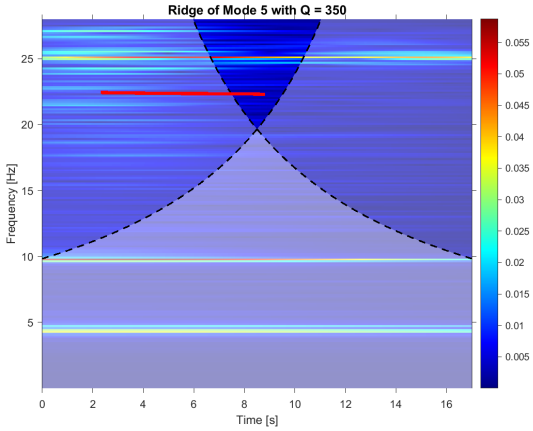

(e)

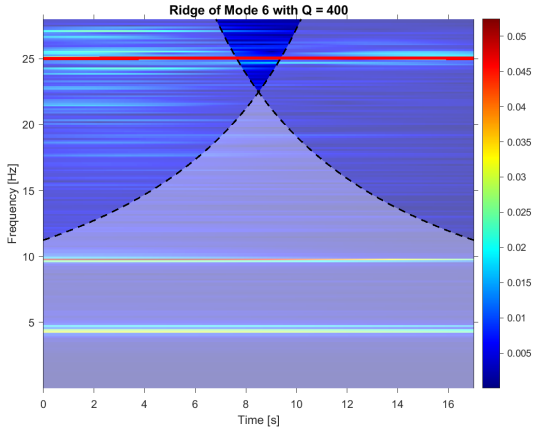

(f)

Figure 7.19: Time–frequency domain using free–decay responses. Ridge extraction for each mode.

➢ *Eigen–modes estimation*

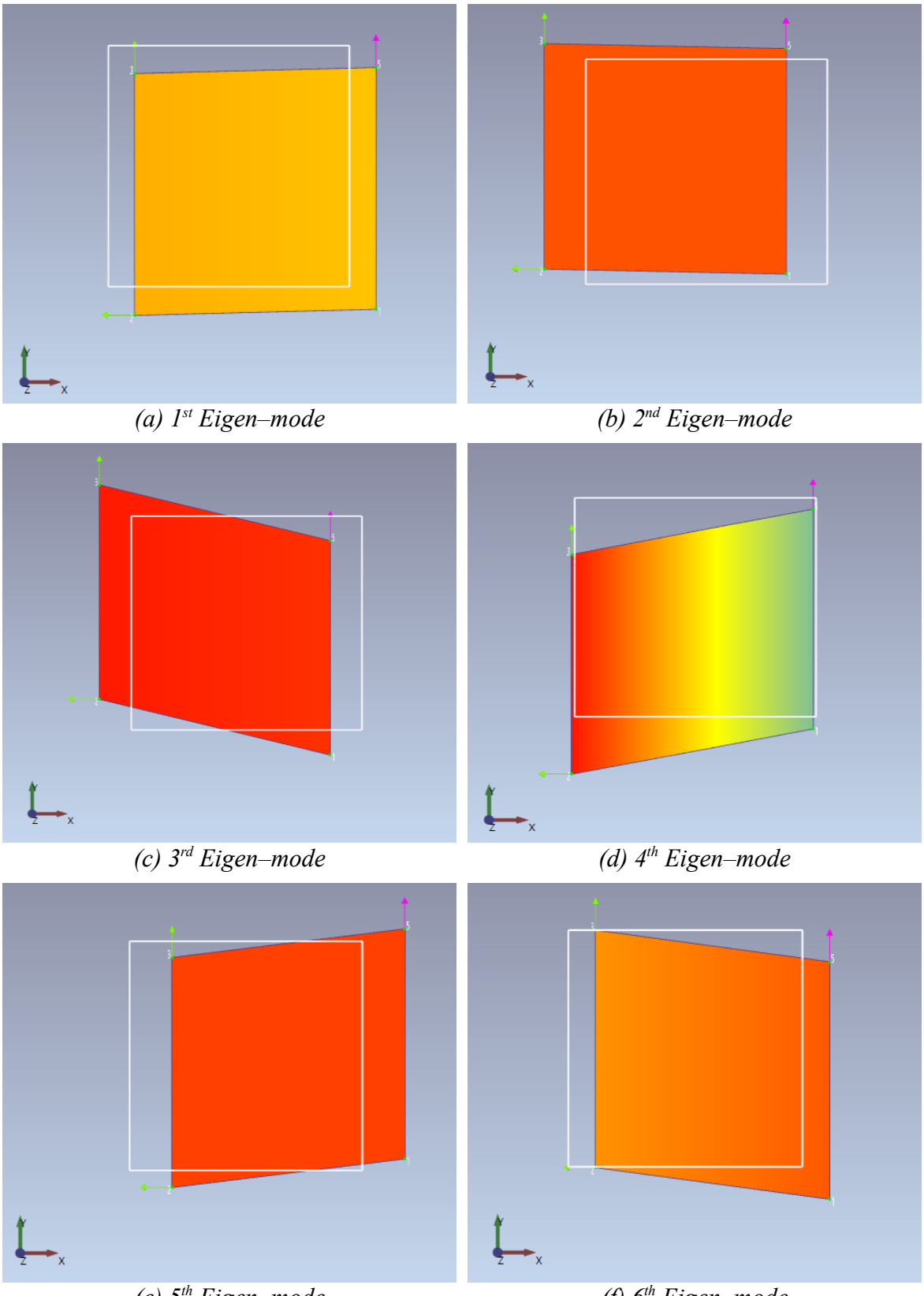

(a) 1st Eigen–mode

(b) 2nd Eigen–mode

(c) 3rd Eigen–mode

(d) 4th Eigen–mode

(e) 5th Eigen–mode

(f) 6th Eigen–mode

Figure 7.20: Eigen–modes estimation from ARTeMIS Modal.

➢ *Signal Reconstruction*

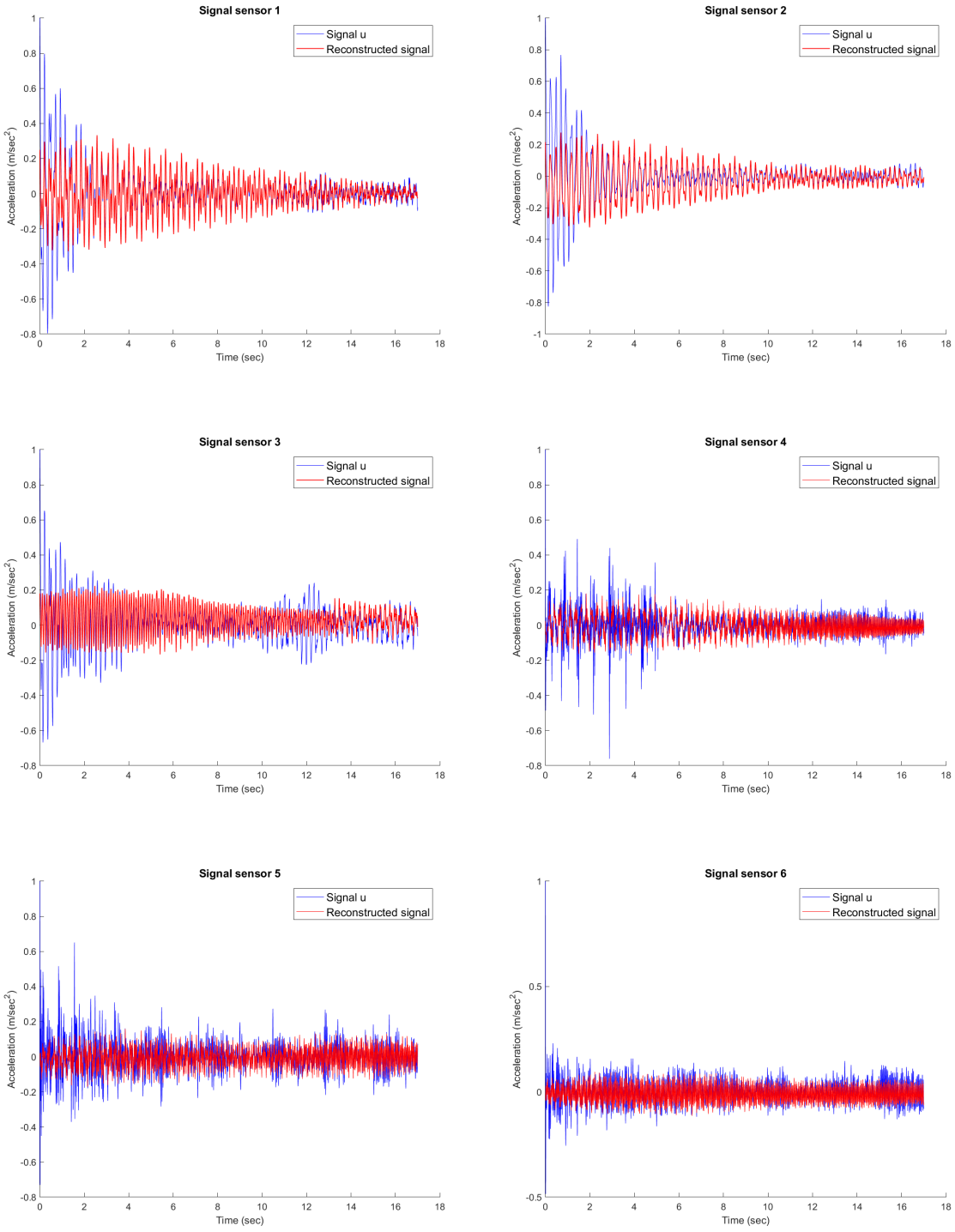

Figure 7.21: Reconstructed signals compared to the normalized signals

- *Eigen–frequencies*

Mode	MACEC	Shape	ACWT	FFT	SSI–COV (ARTeMIS Modal)
1	4.102	Trans	4.087	4.12	4.34
2	4.199	Trans	4.37	4.353	4.36
3	9.668	Tors	9.769	9.647	9.726
4	21.191	Coupled	21.135	(–)	21.504
5	22.363	Coupled	22.496	(–)	22.652
6	(–)	Coupled	25.03	25	25

- *Damping ratios*

Mode	MACEC	ACWT (linFit)	expoFit	SSI–COV (ARTeMIS Modal)
1	0.0304	0.00424	0.014	0.03154
2	0.0342	0.00752	0.0136	0.01772
3	0.008	0.002	0.00605	0.00814
4	0.0135	0.001446	0.0028	0.01474
5	0.0075	0.00165	0.0026	0.02413
6	(–)	0.00062	0.0023	0.00279

Addition of noise and comparison of the eigen–values using the signal–to–noise ratio.

- *Eigen–frequencies*

	SNR = ∞ (no additional noise)	**SNR = 28.7**		
Mode	**ACWT**	**FFT**	**ACWT**	**SSI–COV (ARTeMIS Modal)**
1	4.087	4.118	4.085	4.297
2	4.37	4.353	4.37	4.395
3	9.769	9.647	9.766	9.744
4	21.135	(–)	21.13	(–)
5	22.496	(–)	22.394	(–)
6	25.03	25	25.03	25.024

	SNR = 4.55			SNR ≈ 0		
Mode	**FFT**	**ACWT**	**SSI–COV (ARTeMIS Modal)**	**FFT**	**ACWT**	**SSI–COV (ARTeMIS Modal)**
1	4.18	4.085	4.342	(–)	(–)	(–)
2	4.353	4.372	4.363	(–)	(–)	(–)
3	9.647	9.79	9.732	(–)	(–)	(–)
4	(–)	21.09	(–)	(–)	(–)	(–)
5	(–)	22.366	(–)	(–)	(–)	(–)
6	25	25.032	24.974	(–)	(–)	(–)

.

- *Damping ratios*

	SNR = ∞ (no additional noise)	SNR = 26.82		SNR = 3.42		SNR ≈ 0	
Mode	**ACWT**	**ACWT**	**SSI–COV (ARTeMIS Modal)**	**ACWT**	**SSI–COV (ARTeMIS Modal)**	**ACWT**	**SSI–COV (ARTeMIS Modal)**
1	0.00424	0.0044	0.0228	0.00786	0.02101	(–)	(–)
2	0.00752	0.00717	0.03518	0.0063	0.05085	(–)	(–)
3	0.002	0.00197	0.01626	0.00265	0.01364	(–)	(–)
4	0.001446	0.00152	(–)	0.00176	(–)	(–)	(–)
5	0.00165	0.00135	(–)	0.00141	(–)	(–)	(–)
6	0.00062	0.00062	0.00737	0.00042	0.00791	(–)	(–)

8. Application to Z24 Bridge

8.1 Description of the Z24−bridge

The Z24 bridge was located in the canton Bern near Solothurn, Switzerland. It was part of the road connection between the villages of Koppigen and Utzenstorf, over−passing the A1 highway between Bern and Zürich. It was a classical post−tensioned concrete two−cell box−girder bridge with a main span of 30 m and two side spans of 14 meters (*Figure 8.2*). The bridge was built as a freestanding frame with the approaches backfilled later. Both abutments consisted of triple concrete columns connected with concrete hinges to the girder. Both intermediate supports were concrete piers clamped into the girder. An extension of the bridge girder at the approaches provided a sliding slab. All supports were rotated with respect to the longitudinal axis, which yielded a skew bridge. The bridge, which dated from 1963, was demolished at the end of 1998, because a new railway adjacent to the highway required a new bridge with a larger side span. More information about the Z24 bridge can also be found in [44][45].

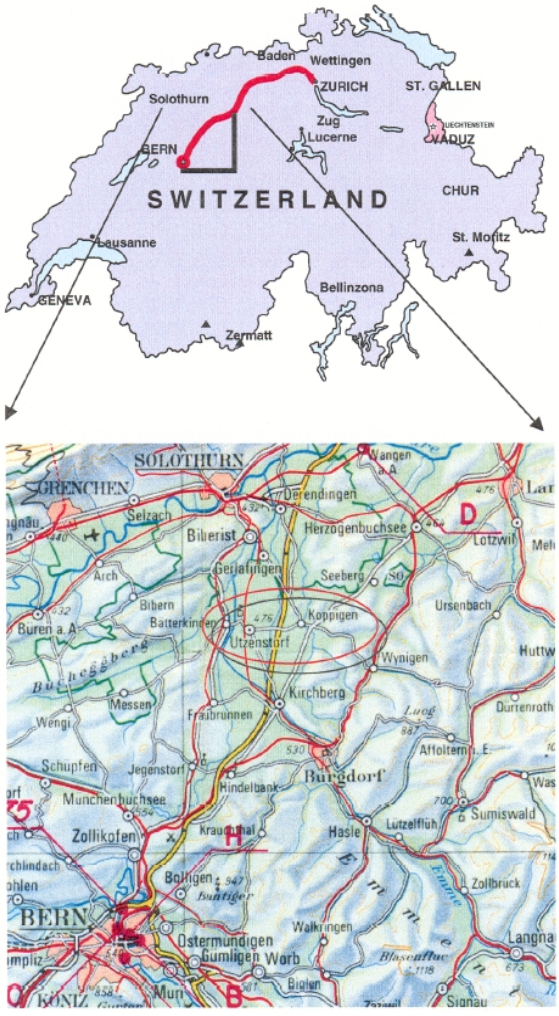

Figure 8.1: Geographical location of the Z24 Bridge [48].

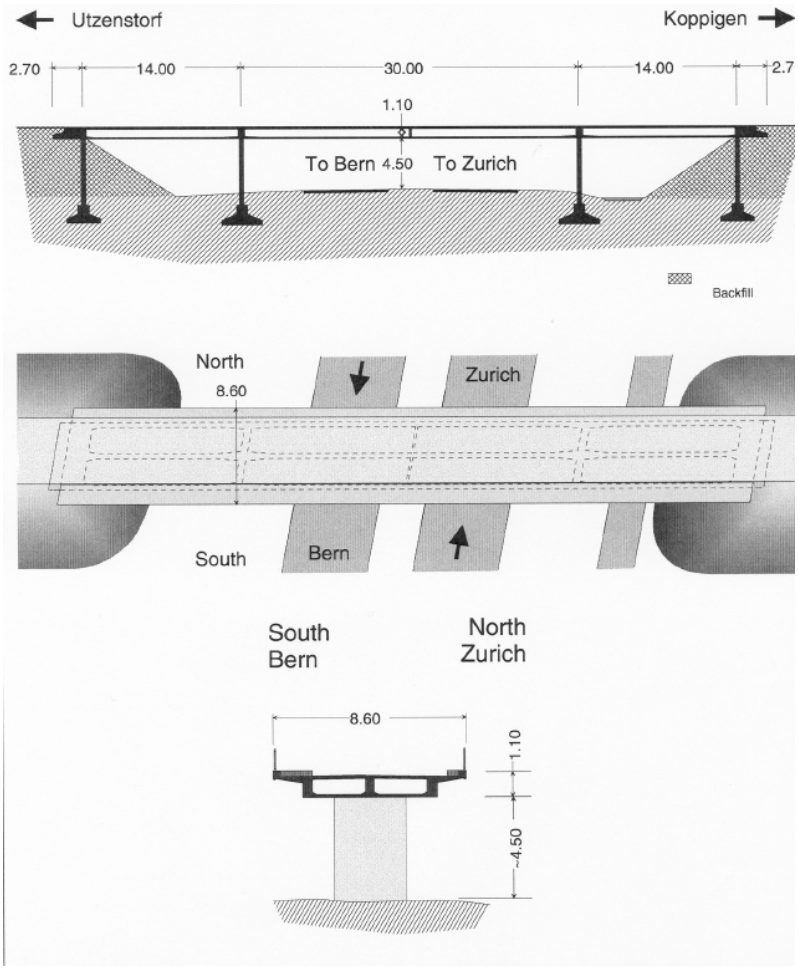

Figure 8.2: Plans of the Z24 Bridge [48].

8.2 Brite−EuRam Project SIMCES

The Z24 Bridge's tests, have been performed in the framework of the European Brite EuRam research project BE−3157, "System Identification to Monitor Civil Engineering Structures" (SIMCES) [46].

The project was coordinated by KU Leuven (Department of Civil Engineering, Structural Mechanics Section). The other partners in the project were: Aalborg University (Institut for Bybninbsteknik); EMPA (Swiss Federal Laboratories for Materials Testing and Research, Concrete Structures Section); LMS (Leuven Measurement and Systems International N.V.; Engineering and Modeling); WS Atkins Consultants Ltd (Science and Technology); Sineco Spa (Ufficio Promozione e Sviluppo); Technische Universität Graz (Structural Concrete Institute). [47]

The SIMCES project programme refers to a monitoring system. One of the main objectives of the SIMCES project was to deliver a proof of feasibility for vibration–based structural health monitoring of civil engineering structures by full−scale, long−term tests and progressive failure tests of a representative structure, the Z24 Bridge. Ideas of the purpose of this monitoring system ranged from 'prototype damage monitoring system' to 'getting an idea of the environmental behavior of the test bridge'. [48]

8.3 Bridge instrumentation

One big issue was the type of instrumentation to be used for the dynamic measurements. Considerations centered to the kind of dynamic characteristics which later might be useful for damage detection. More or less directly measurable characteristics such as frequencies and amplitude ratios could have been supplemented by derivable characteristics such as curvature etc. If curvature would have been considered interesting, sensors would have to be allocated in concentrated or array manner. However, the conclusion was to distribute the instruments over the bridge, at locations where they could pick a maximum number of modes. [48]

8.4 Importing model into ARTeMIS Modal

For simplification purposes and minimization of computational cost, the deck of the three–span bridge was assumed a plane, as well as its pillars. Firstly, the coordinates of total nodes are introduced. Then, the lines and the surfaces are defined, dividing the bridge into smaller rectangles. Subsequently, the acceleration signals are imported into the corresponding degrees of freedom. Due to the big computational cost, the 110 out of 246 signals are imported in order to obtain a good estimation of the eigen−modes. The channels were chosen for the ACWT estimation are 12, 13, 42, 43, 44 and 45.

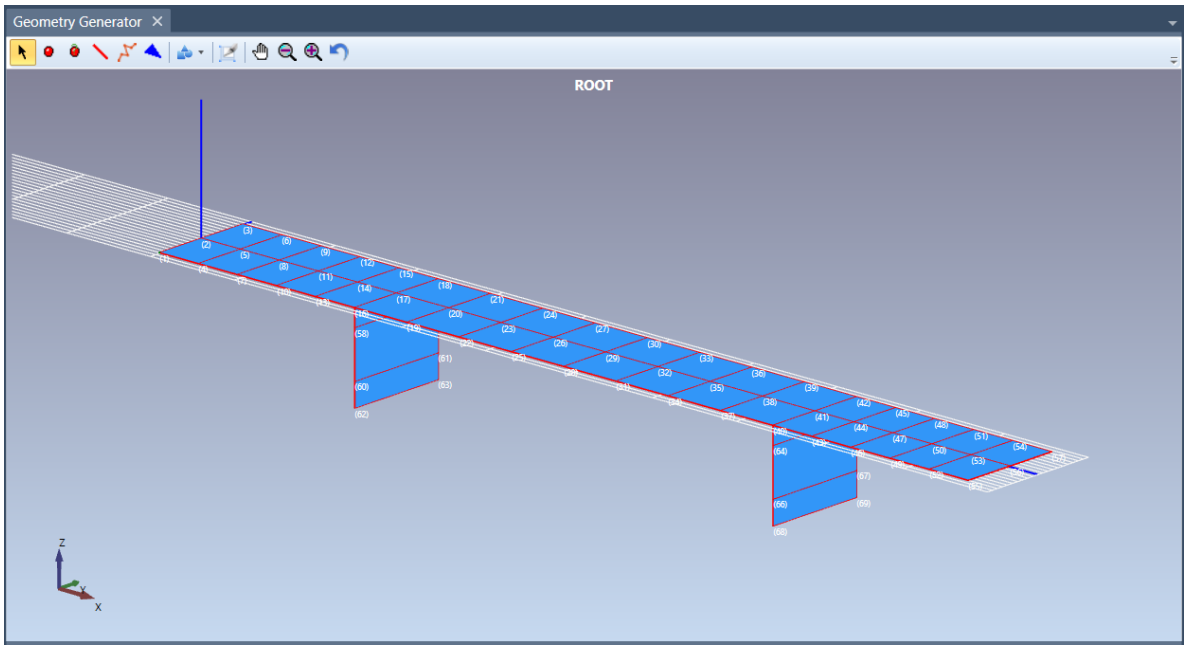

Fugure 8.3: Importing bridge geometry (nodes, lines and surfaces).

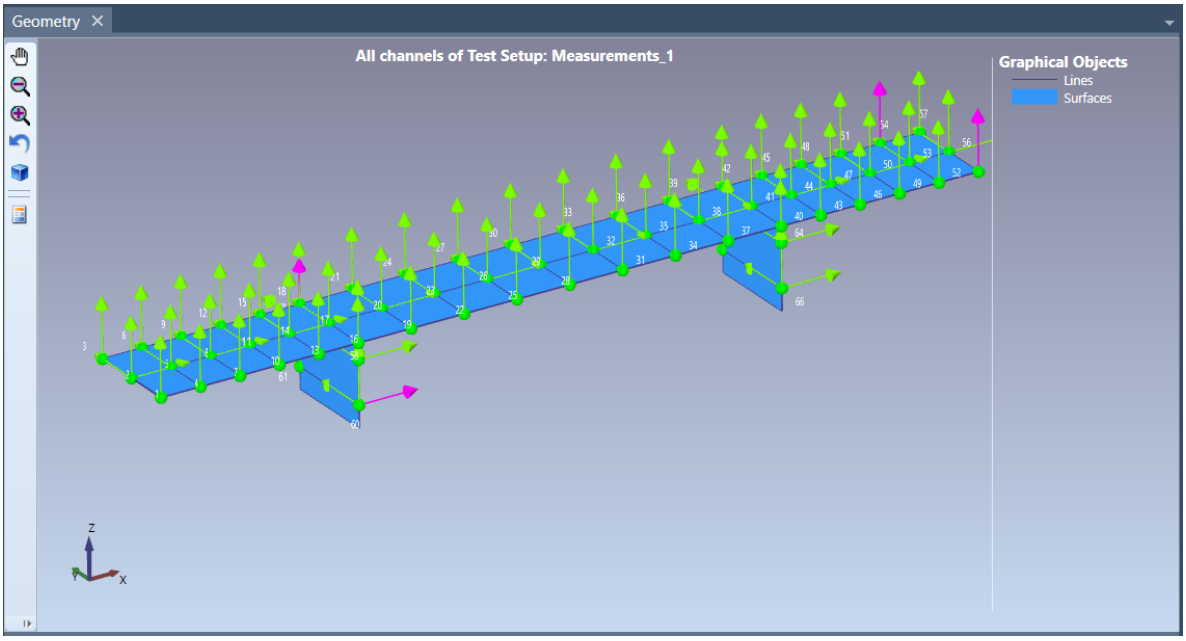

Fugure 8.4: Importing signal channels into the corresponding degree of freedom.

8.5 Long−term continuous monitoring test

A long−term continuous monitoring test took place during the year before demolition. Since the aim of this test was to quantify the environmental variability of the bridge dynamics, all environmental variables that were considered to be of possible importance for the bridge dynamics have been monitored. Sensors to measure air temperature, air humidity, rain true or false, wind speed, and wind direction were installed at the bridge, resulting in five sensors for the atmospheric conditions. A sensor consisting of two inductive loops was installed to detect the presence of vehicles on the bridge. [47]

To monitor the bridge dynamics, 16 accelerations have been measured on the bridge at different points and in different directions. Every hour, 10 scans of environmental data, sampled at 48 sensors, and 8 averages of 8192 acceleration samples, taken at 16 sensors, were collected and stored to a hard disk after compression. The construction works at the new bridge that replaced the Z24, caused the loss of six temperature sensors and damage to one accelerometer. Although the type of accelerometers that had been used was specially designed for long−term use, some showed a considerable drift and a few of them failed during operation. [47]

The chosen dates for the analysis are 10th Nov and 10th Dec of 1997, 9th Jan, 10th Feb, 10th Mar, 10th Apr, 28th May, 18th Jun, 10th Jul, 4th Aug and 9th Sept of 1998 and the hourly recording of the 11 p.m. for each date.

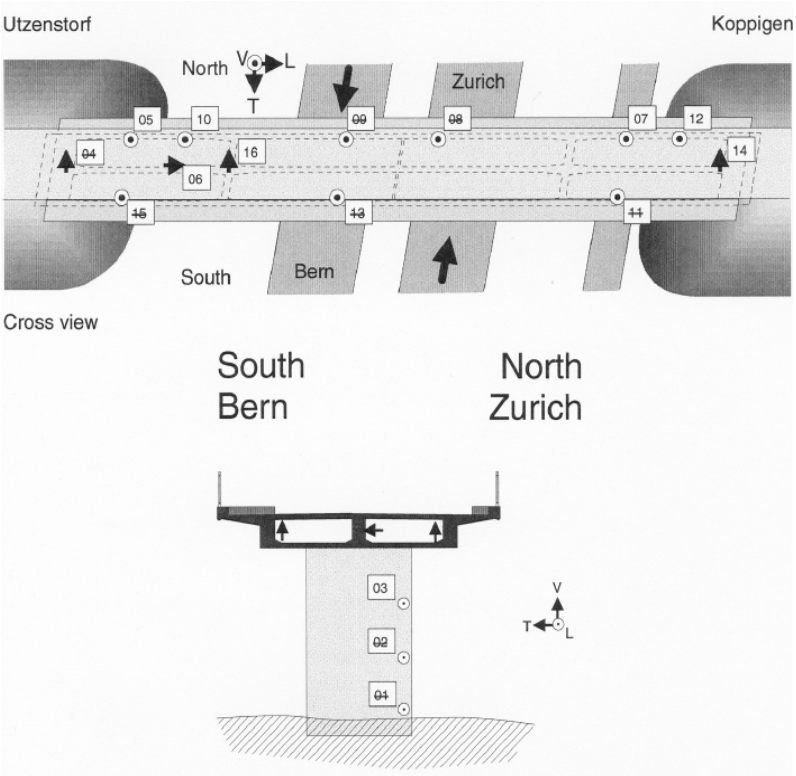

Figure 8.5: Location and orientation of accelerometers [48].

- *Analysis History in ARTeMIS Modal*

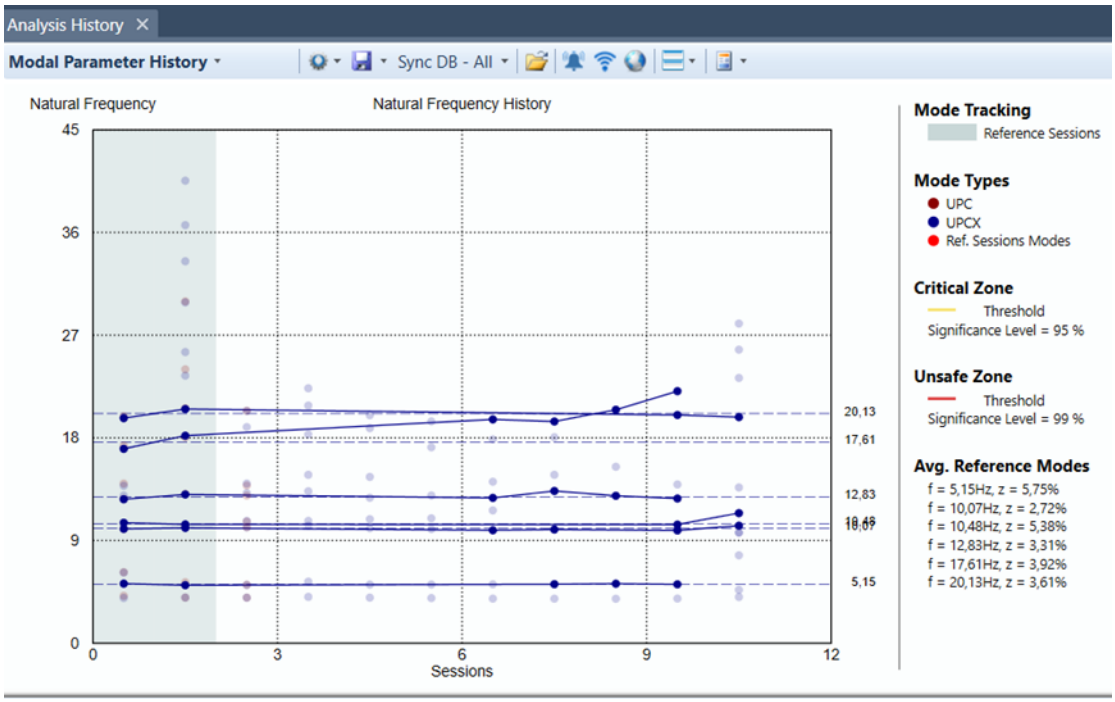

Fugure 8.6: Modal Parameter History, Long−term continuous monitoring test.

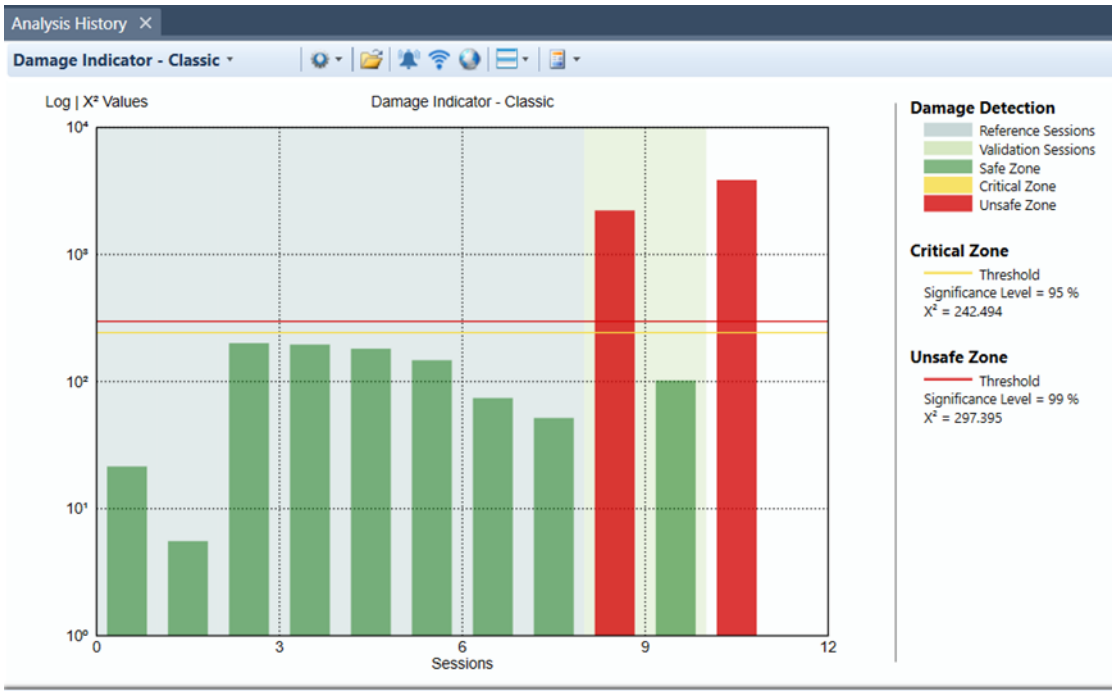

Figure 8.7: Damage Indicator, Long−term continuous monitoring test.

8.6 Short−term progressive damage test

Progressive damage tests took place over a month, shortly before complete demolition of the bridge. The practical significance of these tests was ensured by checking that they were relevant for the safety of the bridge and that the simulated damage occurred frequently. *Table 8.1* gives a complete overview of all progressive damage tests that were performed. Before and after each applied damage scenario, the bridge was subjected to a forced and an ambient operational vibration test. With a measurement grid consisting of a regular 3 × 45 grid on top of the bridge deck and a 2 × 8 grid on each of the two pillars, 291 degrees of freedom have been measured: all displacements on the pillars, and mainly vertical and lateral displacements on the bridge deck. Because the number of degrees of freedom to be measured exceeded the number of available accelerometers and acquisition channels, the data were collected in nine setups using five reference channels. The forced excitation was applied by two vertical shakers, placed on the bridge deck. An 1 kN shaker was placed on the middle span and a 0.5 kN shaker was placed at the Koppigen side span. The shaker input signals were generated using an inverse fast Fourier transform (FFT) algorithm, resulting in a fairly flat force spectrum between 3 and 30 Hz. After scenario 8, a drop weight test was also performed, using a device that allowed to drop a mass of up to 120 kg from a height of up to 1 m in a controlled way. The applied shaker and drop weight forces were periodic with eight periods. A total of 65536 samples was collected at a sampling rate of 100 Hz, using an anti−aliasing filter with a 30 Hz cutoff frequency. [47]

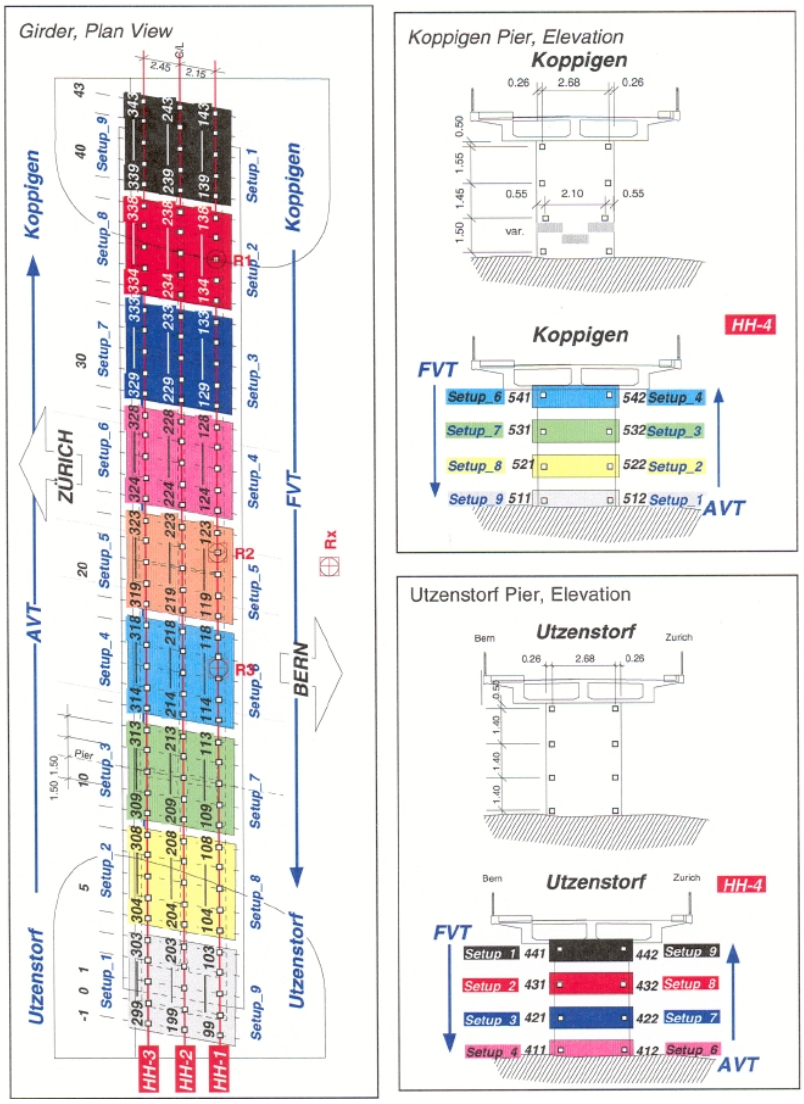

Figure 8.8: Location of accelerometers in short−term progressive damage test [48].

Table 8.1: Chronological overview of applied damage scenarios, indicating on which date a specific scenario was fully realized [47].

Date (1998)	Scenario
4 August	Undamaged condition
9 August	Installation of pier settlement system
10 August	Lowering of pier, 20 mm
12 August	Lowering of pier, 40 mm
17 August	Lowering of pier, 80 mm

18 August	Lowering of pier, 95 mm
19 August	Lifting of pier, tilt of foundation
20 August	New reference condition
25 August	Spalling of concrete at soffit, 12 m^2
26 August	Spalling of concrete at soffit, 24 m^2
27 August	Landslide of 1 m at abutment
31 August	Failure of concrete hinge
2 September	Failure of 2 anchor heads
3 September	Failure of 4 anchor heads
7 September	Rupture of 2 out of 16 tendons
8 September	Rupture of 4 out of 16 tendons
9 September	Rupture of 6 out of 16 tendons

➢ *Analysis History in ARTeMIS Modal*

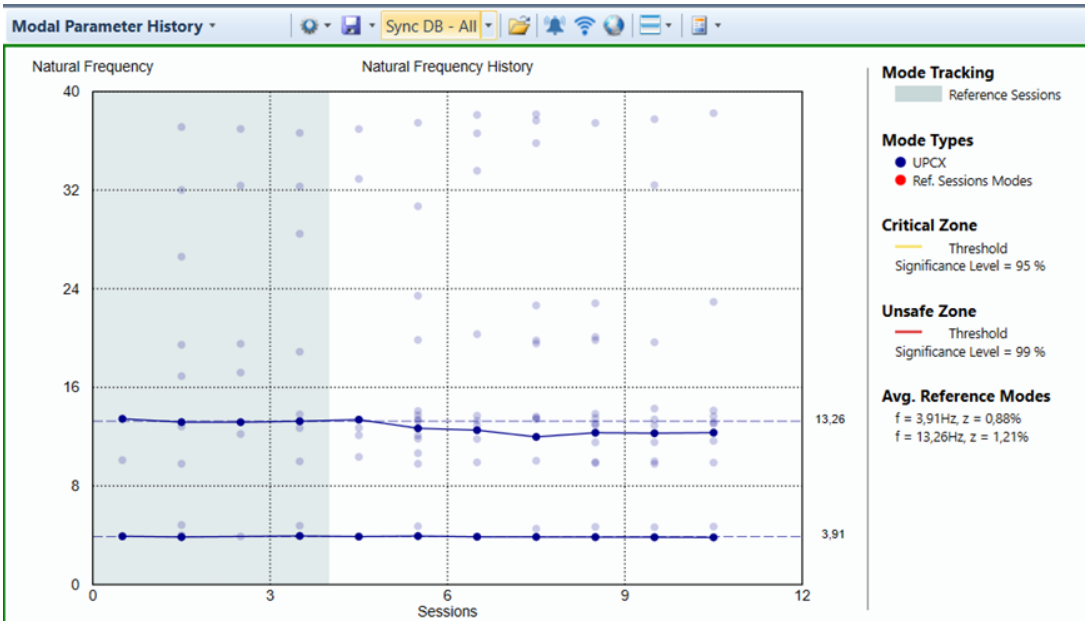

Fugure 8.9: Modal Parameter History, Short−term progressive damage test.

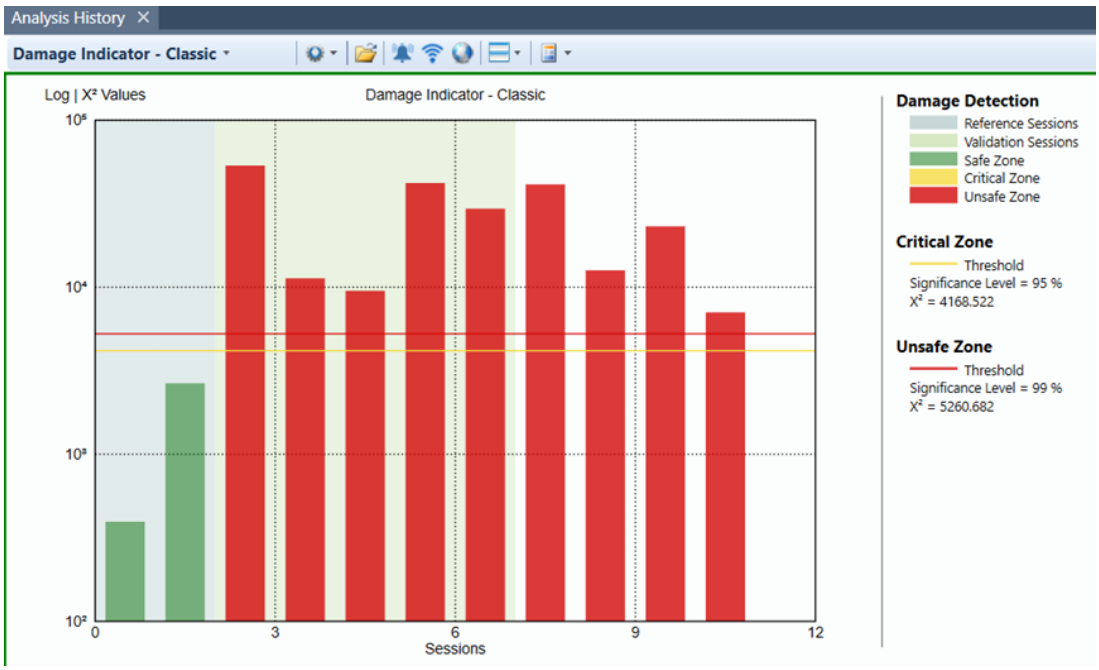

Fugure 8.10: Damage Indicator, Short−term progressive damage test.

To minimize the computational cost, the undamaged scenarios 2−7 were not counted.

8.7 Results

- *Eigen–modes estimation*

KU LEUVEN	ARTeMIS Modal (FDD)
mode 1 - 3.86Hz - 0.8% 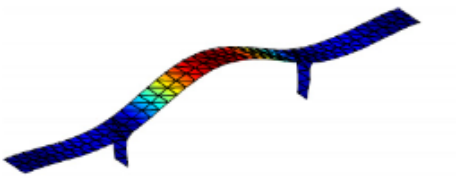	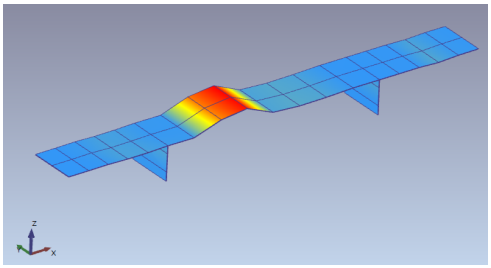
mode 2 - 4.90Hz - 1.4% 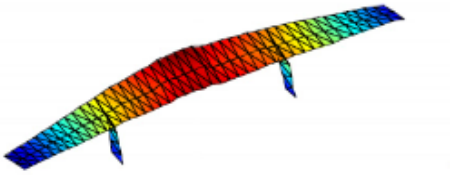	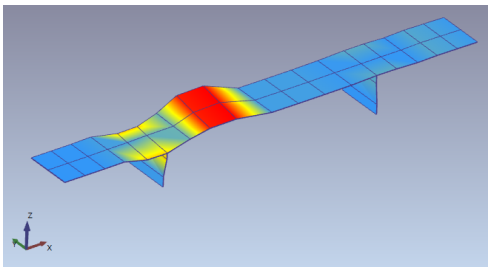
mode 3 - 9.76Hz - 1.4% 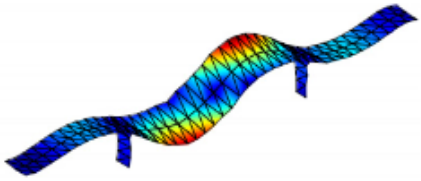	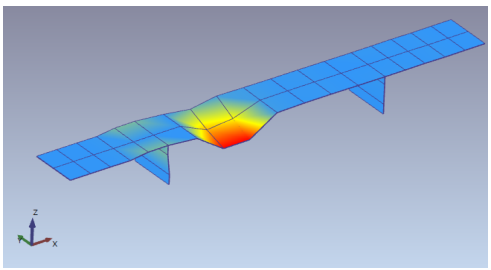
mode 4 - 10.30Hz - 1.3% 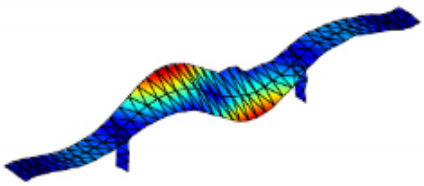	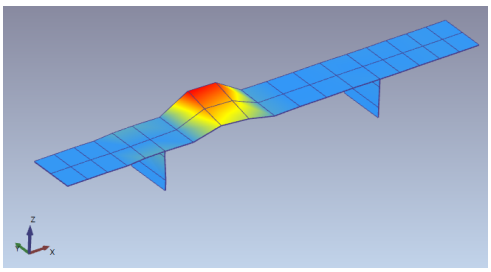

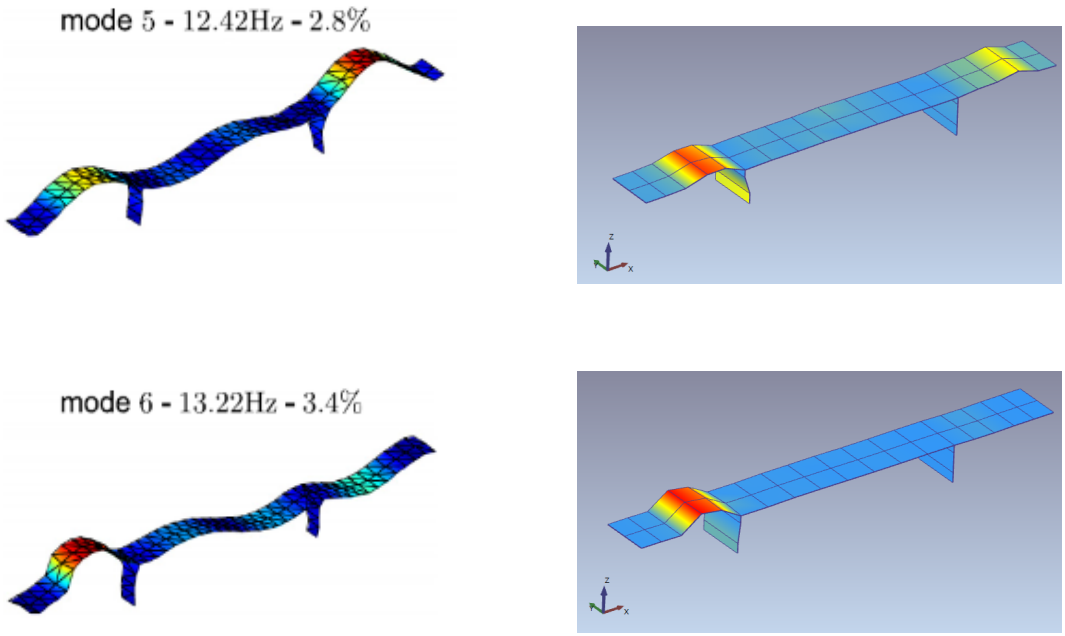

Figure 8.11: Eigen–modes estimation from (a) KU Leuven [47] and (b) ARTeMIS Modal (Scenario 8).

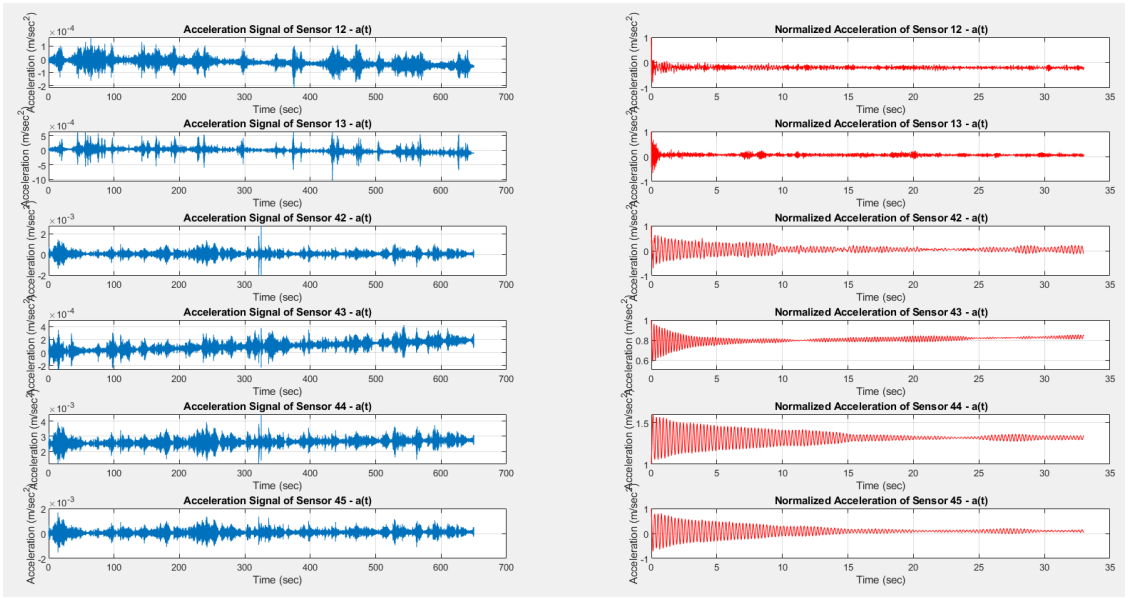

(a) *(b)*

Figure 8.12: Accelerograms (a) Ambient vibrations, (b) Normalized accelerations –free decay responses– after the application of RDT Method (Scenario 8).

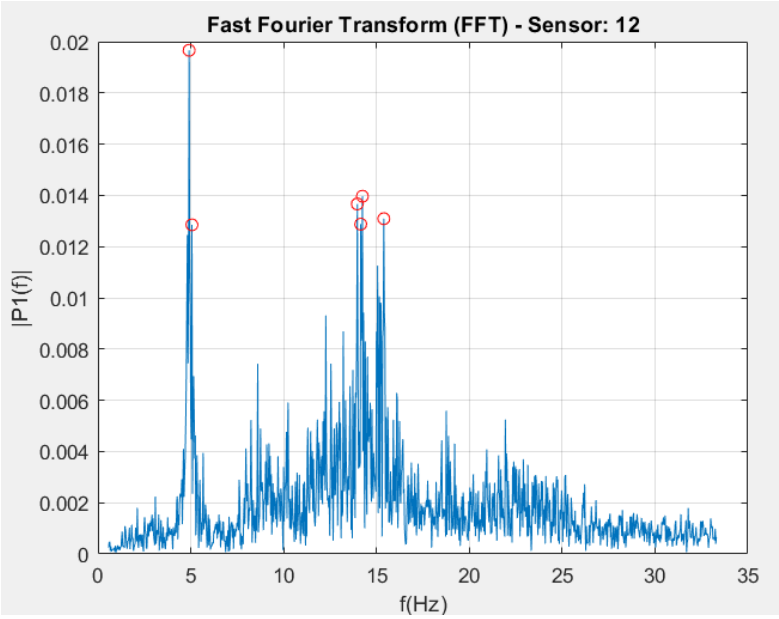

Figure 8.13: Fast Fourier Transform – FFT (Scenario 8).

➢ *Ridges estimation with ACWT*

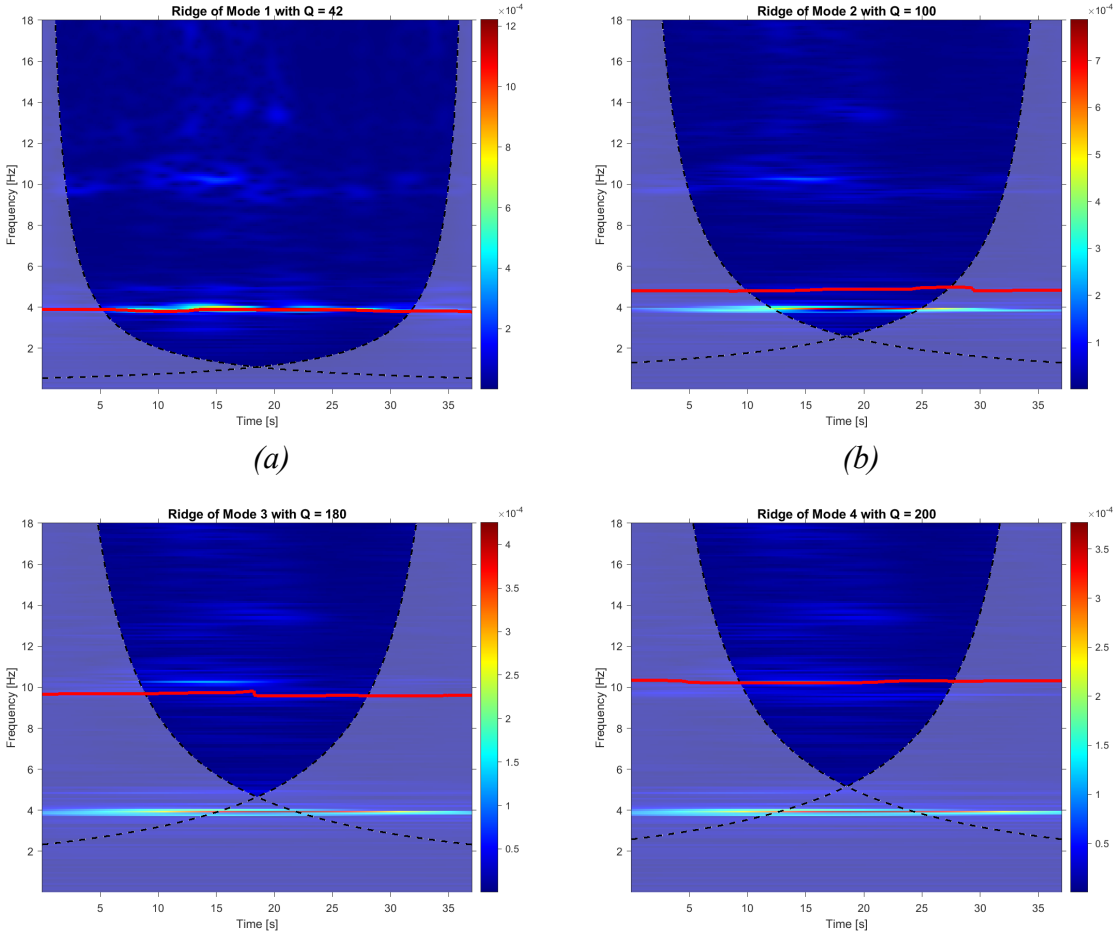

(a) *(b)*

(c) *(d)*

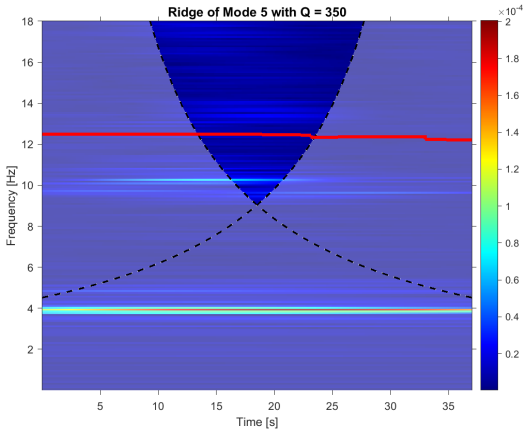

(e)

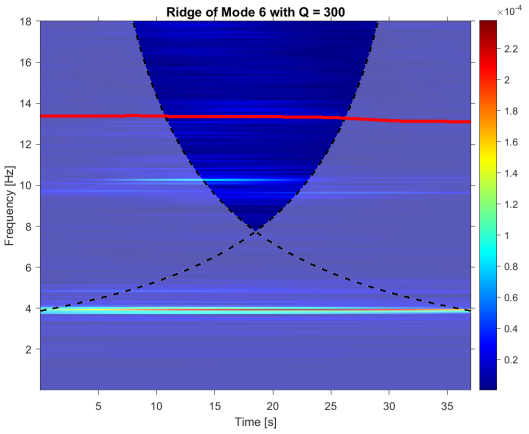

(f)

Figure 8.14: Time–frequency domain using ambient vibrations. Ridge extraction for each mode (Scenario 8).

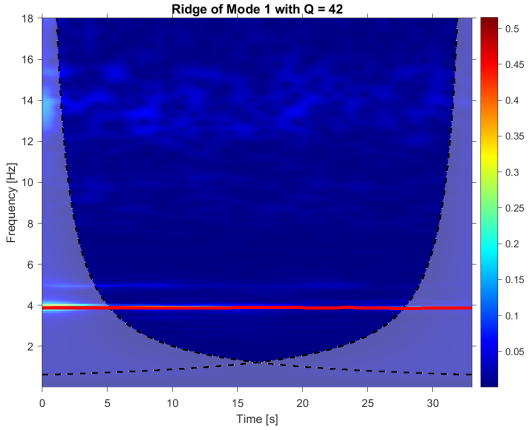

(a)

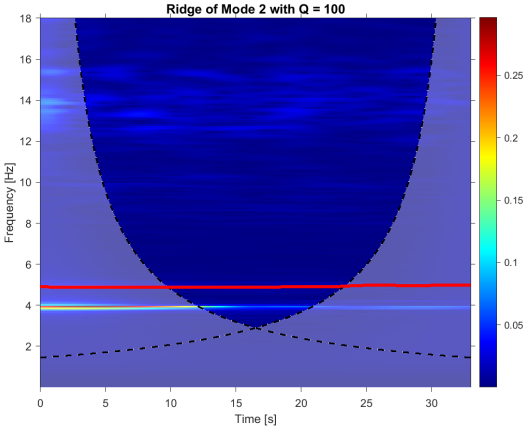

(b)

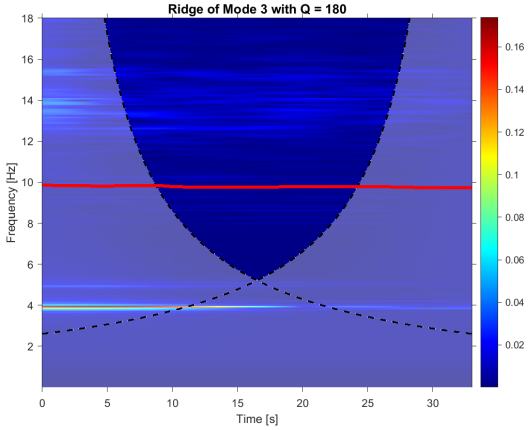

(c)

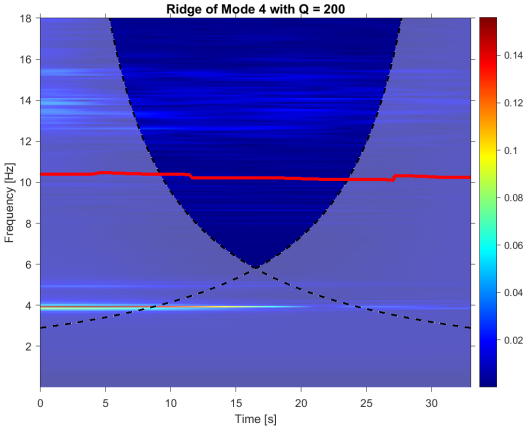

(d)

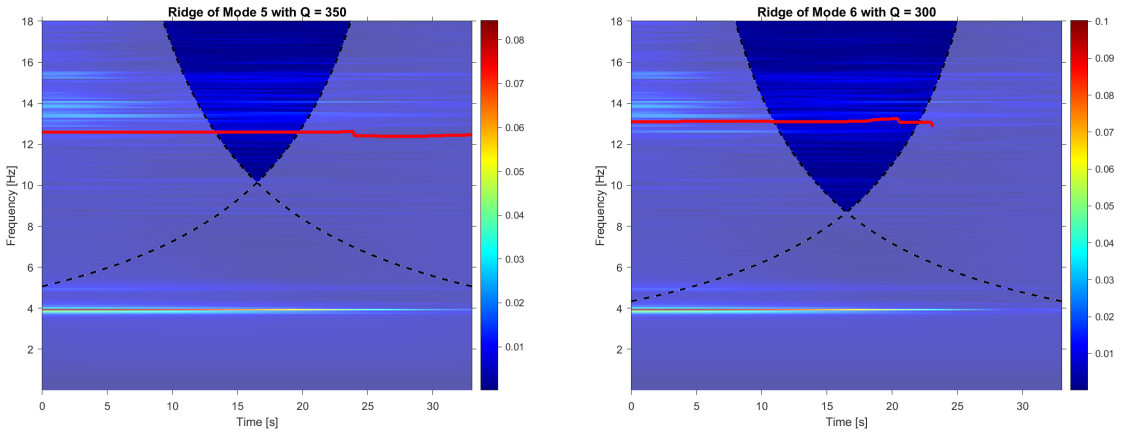

(e) *(f)*

Figure 8.15: Time–frequency domain using free–decay responses. Ridge extraction for each mode (Scenario 8).

- *Scenario 8 – 20th August 1998*

Figure 8.16: Stabilization Diagram of Estimated State Space Models – SSI UPCX (Scenario 8)

Eigen–frequencies					
Mode	**KU LEUVEN**	**Shape** (KU LEUVEN)	**ACWT**	**FFT**	**SSI–COV (ARTeMIS Modal)**
1	3.86	Trans	3.88	(–)	3.863
2	4.90	Coupled	4.87	4.92	4.883
3	9.76	Tors	9.67	9.89	9.802
4	10.30	Tors	10.218	10.05	(–)
5	12.42	Trans	12.475	(–)	12.826
6	13.22	Trans	13.34	13.81	13.18

Damping ratios				
Mode	**KU LEUVEN**	**ACWT (linFit)**	**expoFit**	**SSI–COV (ARTeMIS Modal)**
1	0.008	0.0037	0.0026	0.00684
2	0.014	0.001	0.0021	0.03466
3	0.014	0.000034	0.001	0.01429
4	0.013	0.00061	0.001	(–)
5	0.028	0.000474	0.0008	0.04077
6	0.034	0.00062	0.000765	0.01345

➢ *Scenario 14 – 3rd September 1998*

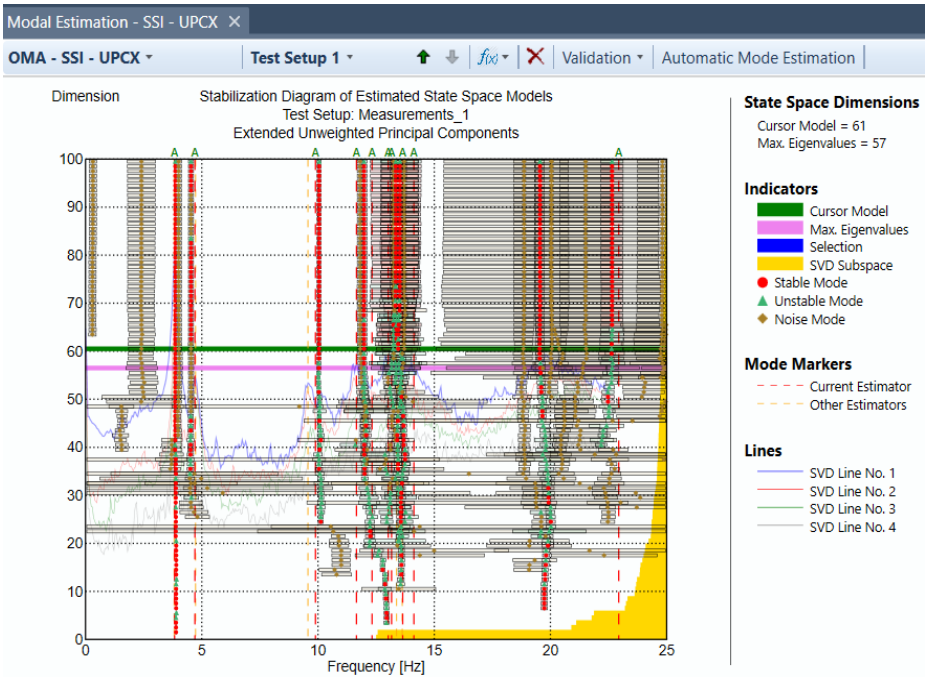

Figure 8.17: Stabilization Diagram of Estimated State Space Models – SSI UPCX (Scenario 14)

1st Mode | 2nd Mode | 3rd Mode

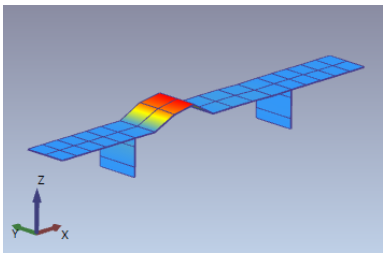

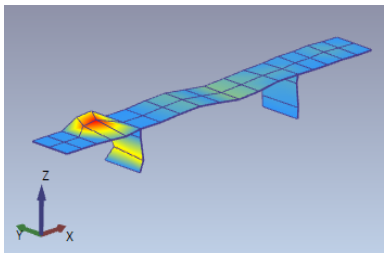

(–)

Trans | Coupled to Coupled*

4th Mode | 5th Mode | 6th Mode

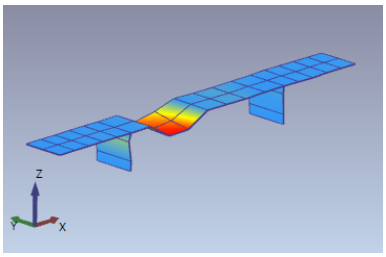

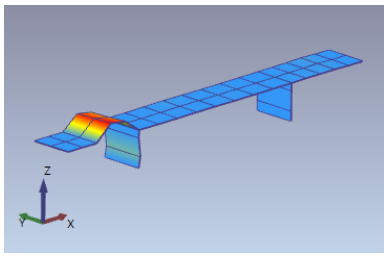

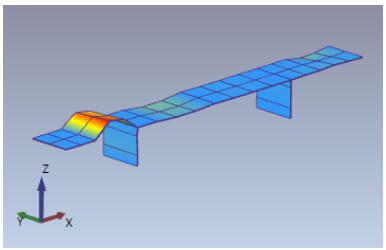

Tors to Coupled | Trans to Trans* | Trans to Coupled

Figure 8.18: Eigen–Modes derived from ARTeMIS Modal (Scenario 14)

Eigen–frequencies			
Mode	**ACWT**	**FFT**	**SSI–COV (ARTeMIS Modal)**
1	3.858	3.86	3.867
2	4.787	4.67	4.532
3	9.834	(–)	(–)
4	10.166	(–)	10.048
5	12.364	12.11	11.983
6	13.339	13.7	13.413

Damping ratios			
Mode	**ACWT (linFit)**	**expoFit**	**SSI–COV (ARTeMIS Modal)**
1	0.002	0.0016	0.01041
2	0.0004	0.00129	0.01611
3	0.0014	0.00062	(–)
4	0.0020	0.0006	0.03255
5	0.00066	0.0005	0.04133
6	0.00017	0.00046	0.06103

➢ *Scenario 16 – 8th September 1998*

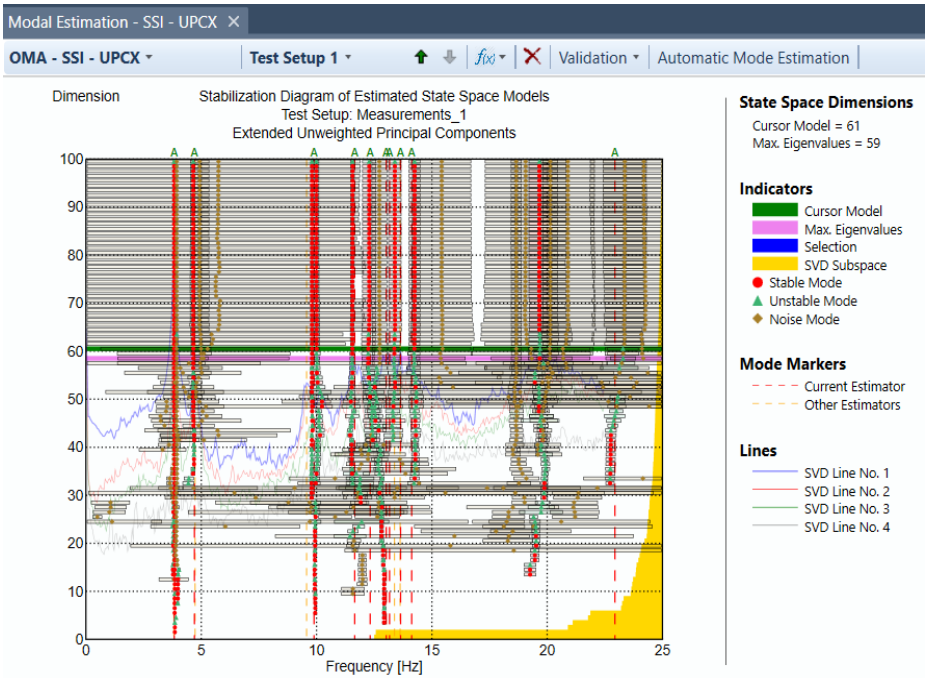

Figure 8.19: Stabilization Diagram of Estimated State Space Models – SSI UPCX (Scenario 16)

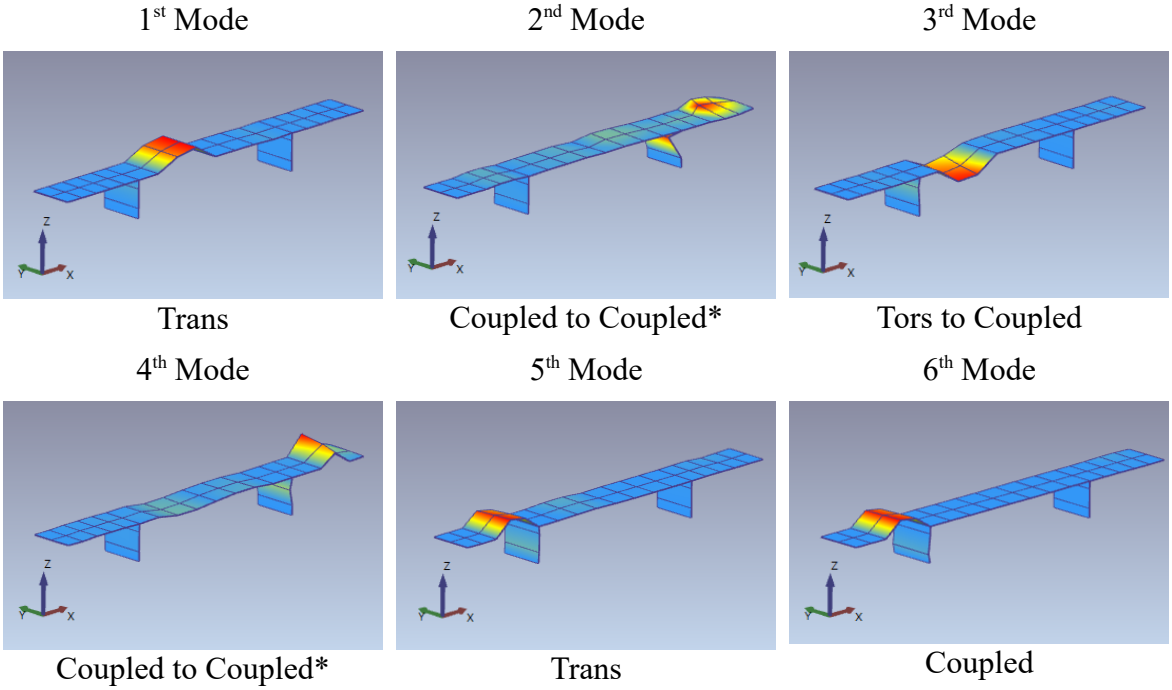

Figure 8.20: Eigen–Modes derived from ARTeMIS Modal (Scenario 16)

Eigen–frequencies			
Mode	**ACWT**	**FFT**	**SSI–COV (ARTeMIS Modal)**
1	3.83	3.84	3.847
2	4.97	4.73	4.654
3	9.796	9.81	9.79
4	10.172	10.35	10
5	12.576	12.22	12.28
6	13.22	13.27	12.914

Damping ratios			
Mode	**ACWT (linFit)**	**expoFit**	**SSI–COV (ARTeMIS Modal)**
1	0.000746	0.000064	0.010
2	0.0015	0.00005	0.0293
3	0.0001	0.000025	0.00865
4	0.00062	0.0000238	0.030
5	0.0012	0.00002	0.035
6	0.000075	0.000018	0.0088

➢ *Scenario 17 – 9th September 1998*

Figure 8.21: Stabilization Diagram of Estimated State Space Models – SSI UPCX (Scenario 17)

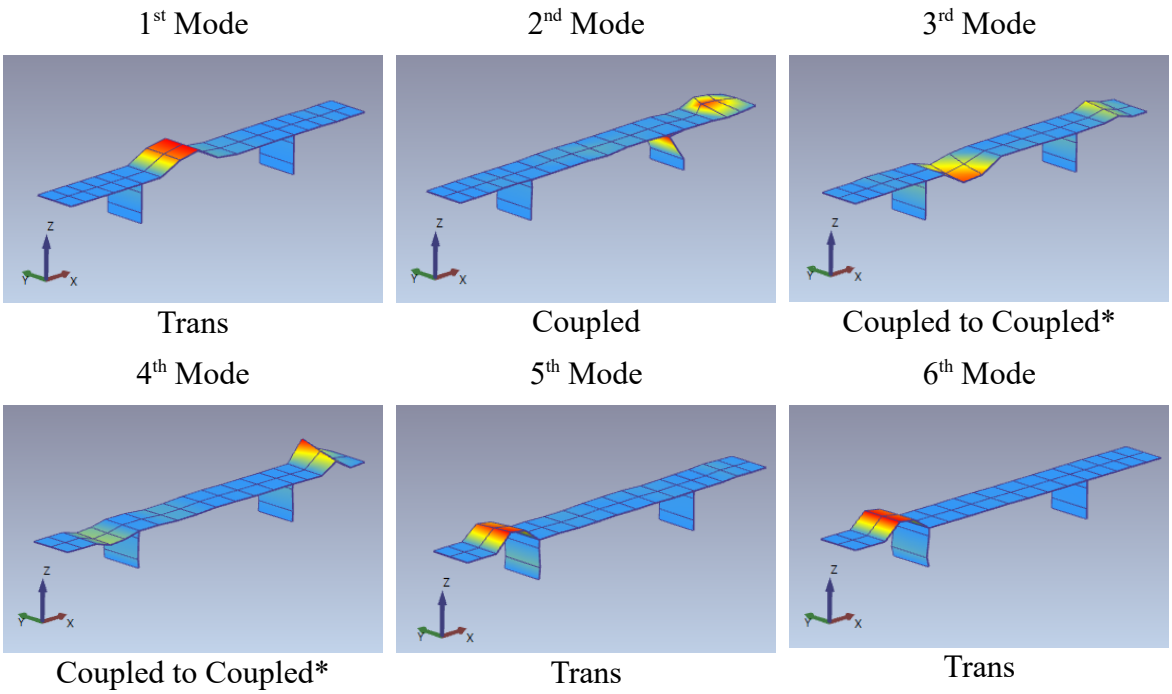

Figure 8.22: Eigen–Modes derived from ARTeMIS Modal (Scenario 17)

Eigen–frequencies			
Mode	**ACWT**	**FFT**	**SSI–COV (ARTeMIS Modal)**
1	3.81	(–)	3.832
2	4.78	4.73	4.707
3	9.675	(–)	9.893
4	10.324	10.13	11.657
5	12.587	12.32	12.328
6	13.25	13.32	13.023

Damping ratios			
Mode	**ACWT (linFit)**	**expoFit**	**SSI–COV (ARTeMIS Modal)**
1	0.00176	0.0016	0.0075
2	0.00143	0.00124	0.03139
3	0.0019	0.00062	0.03226
4	0.0000014	0.00058	0.03366
5	0.00062	0.00049	0.02579
6	0.00004	0.00046	0.01219

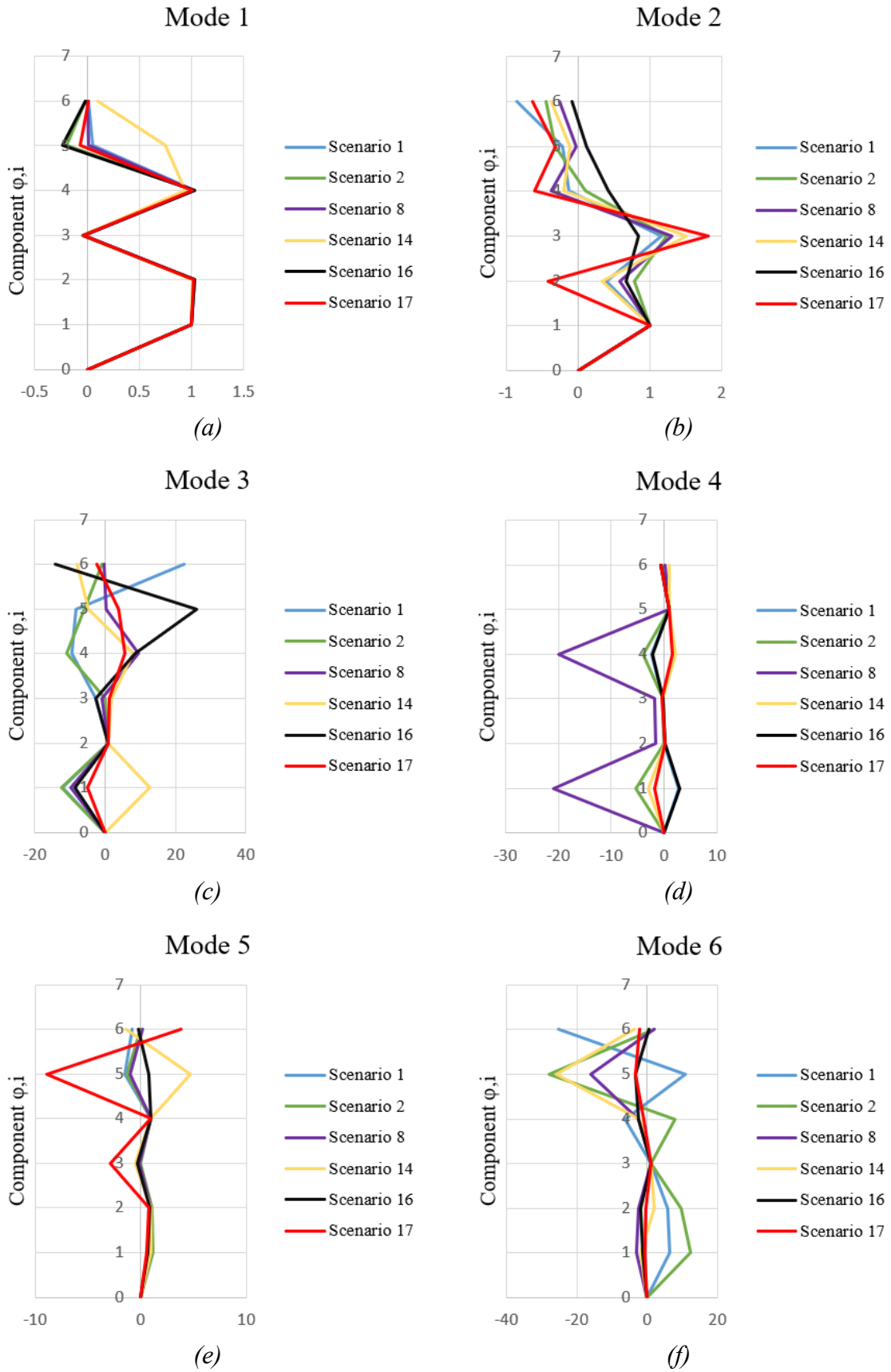

Figure 8.23: Components φ_i of each mode derived from ACWT and comparison throughout the damage scenarios 1, 2, 8, 14, 16, and 17.

9. Conclusions

The current postgraduate thesis has aimed to present the application of the Continuous Wavelet Transform (CWT) in Structural Health Monitoring (SHM). Four systems were presented in total. The CWT was applied in evaluating the modal parameters (eigen–frequencies, damping ratios and eigen–modes) for a 4–storey, an 8–storey and the EuroProteas Project, and subsequently for the Z24 Bridge where the SHM process was applied as well. This road bridge suffered man–made damages before its demolition and the replacement by a railway bridge. The bridge was tested using an on–structure sensing system to monitor its performance through different damage stages. Consequently, damages of a system can be detected comparing the natural frequencies, damping ratios and mode shapes of the different scenarios.

First of all, the background of the CWT, the importance of the mother wavelet choice and the *Q* factor choice were described (edge effect etc.). Afterwards, the sensitivity of the methods in embedded noise effects was presented in Chapter 7 using the signal–to–noise ratio (SNR). The CWT showed more efficient use in high noise phenomena (as the SNR tends to zero), compared to the FFT and ARTeMIS Modal results, maintaining the ability to locate the eigen–frequencies, under very noisy conditions.

Subsequently, the method was applied in order to detect differences in modal parameters through the recordings of the progressive damage scenarios of Z24 Bridge. Initially, the time–frequency domains of the new reference condition (Scenario 8) were presented. The results compared with those derived from the research of KU Leuven (Department of Civil Engineering, Structural Mechanics Section) and they showed good agreement. Furthermore, the eigen–shapes obtained from ARTeMIS Modal were illustrated and compared (*Figure 8.11*).

Thereafter, the components φ_i^l of the "instantaneous" complex mode l of each scenario were compared and demonstrated in the same figures (*Figure 8.23*), in order to reveal the differences of the graphs from the undamaged state (Scenario 1) to the final damaged state (Scenario 17). At the final Scenario the components have bigger values in modes 2 and 5, while in modes 3, 4 and 6 the values of components have been significantly reduced. The only eigen–mode, where the components φ_i^l seem to remain invariant, is the first one.

Concurrently, damage detection was performed in ARTeMIS Modal using the tool "SHM Configuration" and "Analysis History". The monthly recordings of long−term continuous monitoring test and the recordings of short−term progressive damage test were imported into the modal analysis software. The Modal Parameter History aimed to calculate the reference modes and then the Damage Indicator showed the expected time period of the failures (*Figures 8.6−8.7* and *Figures 8.9−8.10*) using statistical analysis and showing dynamic changes of the structure through X^2 value.

The damage state and the dynamic changes of the bridge can also be obtained from the eigen−shapes of the model. As we can see, the only mode without changes is the first

transition mode. During the Scenario 14, after lowering of pier, landslide at abutment, spalling of concrete and failure anchor heads, the shapes of 2nd and 4th mode have significantly changed their form to coupled modes, especially the 2nd mode, while the middle span and the pillars have been activated in the 5th and 6th mode. Eventually, in the ultimate damage scenarios (Scenarios 16 and 17), after tendons rupture, the 2nd, 3rd, 4th, 5th and 6th mode have changed their behavior anew. A remarkable change can be noticed in the 4th mode, where the middle span has been deactivated in comparison to the initial Scenario 8.

Finally, the changes in the system's dynamics can be observed from the decrease in the values of the eigen–frequencies resulting from the automatic estimation with the OMA SSI CPUX method in ARTeMIS Modal. At the same time, there is an increase in the values of the damping ratios in comparison to the undamaged condition. These changes can also be observed in the ACWT results, where the complex modes have given much lower values for the damping ratios which indicates the dissimilar state of the system's dynamics.

Summarizing, the CWT is a reliable method of calculating the modal parameters of a system. In comparison with other methods, it showed better performance in the presence of significant noise. Another ascendancy is the potentiality of the signal presentation in the time domain and the frequency domain at the same time, which is not possible in FFT. In addition, it is an important tool in the application of SHM, giving satisfactory information for the system dynamic characterization, reflecting the condition and functionality of the structure. Therefore, the necessary decisions can be made either for possible required interventions or, in general, for the structure's future, and importantly to ensure the safety of the users.

10. Literature and References

[1] Boashash B., (2016). "Time−Frequency Signal Analysis and Processing, A Comprehensive Reference", 2nd Ed., Academic Press.

[2] Carmona R., Hwang W−L., Torrésani B. (1998). "Practical Time–Frequency Analysis, Gabor and Wavelet Transforms with an Implementation in S", Wavelet Analysis and its Applications, Vol. 9, Academic Press.

[3] Chui C.K., in: Charles K. Chui (Ed.) (1991). "An Introduction to Wavelets", Academic Press.

[4] Daubechies, I. (1990). "The wavelet transform time–frequency localization and signal analysis", IEEE Trans. Inform. Theory, 36, 961–1004.

[5] Debnath L. (2002). "Wavelet Transforms and Their Applications", Birkhäuser Boston.

[6] Delprat N., Escudie B., Guillemain P., Ronland–martinet R.K., Tchamichian Ph., Torrésani B. (1992). "Asymptotic wavelet and Gabor analysis: extraction of instantaneous frequencies", IEEE 38 , 644–664.

[7] Gram−Hansen K., Dorize K., "On the choice of parameters for time–frequency analysis", in: Y. Meyer (Ed.), Wavelets and Applications, Proceedings of the International Conference, Masson, Parts, 1991, pp. 86–92.

[8] Harris F.J. (1978). "On the Use of Windows for Harmonic Analysis with the Discrete Fourier Transform", Proceedings of the IEEE 66, no. 1, 51–83.

[9] Kaiser G. (2011). "A Friendly Guide to Wavelets", 1st Ed., Modern Birkhäuser Classics, Birkhäuser Boston.

[10] Le T–P., Argoul P. (2004). "Continuous wavelet transform for modal identification using free decay response", Journal of Sound and Vibration , 277, 73–100.

[11] Lilly J. M. (2017). "Element analysis: a wavelet–based method for analyzing time localized events in noisy time series." Proceedings of the Royal Society A. Volume 473: 20160776, pp. 1–28.

[12] Liner C. (2010). An overview of wavelet transform concepts and applications, University of Houston, 1–17, 26.

[13] Ljung L., Glover K. (1981). Frequency domain versus time domain methods in system identification, Automatica, Volume 17, Issue 1,Pages 71–86.

[14] Misiti M., Misiti Y., Oppenheim G., Poggi J.M.: Wavelet Toolbox: User's guide ver.R2023a, MathWorks.

[15] Morlet J., (1980). "Sampling theory and wave propagation", Proceedings of the 51st Annual Meeting Soc. Explor. Geophys. Los Angeles.

[16] Grossmann A., Morlet J. (1985). “Decomposition of functions into wavelets of constant shape, and related transforms”, In: Mathematics and Physics, Lecture on Recent Results L. Streit, Editor. World Scientific Publishing (Singapore).

[17] Nobach H., Tropea C., Cordier L., Bonnet J. P., Delville J., Lewalle J., Farge M., Schneider K., and R. J. Adrian (2007). "Review of Some Fundamentals of Data Processing." Springer Handbook of Experimental Fluid Mechanics (C. Tropea, A. L. Yarin, and J. F. Foss, eds.). Berlin, Heidelberg: Springer, pp. 1337–1398.

[18] Signal Processing in Earthquake Engineering, lecture notes, Fragiadakis M. and Taflampas I., ADERS 2020–2021.

[19] Proakis J.G., Manolakis D.G. (1996). “Digital Signal Processing: principles, algorithms and applications, 3rd Ed., Prentice–Hall, Inc., New Jersey.

[20] Todorovska M. (2001). “Estimation of Instantaneous Frequency of Signals Using the Continuous Wavelet Transform”, Technical Report CE 01–07, University of Southern California, Los Angeles.

[21] Torrence C., Compo G.P. (1998). “A Practical Guide to Wavelet Analysis”, Bulletin of the American Meteorological Society, Vol. 79(1):61–78.

[22] Tuzlukov V. (2010), “Signal Processing Noise”, Electrical Engineering and Applied Signal Processing Series, CRC Press.

[23] Staszewski W.J., Cooper J.E. (1995). “Flutter data analysis using the wavelet transform”, Proceedings of the international congress MV2: new advances in modal synthesis of large structures, non linear, damped and non deterministic cases. Lyon, France, 5–6 October 2 1995, 549–561.

[24] Wang, S., Zhao, W., Zhang, G., Xu, H., Du, Y. (2021). “Identification of structural parameters from free vibration data using Gabor wavelet transform”, Mechanical Systems and Signal Processing, Volume 147.

[25] Hera Yanni (2022). “Modal Parameter Identification using the Continuous Wavelet Transform”, National Technical University of Athens, Greece

[26] Wikipedia, Complex number, https://en.wikipedia.org/wiki/Complex_number

[27] Mallat, S. (1989). “A theory of multiresolution signal decomposition: The wavelet representation.” IEEE Transactions on Pattern Analysis and Machine Intelligence, 11:674–693.

[28] Grossmann, A. and Morlet, J. (1984). “Decomposition of Hardy functions into square integrable wavelets of constant shape.” SIAM Journal on Mathematical Analysis, 15(4):723–736.

[29] Carpine R., Ientile S., Vacca N., Boscato G., Rospars C., Cecchi A., Argoul P. (2021). “Modal identification in the case of complex modes – Use of the wavelet analysis applied to the after–shock responses of a masonry wall during shear compression tests.”, Mechanical Systems and Signal Processing, 160, 107753.

[30] Carpine R. (2022). “Détection de défauts dans les structures de génie civil par analyse en ondelettes de réponse vibratoire.”, PhD thesis of Paris–Est University, in French.

[31] Le T.–P., Argoul, P. (2004). “Continuous wavelet transform for modal identification using free decay response”, Journal of Sound and Vibration, 277(1–2), 73–100.

[32] Torrésani, B. (2012). “Analyse continue par ondelettes.”, EDP Sciences, 256 pages.

[33] Lilly, J. M., & Olhede, S. C. (2010). “On the Analytic Wavelet Transform.” IEEE Transactions on Information Theory, 56(8): 4135–4156.

[34] Carmona, R., Hwang, W. L., & Torr´esani, B. (1995). “Identification of chirps with continuous wavelet transform.” In P. Bickel, P. Diggle, S. Fienberg, K. Krickeberg, I. Olkin, N. Wermuth, S. Zeger, A. Antoniadis, & G. Oppenheim (Eds.), Wavelets and Statistics, 103:95–108. New York.

[35] Geradin M. & Rixen D.−J. (2015). “Mechanical Vibrations: Theory and Application to Structural Dynamics”, John Wiley & Sons, 616 pages.

[36] Erlicher, S., Argoul, P. (2007). “Modal identification of linear non–proportionally damped systems by wavelet transform.” Mechanical Systems and Signal Processing, 21(3): 1386–1421.

[37] Argoul P. and Erlicher S. (2005). “Mechanical modelling and computational issues in civil engineering”, Volume 23 of Lecture Notes in Applied and Computational Mechanics, In “On the use of continuous wavelet analysis for modal identification”,359–368. Springer.

[38] Ruzzene M., Fasana A., Garibaldi L., & Piombo B., (1997). “Natural frequencies and dampings identification using wavelet transform: application to real data”, Mechanical Systems and Signal Processing, 11(2): 207–218.

[39] Lardies, J., Gouttebroze, S. (2002). “Identification of modal parameters using the wavelet transform.” International Journal of Mechanical Sciences. 44(11): 2263–2283.

[40] Argoul P. and Fragiadakis M. (2023). “Application of the Wavelet Transform Inverse Analysis for Modal Identification and Damage Detection.” COMPDYN 2023, 9th ECCOMAS Thematic Conference on, Computational Methods in Structural Dynamics and Earthquake Engineering.

[41] Yashodhya Swarna Sri Dhanapala Liyana Kankanamge (2016). “Application of Wavelet Transform in Structural Health Monitoring”, Western Michigan University.

[42] Dimitris Pitilakis, Despina Lamprou, Maria Manakou, Emmanuil Rovithis, Anastasios Anastasiadis (2014), "System identification of soil−foundation structure systems by means of ambient noise records: The case of EuroProteas model structure in Euroseistest"

[43] https://en.wikipedia.org/wiki/Signal–to–noise_ratio

[44] J. Maeck and G. De Roeck (2003), Description of Z24 benchmark, Mechanical Systems and Signal Processing, 17(1):127–131

[45] E. Reynders and G. De Roeck. (2015) Vibration–based damage identification: the Z24 benchmark. In M. Beer, I.A. Kougioumtzoglou, E. Patelli, and I.S.–K. Au, editors, Encyclopedia of Earthquake Engineering.

[46] G. De Roeck. (2003) The state–of–the–art of damage detection by vibration monitoring: the SIMCES experience. Journal of Structural Control, 10:127–143

[47] KU Leuven, Structural Mechanics, Z24 Bridge, https://bwk.kuleuven.be/bwm/z24

[48] EMPA, Section116, Project: SIMCES, Deliverable Code a3: Results of Tasks A1 & A2

[49] Staszewski W.J. (1997). "Identification of damping in MDOF systems using time–scale decomposition", Journal of Sound and Vibration, 203(2): 283–305.

Cover image:

(1) Øresund/Öresund Bridge, located between Denmark and Sweden, is presented in the cover. The image is available in https://www.itsinternational.com/its9/its4/feature/oresund–bridges–front–line–border–crossing–traffic, and it has been modified with the wavelet design for the needs of the thesis.

Youtube links:

(1) Webinar on Structural Health Monitoring (SHM) using ARTeMIS Modal, https://www.youtube.com/watch?v=sfQaGghX_8o&t=2099s